MODELING OF MOLECULAR WEIGHT DISTRIBUTIONS IN ZIEGLER-NATTA CATALYZED ETHYLENE COPOLYMERIZATIONS

by

Duncan Edward Thompson

A thesis submitted to the Department of Chemical Engineering

in conformity with the requirements for the degree of

Doctor of Philosophy

Queen's University

Kingston, Ontario, Canada

(May, 2009)

Abstract

The objective of this work is to develop mathematical models to predict molecular weight distributions (MWDs) of ethylene copolymers produced in an industrial gas-phase reactor using a Ziegler-Natta (Z-N) catalyst. Because of the multi-site nature of Z-N catalysts, models of Z-N catalyzed copolymerization tend to be very large and have many parameters that need to be estimated. It is important that the data that are available for parameter estimation be used effectively, and that a suitable balance is achieved between modeling rigour and simplification.

In the thesis, deconvolution analysis is used to gain an understanding of how the polymer produced by various types of active sites on the Z-N catalyst responds to changes in the reactor operating conditions. This analysis reveals which reactions are important in determining the MWD and also shows that some types of active sites share similar behavior and can therefore share some kinetic parameters. With this knowledge, a simplified model is developed to predict MWDs of ethylene/hexene copolymers produced at 90 °C. Estimates of the parameters in this isothermal model provide good initial guesses for parameter estimation in a subsequent more complex model.

The isothermal model is extended to account for the effects of butene and temperature. Estimability analysis and cross-validation are used to determine which parameters should be estimated from the available industrial data set. Twenty model parameters are estimated so that the model provides good predictions of MWD and comonomer incorporation. Finally, D-, A-, and V-optimal experimental designs for improving the quality of the model predictions are determined. Difficulties with local minima are addressed and a comparison of the optimality criteria is presented.

Co-Authorship

The material presented in Chapters 2, 3, and 4 has been submitted and published in refereed journals as indicated in the chapter introductions. I prepared the first and subsequent drafts for all of the manuscripts, performed all of the calculations and made all of the Figures and Tables. Dr. Km McAuley and Dr. Jim McLellan were co-authors of these papers and have edited and suggested revisions for this thesis, assisted with the organization of the material, and provided technical advice.

Acknowledgements

First, I would like to thank my family for all of their love and support. I would not be in the position I am without the opportunities and guidance they gave to me. I would also like to thank my many friends who have helped me along the way.

I would especially like to thank my supervisors Dr. Kim McAuley and Dr. Jim McLellan. I have been blessed to have two exceptionally smart, dedicated, and kind people to guide me through my time as a graduate student.

I would also like to thank Jean-Richard Llinas and Pierre Sere Peyrigain from INEOS Technologies. Their support and guidance has been of great help to me. I would also like to thank them for the opportunities they gave me to work with them at the INEOS Technologies research center in Lavéra, France.

I also thank all of my lab-mates, especially Saeed Varziri and Shauhoa (Roy) Wu. Our discussions have been a great source of enjoyment for me.

Finally, I would like to thank INEOS Technologies for providing me with experimental data and for their financial support. I would also like to thank MITACS and Queen's University for financial support, and Queen's University and the Province of Ontario for scholarship support.

Table of Contents

List of Figures

List of Tables

Chapter 1

Introduction

1.1 Problem Description

This work focuses on the development of mathematical models for predicting the molecular weight distribution (MWD) of polyethylene (PE) produced using α-olefin comonomers and a particular Ziegler-Natta (Z-N) catalyst in a gas-phase process. Polyethylene, the most widely produced polymer in the world, is generally classified as low-density (LDPE), high-density (HDPE), or linear-low-density (LLDPE).[1.1] LDPE is usually produced by free-radical polymerization and features long-chain branches. HDPE and LLDPE are commonly produced using Z-N catalysts and are generally linear polymers. An α-olefin such as butene or hexene is often used to add short-chain branches to the polymer in order to control its density (a measure of comonomer incorporation and polymer crystallinity). There are several types of active sites on Z-N catalysts. Because of this multi-site nature, polyethylene produced using Z-N catalysts tends to have a broader MWD than PE produced using single-site catalysts. Mechanistic models of PE produced by Z-N catalysts tend to be very complex because of the large number of possible reactions and because each type of active site requires a different set of reaction rate constants.[1.2-1.7] Consequently, these large models with many reactions have a substantial number of kinetic parameters that need to be estimated if the model is to be used to provide accurate predictions. It is difficult to estimate large numbers of parameters, especially if limited data are available. Therefore, simpler models with fewer parameters and effective techniques to help with parameter estimation are desirable.

The kinetics of ethylene copolymerization with Z-N catalysts have been well characterized by Kissin.[1.8] Generally, the average molecular weight of the polymer is controlled by the presence of hydrogen in the reactor. The most common cause for chain termination is chain transfer to hydrogen; thus, when more hydrogen is present, more chain-stopping events take place, thereby lowering the resulting molecular weight of the polymer. Other reactor conditions such as temperature and the various monomer concentrations also have an effect on the MWD. Many efforts have been made to model copolymerizations using Z-N catalysts. de Carvalho et al.[1.2] have developed a commonly used reaction scheme to model the polymerization. If this standard scheme is used, there are about 20 reactions included in the model. Each of these reactions requires a separate kinetic rate constant and activation energy for each type of active site on the catalyst. As a result, when this complete reaction scheme is used to model the PE MWD produced by a catalyst with five types of active sites, there are up to 200 different kinetic rate parameters (rate constants plus activation energies) that need to be estimated. This is an impossible task, given a reasonable amount of data. Therefore, some simplifying assumptions must be made to reduce the number of parameters in the model to a manageable number.

Even with a simplified reaction scheme and model, the parameter estimation may still be difficult. Many modellers have assumed arbitrary values for all of their model parameters.[1.3, 1.9-1.11] Other modellers have adjusted a few key parameters to match available data.[1.4, 1.5, 1.12-1.14] Many modellers have assumed the presence of only one or two types of active sites on the catalyst.[1.3, 1.4, 1.9, 1.10, 1.12-1.20]

1.2 Process Description

The model to be developed predicts MWDs and comonomer incorporation of ethylene/butene and ethylene/hexene copolymers. These copolymers are produced in a gas-phase

process, developed by Naphtachimie in France[1.21] and later transferred to BP Chemicals[1.1] and then to INEOS. This process is known as the Innovene™ process. A simplified schematic is shown in Figure 1.1.1. The MWD is determined by the catalyst and by the operating conditions in the reactor. Although a large number of reactor operating conditions are monitored and controlled, the reactor temperature and the gas-phase partial pressures of the various reactants are of particular interest because they influence the polymer MWD. The gas-phase ratios of the reactants (butene/ethylene, hexene/ethylene, and hydrogen/ethylene) are used to control the polymer molecular weight and density.

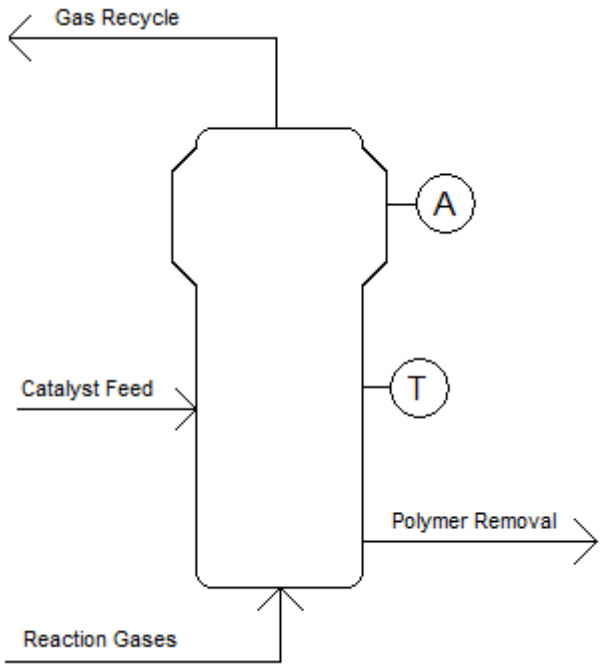

Figure 1.1 Simplified Process Flow Diagram.

The MWDs are measured using high-temperature gel permeation chromatography (GPC). In GPC, a dilute polymer solution is passed through a column containing a porous gel. The

polymer is thereby separated by size. Smaller polymer chains enter the pores in the gel and thus take longer to pass through the column compared to the longer polymer chains that pass through the column without spending time in the pores.[1.22] Thus the molecular weight of each polymer fraction is determined by the amount of time it takes to pass through the column. The MWD is determined based on the fraction of the polymer that exits the column at a given time. The comonomer incorporation (the fraction of the polymer chain that is made up of comonomer rather than ethylene) can be determined by infrared (IR) spectroscopy.[1.22]

1.3 Modeling Approach

Modeling involves not only the derivation of model equations but also obtaining estimates of the model parameters. Without good parameter estimates, the model can only provide qualitative predictions that may be unreliable. The process of modeling involves several steps: i) developing an understanding of the process to be modeled, ii) derivation of mathematical equations to represent the process, iii) the collection of data, iv) the estimation of model parameters, and v) the validation of model predictions. [1.23, 1.24] There is not always a clear beginning or end to this process, because improved model equations are often derived after parameters are estimated and predictions are tested. Additional experiments are often performed after some of the parameters are estimated, in an effort to obtain better information that will lead to better parameter estimates and model predictions. In short, modelling is usually an iterative or cyclical process in which information is obtained, learning occurs, and model improvements are made (see Figure 1.2).

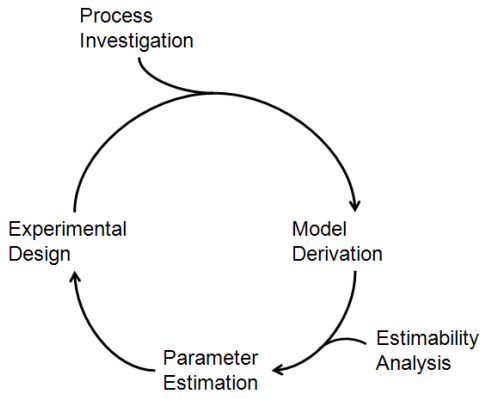

Figure 1.2 Model development cycle

Models can either be empirical models or fundamental mechanistic models. Empirical models do not require prior knowledge of the process; they simply fit parameters to relate input variables to responses. As a result, empirical models are easy to build but have the disadvantage that they are only applicable to the operating region for which they were developed. Mechanistic models on the other hand are based on the underlying physical relationships between input variables and responses. This makes the models more rigorous and more applicable over a larger operating region, but means that they are harder to develop and to estimate. The model presented in this work is a semi-empirical model. Fundamental knowledge of the system is included, but simplifications are made and parameters are estimated in an empirical manner to get a semi-empirical model for the particular system. Depending on the quality of data available and the complexity of the model, different levels of simplification are appropriate to achieve a final semi-empirical model that can be used for making predictions. In this work, good model predictions are more important than the physical veracity of the parameter estimates.

1.4 Thesis Outline and Objectives

The objectives of this thesis are: i) to develop a mathematical model to predict MWD of ethylene/butene and ethylene/hexene copolymers produced by Z-N catalysts, ii) to estimate model parameters using data supplied by our industrial sponsor, and iii) to design additional experiments aimed at improving model predictions. As a first step in the model development process, an empirical, deconvolution-based, analysis of industrial ethylene copolymerization data is performed in Chapter 2 to obtain information about relevant phenomena that should be included in mechanistic MWD models. In Chapter 3, a mechanistic model is developed to predict MWD and comonomer incorporation for ethylene/hexene copolymers produced isothermally at 90 °C. The reaction scheme and the resulting model are simplified so that reasonable estimates can be obtained for key model parameters. In Chapter 4, the isothermal MWD model is extended to account for operation at a variety of temperatures and with butene comonomer. Parameter estimability analysis and cross-validation are used to determine which parameters should be estimated from the available data. The predictive ability of the model is demonstrated by using the model to predict experimental results not used in parameter estimation (cross-validation). The final parameter values that are reported make use of information from all of the available data. In Chapter 5, sequential experiments are designed that should lead to improved parameter estimates and model predictions. These new experiments are of interest to our industrial sponsor.

In addition to the models, parameter values, and suggested experiments described above, this thesis provides up-to-date reviews of mathematical models of polyethylene reactors and of parameter estimation in complex mechanistic models within the various chapters. This thesis further develops the estimability analysis tool for parameter ranking that has been used by previous researchers in our group.[1.25-1.28] Appropriate uncertainty-based scaling factors are

developed and are described in Chapter 4. This scaling has subsequently been used by other students in our group.[1.29, 1.30] Cross-validation is proposed for deciding how many parameters to estimate from the ranked parameter list determined via estimability analysis. Finally, features of A-, D- and V-optimal sequential experimental designs are compared and recommendations are made about problems related to local optima.

This thesis is presented in manuscript format. Chapters 2 and 3 have been published in the journal *Macromolecular Reaction Engineering*, and Chapter 4 has been accepted for publication in the same journal.

1.5 References

[1.1] T. Xie, K. B. McAuley, J. C. C. Hsu, D. W. Bacon, *Ind. Eng. Chem. Res.* **1994**, *33*, 449.

[1.2] A. B. de Carvalho, P. E. Gloor, A. E. Hamielec, *Polymer* **1989**, *30*, 280.

[1.3] G. Dompazis, V. Kanellopoulos, C. Kiparissides, *Macromol Mater. Eng.* **2005**, *290*, 525.

[1.4] K. B. McAuley, J. F. MacGregor, A. E. Hamielec, *AIChE J.* **1990**, *36*, 837.

[1.5] N. P. Khare, K. C. Seavey, Y. A. Liu, S. Ramanathan, S. Lingard, C.-C. Chen, *Ind. Eng. Chem. Res.* **2002**, *41*, 5601.

[1.6] V. Kanellopoulos, B. Gustafsson, C. Kiparissides, *Macromol. React. Eng.* **2008**, *2*, 240.

[1.7] A. Dashti, S. A. A. Ramazani, *Iranian Journal of Chemistry & Chemical Engineering – International English Edition* **2008**, *27*, 13.

[1.8] Y. V. Kissin, *J. Polym. Sci., Part A: Pol. Chem.* **2001**, *39*, 1681.

[1.9] T. Xie, K. B. McAuley, J. C. C. Hsu, D. W. Bacon, *AIChE J.* **1995**, *41*, 1251.

[1.10] B. M. Shaw, K. B. McAuley, D. W. Bacon, *Polym. React. Eng.* **1998**, *6*, 113.

[1.11] K. Y. Choi, S. Tang, A. Sirohi, *Ind. Eng. Chem Res.* **1997**, *36*, 1095.

[1.12] V. Matos, A. G. Mattos Neto, J. C. Pinto, *J. Appl. Polym. Sci.* **2001**, *79*, 2076.

[1.13] Z. G. Xu, S. Chakravarti, W. H. Ray, *J. Appl. Polym. Sci.* **2001**, *80*, 81.

[1.14] M. Hamba, G. C. Han-Adebekun, W. H. Ray, *J. Polym. Sci., Part A: Pol. Chem.* **1997**, *35*, 2075.

[1.15] R. Galvan, M. Tirrell, *Chem Eng. Sci.* **1986**, *41*, 2385.

[1.16] A. G. Mattos Neto, M. F. Freitas, M. Nele, J. C. Pinto, *Ind. Eng. Chem Res.* **2005**, *44*, 2697.

[1.17] G. B. Meier, G. Weickert, W. P. M. van Swaaij, *J. Polym. Sci., Part A: Pol. Chem.* **2001**, *39*, 500.

[1.18] J. J. C. Samson, B. van Middelkoop, G. Weickert, K. R. Westerterp, *AIChE J.* **1999**, *45*, 1548.

[1.19] M. R. Pourhossaini, E. Vasheghani-Farahani, M. Gholamian, M. Gholamian, *J. Appl. Polym. Sci.* **2006**, *100*, 3101.

[1.20] L. D'Agnillo, J. B. P. Soares, G. H. J. van Doremaele, *Macromol. Mater. Eng.* **2005**, *290*, 256.

[1.21] US 3922322, (1975), Naphtachimie, R. Dormenval, L. Havas, P. Mangin.

[1.22] Y. V. Kissin, *"Isospecific Polymerization of Olefins with Heterogeneous Ziegler-Natta Catalysts"*, Springer-Verlag Inc., New York 1985.

[1.23] B. A. Foss, B. Lohmann, W. Marquardt, *J. Proc. Cont.* **1998**, *8*, 325.

[1.24] G. Box, *Journal of Applied Statistics* **2001**, *28*, 285.

[1.25] B. Kou, K. B. McAuley, C. C. Hsu, D. W. Bacon, K. Z. Yao, *Ind. Eng. Chem. Res.* **2005**, *44*, 2428.

[1.26] B. Kou, K. B. McAuley, C. C. Hsu, D. W. Bacon, K. Z. Yao, *Ind. Eng. Chem. Res.* **2005**, *44*, 2443.

[1.27] K. Z. Yao, B. M. Shaw, B. Kou, K. B. McAuley, D. W. Bacon, *Polym. React. Eng.* **2003**, *11*, 563.

[1.28] J. E. Puskas, S. Shaikh, K. Z. Yao, K. B. McAuley, G. Kaszas, *European Polymer Journal*, **2005**, *41*, 1.

[1.29] D. A. Latham, "Mathematical Modelling of an Industrial Steam Methane Reformer", M. Sc. Thesis, Queen's University, 2008.

[1.30] V. I. Koeva, S. Daneshvar, R. J. Senden, A. H. M. Imam, L. J. Schreiner, K. B. McAuley, "Mathematical Modeling of PAG and NIPAM-Based Polymer Gel Dosimeters contaminated by oxygen and inhibitor" Submitted to: Macromolecular Theory and Simulation, April 2009.

Chapter 2

Exploring Reaction Kinetics of a Multi-Site Ziegler-Natta Catalyst Using Deconvolution of Molecular Weight Distributions for Ethylene-Hexene Copolymers

Duncan E. Thompson, Kim B. McAuley*, and P. James McLellan

Department of Chemical Engineering, Queen's University, Kingston, ON, K7L 3N6, Canada

Fax: 1-(613)-533-6637, email: mcauleyk@chee.queensu.ca

Keywords: copolymerization, deconvolution, molecular weight distribution / molar mass distribution, Ziegler-Natta polymerization

2.1 Summary

Industrial ethylene-hexene copolymer samples produced using a supported Ti-based Ziegler-Natta catalyst were deconvoluted into five Flory molecular weight distributions (MWDs). Relationships between reactor operating conditions and deconvolution parameters confirmed that temperature and hydrogen and hexene concentrations influenced the MWD. The two sites that produced low-molecular-weight polymer responded similarly to changes in reactor operating conditions, as did the three sites that produce high-molecular-weight polymer. Increasing hexene concentration resulted in relatively more polymer being produced at the two low-molecular-weight sites and less at the high-molecular-weight sites. The information obtained will be useful for making simplifying assumptions during kinetic model development.

This work was published in *Macromolecular Reaction Engineering* in 2007.

2.2 Introduction

Polyethylene, the polymer with the highest annual world-wide production, is commonly used for films and packaging as well as automotive applications. Polyethylene and its copolymers are generally classified as either low-density (LDPE), high-density (HDPE), or linear-low-density (LLDPE) polyethylene.[2.1] LDPE, which contains long branches, is made using high-pressure free-radical polymerization, whereas HDPE and LLDPE, which are linear polymers, are most often made using Ziegler-Natta catalysts. In HDPE and LLDPE production, an α-olefin comonomer (e.g., hexene or butene) is incorporated to produce short-chain branches. Increasing levels of comonomer incorporation result in lower polymer density.[2.1] HDPE and LLDPE are made in solution and slurry processes, but the gas-phase process is most economical for large-scale production.[2.2] World-wide production of all types of polyethylene is growing, but HDPE and LLDPE production are growing faster than production of LDPE.[2.2]

Polyolefins made using Ziegler-Natta catalysts have very broad MWDs. A polymer's MWD influences its end-use properties[2.3] such as its Young's modulus, impact strength, and melting point. Industrial reaction engineers would like to have kinetic models that predict the MWD (and comonomer incorporation) from the reactor operating conditions. End-use properties could then be predicted from reactor operating conditions, assuming that structure-property relationship models are available to predict end-use properties from MWD (and composition). Mathematical models enable engineers to determine the properties of copolymer currently being produced in a reactor, and to select the appropriate reactor conditions to make polymer grades with desired properties. In gas-phase polyethylene reactors, the polymerization rate, polymer density and average molecular weight are controlled by adjusting the catalyst feed rate, the comonomer feed rate, the hydrogen (a chain transfer agent) feed rate and the temperature.

Polymerization proceeds faster at higher temperatures, so reactors are usually operated at high temperature (typically over 80 ºC) to maintain high reaction rates without using excessive amounts of catalyst. If the temperature is too high in gas-phase reactors, serious problems such as particle agglomeration can arise. Since different polyethylene grades have different particle-softening temperatures, different grades are produced at different temperatures. The more hydrogen that is present in the reactor, the lower the average molecular weight of the polymer (and the higher the melt index) that is produced. The amount of comonomer in the reactor is used to control the density of the copolymer. Short-chain branches, produced by comonomer incorporation, disrupt crystallization, resulting in relatively more amorphous polymer (which is less dense) and relatively less crystalline polymer (which is more dense).

A variety of different HDPE polymer grades are produced commercially to satisfy customers who require polyethylene with different densities and average molecular weights. Table 2.1 shows the scaled reactor operating conditions used to produce the ethylene/hexene copolymer samples that were used in the current study. These sample MWDs were produced using a supported Ti-based Ziegler-Natta catalyst in gas-phase commercial and pilot plants over a 28ºC temperature range. Some of the runs are replicates of each other. Figure 2.1a) to c) show MWDs for the three pairs of replicate runs from Table 2.1. Although the two MWDs shown in Figure 2.1 a) are very close to each other, Figure 2.1 b) and c) show more variability between replicates. Some of these runs were conducted several months apart, and so the larger differences between some of the replicates could be the result of small batch-to-batch differences in the catalyst, impurities in the reactors, disturbances away from operating setpoints, and GPC drift. The replicate runs were produced using the same operating conditions; however, it is also possible to produce the same grade of polymer (same melt index and density) at different

operating conditions. For example, runs 1, 2, and 12 produced the same grade, as did runs 3, 5, 9, and 10. Since the samples being examined resulted from industrial test runs performed for a variety of purposes unrelated to the current work, only a limited range of experimental conditions were used to generate the data. Although we would like to have a richer data set, this was not possible.

Table 2.1 Scaled reactor operating conditions for sixteen ethylene/hexene copolymerization runs and weight-average molecular weight and density of the resulting copolymer. Reactor operating conditions were scaled to protect proprietary information.

Run	Temperature	H_2/C_2 Ratio	C_6/C_2 Ratio	P_{C2}	Mw ($g\ mol^{-1}$)	Density ($kg\ m^{-3}$)
1	0	0.54	1	0.67	68372	931.2
2	0	0.68	1	0.67	70660	933
3	0.36	0.46	0.08	0.67	99150	952
4	0.36	1	0.34	0.83	65234	947.5
5	0.36	0.46	0.08	0.67	95806	952.3
6	0.36	0.46	0.27	0.33	83049	946.5
7	0.36	0.27	0	1	122470	955.3
8	0.36	0.86	0.015	0.73	85943	957.2
9	0.36	0.46	0.16	0.67	86600	951
10	0.36	0.46	0.16	0.67	89450	950.5
11	0	0.49	0.89	0.67	83000	937.9
12	0	0.54	1	0.67	72300	933
13	0.57	0.14	0.74	0	73000	934.5
14	0.71	0	0.66	0.03	78700	936.5
15	0.57	0.08	0.81	0	75400	935.7
16	1	0	0.14	0.47	82600	947.9

a)

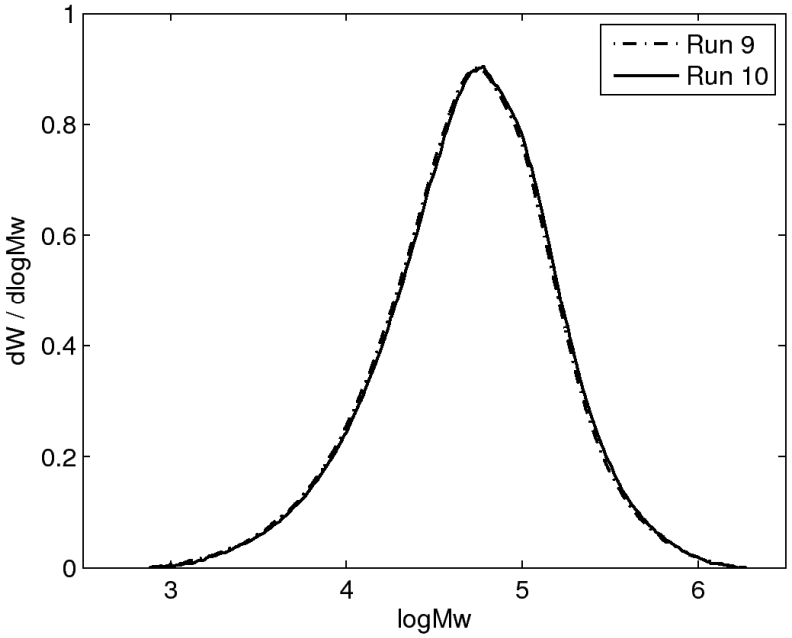
Run 9
Run 10
dW / dlogMw
logMw
0
0.2
0.4
0.6
0.8
1
3
4
5
6

b)

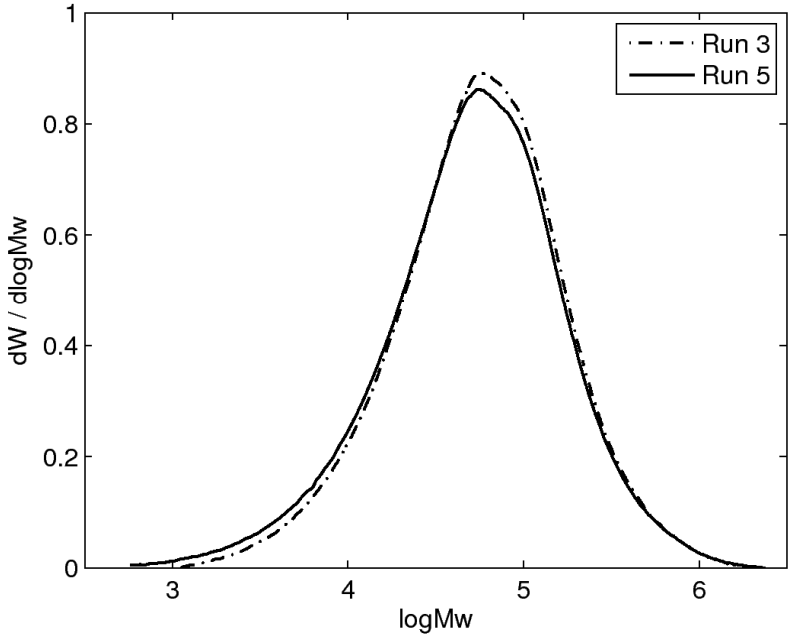
Run 3
Run 5
dW / dlogMw
logMw
0
0.2
0.4
0.6
0.8
1
3
4
5
6

c)

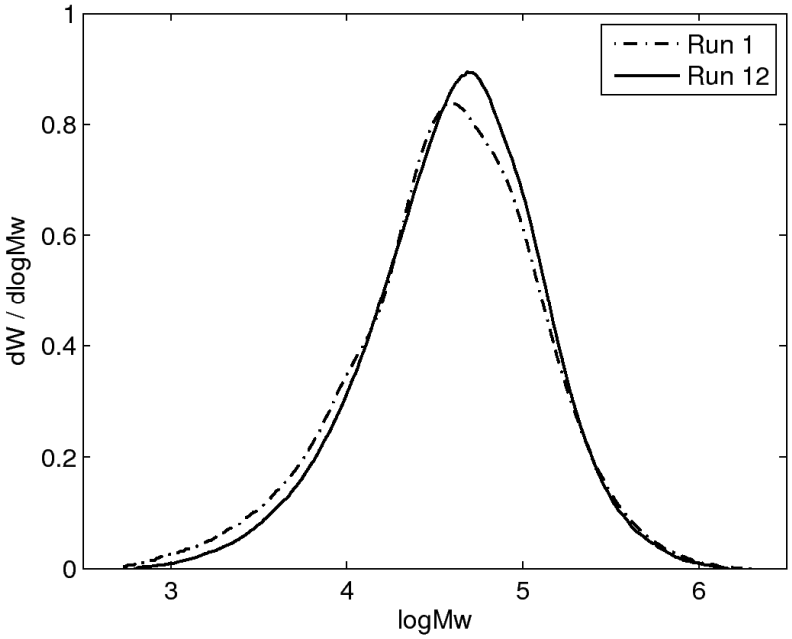

Figure 2.1 a) Measured MWDs from replicate runs 9 and 10. b) Measured MWDs for replicate runs 3 and 5. c) Measured MWDs of replicate runs 1 and 12.

The broad MWDs of polyethylene copolymers produced using heterogeneous Ziegler-Natta catalysts are the result of several types of active sites on the catalyst.[2.4] The multi-site nature of the catalyst makes it difficult to develop kinetic models that can predict MWD and comonomer composition. Because each site type can have different kinetic behaviour, large numbers of kinetic parameters are needed. As a result, many modellers only assume two or three types of active sites and make many simplifying assumptions, but almost all end up with a very large number of kinetic parameters[2.5-2. 9] that need to be estimated.

In theory, each type of active site produces polymer with an instantaneous MWD that can be described by Flory's most probable distribution,[2.4, 2.10, 2.11] assuming that temperature, hydrogen and monomer concentrations are uniform in the amorphous phase of the polymer

throughout the reactor. Vickroy et al.[2.10] originally proposed deconvolution analysis as a technique for decomposing MWDs into their component Flory distributions. Soares and Hamielec clearly outlined the methodology that is most often used to deconvolute experimental MWDs.[2.11] Using nonlinear regression techniques, the average molecular weight of polymer produced at each site, as well as the mass fraction of polymer produced at each site, can be determined.

Kissin and others have found that five to seven Flory components are often needed to adequately match the MWD of polyolefins produced using Ziegler-Natta catalysts.[2.4, 2.10, 2.12, 2.13] However, it is widely believed that there are not this many chemically distinct types of active sites on Ziegler-Natta catalysts. In fact, by broadening the component distributions to account for site-surface interactions, Soares found that broad MWDs could be explained using only two or three chemically distinct types of active sites.[2.14] Although using a broadened Flory component distribution reduces the number of sites, it would require that additional broadening parameters be included in the model. Therefore, this method has not been pursued. Maschio et al. used log-normal distributions, which are broader than Flory distributions, to represent individual components of MWDs,[2.15] as proposed by Keii.[2.16] Log-normal distributions could model the polymer produced by "a group of relatively similar active sites producing polymer with $\overline{M}_w / \overline{M}_n < 3$",[2.15] whereas the Flory distribution only models a single site type with a theoretical polydispersity of two. Maschio and Scali compared two deconvolution methods to determine the effects of mass-transfer phenomena on the MWD in free radical polymerizations.[2.17] A two-peak method in which one peak characterized polymer produced early in a reaction under chemical control, and the second peak characterized higher-molecular-weight polymer produced under diffusive control was used to predict MWDs. A multi-peak method that had peaks corresponding

to many different conversions was also used. They found that the multi-peak method "…is potentially much superior, but the results prove to be more sensitive to the quality of the experimental part."[2.17] Pinto's group found that fewer sites were needed for deconvolution of MWDs produced in unsteady-state reactions if dynamic models were used rather than the more traditional steady-state models.[2.18]

Pinto's group also found that, under some circumstances, it was easier to use cumulative probability distributions[2.19, 2.20] for deconvolution rather than the usual differential distribution approach.[2.11] Because the cumulative distribution is always a monotonic increasing function constrained between 0 and 1, the cumulative-distribution approach can encounter fewer numerical problems than the traditional differential-distribution approach, particularly for multimodal MWDs.

Deconvolution analysis has been used to explore polymerization kinetics at various types of sites, with the aim of developing kinetic models. Khare et al.[2.13] and Soares et al.[2.21] used traditional deconvolution techniques[2.11] to determine the number of sites needed to model the MWD of polymer produced using a Ziegler-Natta catalyst. Deconvolution has also been used by Pinto's group[2.19, 2.20] to develop a method for the quantitative evaluation of kinetic constants in Ziegler-Natta and metallocene-catalyzed olefin polymerizations for both conventional[2.19] and high-activity catalysts.[2.20] Nele and Pinto[2.22] used MWD deconvolution to predict whether the polymers that are produced would have bimodal MWDs.

Kissin has done extensive work using deconvolution to better understand the kinetics of ethylene polymerization with heterogeneous Ziegler-Natta catalysts.[2.4, 2.23-2.29] Kissin characterized the effects of important reactor operating conditions on the active sites. Hydrogen is a chain-transfer agent and so, not surprisingly, it was found that an increase in hydrogen

concentration reduced the average molecular weight of polymer produced at all sites.[2.23-2.25, 2.29] Hydrogen also suppresses overall catalyst activity[2.30] and polymerization rates. Higher temperatures were found to decrease the average molecular weight of the polymer produced, and to increase the activity of the catalyst.[2.25] In copolymerization with hexene, high temperatures make the catalyst more effective at incorporating comonomers.[2.25] Kissin also found that the pressure of ethylene in the reactor had very little effect on the average molecular weight and mass fraction of polymer produced by individual active sites.[2.23, 2.29]

In copolymerization reactions using hexene, Kissin found that the presence of hexene greatly increased the amount of polymer produced by low-molecular-weight sites, since these sites more easily incorporate comonomer than high-molecular-weight sites do.[2.23, 2.25, 2.28, 2.31] In batch or semi-batch reactors, the low-molecular-weight sites dominate during the early stages of polymerization, whereas the high-molecular-weight sites dominate during the later stages.[2.23] Kissin also found that, in the presence of hydrogen and hexene, the low-molecular-weight sites reactivate after chain-transfer reactions much more quickly than the high-molecular-weight sites.[2.23] In homopolymerization, all of the sites reactivate after chain-transfer reactions at about the same rate. Therefore, deconvolution has proven a useful tool for exploring the behaviour of multi-site catalysts. By examining the effects of reactor operating conditions on different types of active sites, useful information for developing fundamental kinetic models can be found.

In the current work, sixteen MWDs are deconvoluted, and the relationships among the deconvolution parameters, and between the deconvolution parameters and the reactor operating conditions, are examined. Density measurements, which are related to copolymer composition, were also obtained for the same industrial samples. Unfortunately, we were not provided with

composition distribution measurements, so we do not have any direct information about the composition of the copolymer produced at the different sites.

In this work, the method used to perform deconvolution is described, and difficulties associated with ill-conditioning of the deconvolution parameter-estimation problem are explored. To explore the reaction kinetics, the relationships between the deconvolution parameters for the active sites and the reactor operating conditions are examined using scatter plots and correlation coefficients. Important correlations are identified, and recommendations for using this information during kinetic-model development are made. We show that the two apparent low-molecular-weight sites respond similarly to reactor operating conditions, as do the three apparent high-molecular-weight sites, helping to confirm that there are not five chemically distinct types of active sites on the catalyst.

2.3 Deconvolution of MWDs

The method of Soares and Hamielec[2.11] was used to deconvolute the MWDs for the sixteen runs into their component Flory distributions, as shown for run 9 in Figure 2.2. The samples were taken from continuous steady-state gas-phase processes with long residence times. Therefore, it is assumed that the reaction conditions were constant, and that any heat or mass-transfer resistances early on in the particle life have little influence on the MWD. It was found that five sites were needed to adequately fit the MWDs. If four sites were used, then the deconvolution often failed to provide a good fit of the tails of the MWDs, but no problems of this nature were encountered when five sites were used. Using five sites is also consistent with the findings of Kissin for a similar Ti-based catalyst.[2.4]

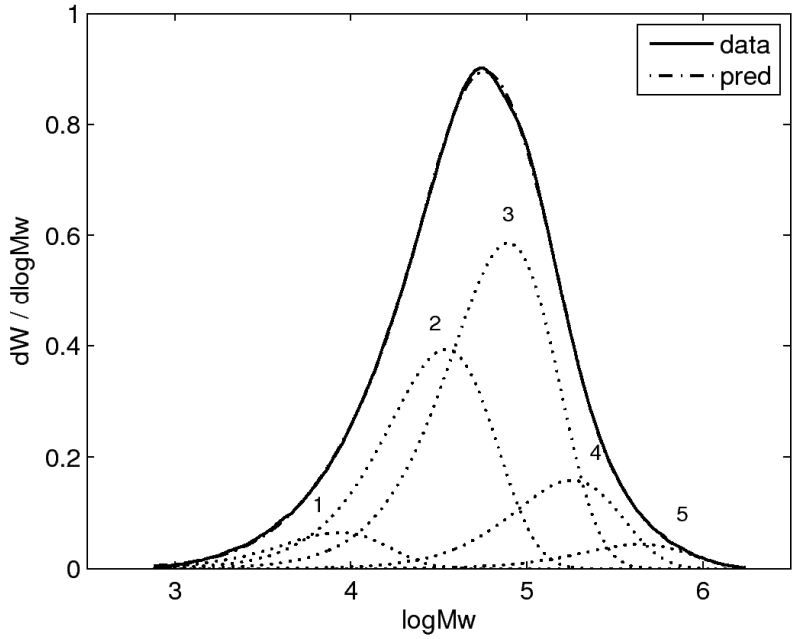

Figure 2.2 The MWD of run 9, deconvoluted into five component Flory distributions.

For each Flory distribution, $w(r,j)$ the weight fraction of chains of length r produced at a site of type j is given by:

$$w(r, j) = \tau_j^2 r \exp\left(-\tau_j r\right) \tag{2.1}$$

where τ_j is the ratio of the rate of chain-terminating events to chain-propagating events at sites of type j.[2.11] We numbered the sites from 1 to 5, with j=1 corresponding to the site that produces the lowest-average-molecular-weight polymer and j=5 corresponding to the site that produces the highest molecular weight. A derivation of how Equation 2.1 is converted into $\frac{dW}{d\log Mw}$ is presented in the appendix. The overall chain-length distribution of the polymer (composed of the individual Flory components) is therefore:

$$W(r) = \sum_{j=1}^{N_S} m_j \cdot w(r, j) \tag{2.2}$$

$W(r)$ is the weight fraction of the polymer of chain-length r produced at all sites, and m_j is the mass fraction of polymer produced by site type j. N_S is the number of site types. Two parameters, τ_j and m_j, must be estimated for each Flory component. The τ_j parameter determines the horizontal position of the component distribution along the chain-length (or molecular weight) axis, and the m_j parameter determines the relative height (see Figure 2.3). The estimated deconvolution parameters, τ_j and m_j, for each of the sixteen samples are shown in Table 2.2.

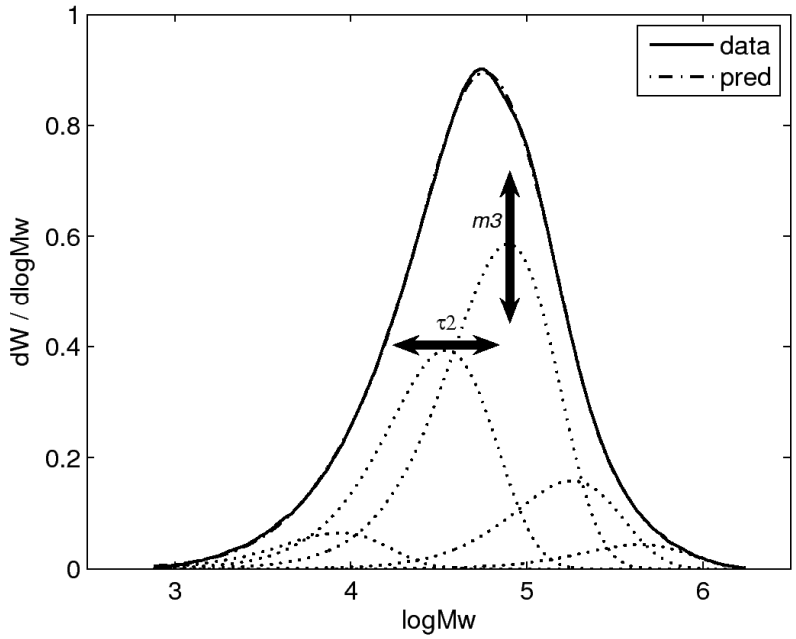

Figure 2.3 Effects of τ_j and m_j. τ_j affects the average molecular weight of polymer produced by a site, and m_j affects the relative size of the component from a site.

Table 2.2 Deconvolution results obtained assuming five site types.

Sample	Mw (g mol^{-1})	τ_1 (*10^3)	τ_2 (*10^3)	τ_3 (*10^3)	τ_4 (*10^3)	τ_5 (*10^3)	m_1	m_2	m_3	m_4	m_5
1	68372	9.977	1.951	0.768	0.305	0.127	0.073	0.384	0.407	0.112	0.022
2	70660	6.064	1.712	0.747	0.335	0.168	0.072	0.372	0.433	0.095	0.028
3	99150	5.939	1.546	0.683	0.297	0.123	0.041	0.290	0.477	0.146	0.046
4	65234	9.349	1.798	0.733	0.286	0.116	0.079	0.440	0.389	0.079	0.013
5	95806	7.434	1.723	0.732	0.313	0.118	0.053	0.266	0.474	0.161	0.046
6	83049	8.912	1.687	0.690	0.281	0.115	0.055	0.384	0.421	0.113	0.026
7	122470	9.753	1.590	0.641	0.257	0.096	0.040	0.277	0.440	0.186	0.057
8	85943	10.070	1.798	0.710	0.276	0.098	0.072	0.362	0.412	0.124	0.029
9	86600	6.497	1.612	0.714	0.309	0.128	0.052	0.316	0.470	0.127	0.035
10	89450	6.338	1.567	0.693	0.301	0.133	0.051	0.312	0.474	0.126	0.038
11	83000	6.170	1.634	0.704	0.286	0.128	0.052	0.349	0.455	0.120	0.024
12	72300	6.544	1.750	0.760	0.337	0.151	0.068	0.361	0.436	0.107	0.028
13	73000	8.928	1.719	0.716	0.290	0.101	0.067	0.420	0.403	0.093	0.017
14	78700	8.744	1.664	0.696	0.282	0.102	0.056	0.411	0.412	0.101	0.020
15	75400	9.154	1.712	0.718	0.286	0.098	0.063	0.420	0.403	0.094	0.019
16	82600	9.255	1.586	0.696	0.292	0.101	0.063	0.382	0.430	0.114	0.022

The active-site parameters, τ_j and m_j, were estimated jointly using least-squares regression to minimize the sum of squared deviations between the model predictions and the dW/dlogM data. Several problems were encountered during deconvolution. For example, the estimates of the mass fractions for some MWDs converged to values that did not sum to one. To address this problem, the sum of m_j values was constrained by defining m_5 as $1-\sum_{j=1}^{4} m_j$. Parameter estimates would sometimes converge to negative values, which make no physical sense. To solve this problem, constraints were imposed during the estimation so that $\tau_j > 0$ and $0 < m_j < 1$. Initial guesses for the values of τ_j and m_j were chosen from within the range of reasonable values for each MWD, (i.e., τ_j values that placed the individual Flory distributions within the range of the measured MWD). Estimates for the τ_js and m_js at different sites were highly correlated. A correlation table for the parameter estimates from the deconvolution of Run 9 is shown in Table 2.3. Note that τ estimates for adjacent sites in the MWD are highly correlated

(e.g., correlation between estimates for τ_2 and τ_3 is 0.89). The mass-fraction estimates are also correlated with the τ estimates for the same site (e.g., the correlation between the estimates of τ_2 and m_2 is -0.96). These high correlations indicate that the parameter estimation was ill-conditioned and that different sets of τ and *m* parameters can give nearly the same MWD curves. Therefore, the deconvolution results are statistically uncertain; however they can provide some information about the behaviour of the catalyst. When only four (rather than five) Flory distributions were used, to reduce the number of parameters, MWDs with the desired shape and breadth were not obtained for some of the samples.

Table 2.3 Correlations between deconvolution parameter estimates from run 9.

	τ_1	τ_2	τ_3	τ_4	τ_5	m_1	m_2	m_3	m_4
τ_1	1	0.69	0.48	0.32	0.23	-0.81	-0.52	0.15	0.40
τ_2	0.69	1	0.89	0.66	0.44	-0.82	-0.96	0.01	0.81
τ_3	0.48	0.89	1	0.89	0.64	-0.59	-0.97	-0.40	0.95
τ_4	0.32	0.66	0.89	1	0.87	-0.38	-0.77	-0.72	0.79
τ_5	0.23	0.44	0.64	0.87	1	-0.22	-0.51	-0.67	0.43
m_1	-0.81	-0.82	-0.59	-0.38	-0.22	1	0.66	-0.20	-0.52
m_2	-0.52	-0.96	-0.97	-0.77	-0.51	0.66	1	0.16	-0.91
m_3	0.15	0.01	-0.40	-0.72	-0.67	-0.20	0.16	1	-0.41
m_4	0.40	0.81	0.95	0.79	0.43	-0.52	-0.91	-0.41	1

As outlined by Matos et al., it is sometimes preferable to perform deconvolution using cumulative MWDs rather than differential ones.[2.19, 2.20] We repeated the deconvolution of the 16 MWDs using this approach, and correlation patterns and confidence intervals for the parameter estimates were similar to those found using the traditional differential distributions. Since we did not observe any benefits, for our particular deconvolution problem, we decided to show the results from the more widely used method described by Soares and Hamielec.[2.11]

2.4 Interpreting Deconvolution Results

To examine the influence of reactor operating conditions on the molecular weights and mass fractions of the polymer produced by the various catalyst sites, large numbers of scatter plots (e.g., Figure 2.4 to Figure 2.8) were examined.[2.32] To make physical interpretations easier, each τ variable was converted to an approximate weight average molecular weight:

$$M_w = 2M_n = 2\frac{M_m}{\tau} \tag{2.3}$$

where M_m is the molecular weight of ethylene (28 g/mol). In some cases, we observed that a particular operating condition was correlated with the molecular weight or mass fraction of polymer produced at a particular active site. For instance, Figure 2.4 suggests that the site 2 mass fraction tends to increase with increased hexene-to-ethylene ratio.

Figure **2.5** suggests that the average molecular weight of polymer produced at site 2 may tend to decrease as the hydrogen to ethylene ratio increases. Figure 2.6 suggests that the molecular weight of polymer produced by site 1 maybe seems to decrease as the reaction temperature increases. These effects were expected.

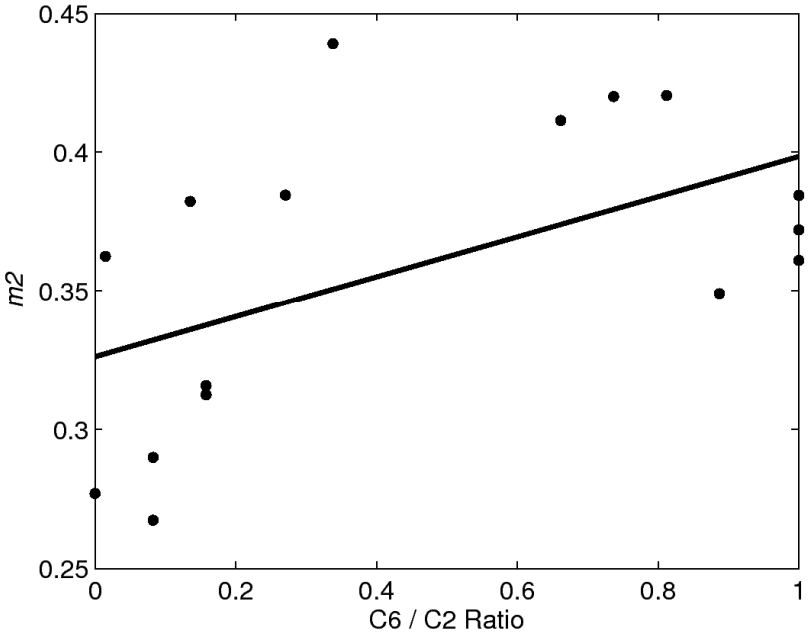

Figure 2.4 Scatter plot showing that site 2 mass fraction increases with hexene-to-ethylene ratio.

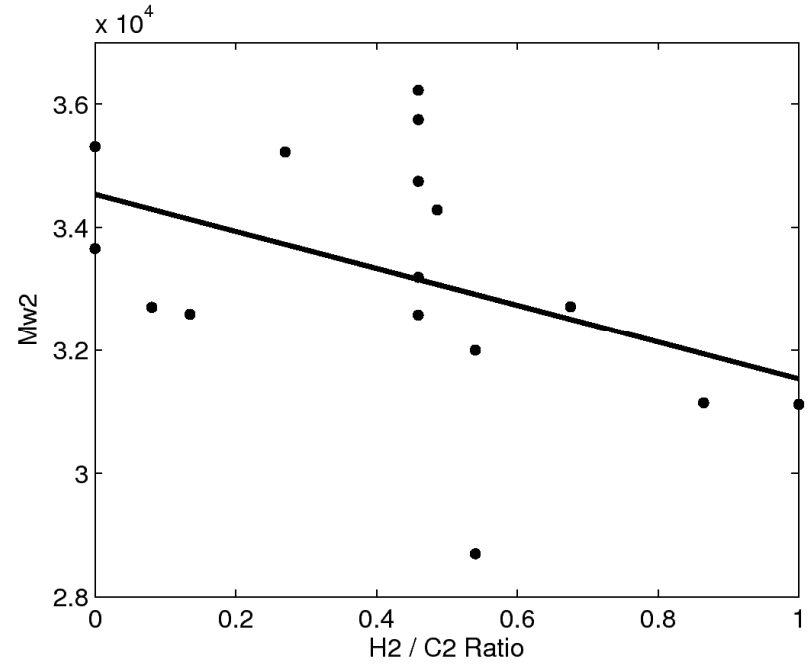

Figure 2.5 Scatter plot showing that site 2 average molecular weight decreases with increasing hydrogen-to-ethylene ratio.

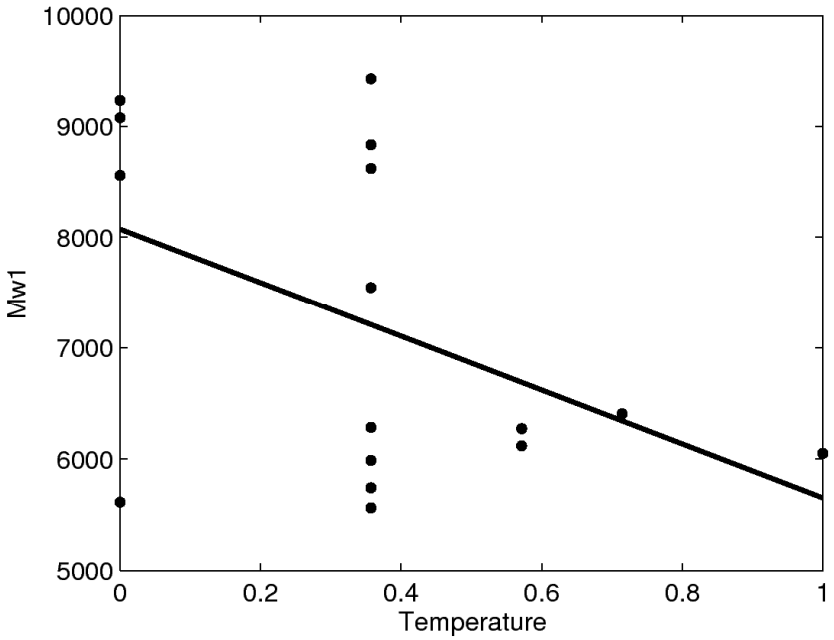

Figure 2.6 Scatter plot showing that site 1 molecular weight decreases with increaing temperature.

Other effects that could be seen in the scatter plots were somewhat less expected. For example, it seems that the hydrogen-to-ethylene ratio has either no effect on the molecular weight of polymer produced at site 1, or that it may even increase with the hydrogen-to-ethylene ratio (Figure 2.7). Also unexpectedly, the average molecular weight of polymer produced at site 5 seems to increase with higher temperatures (Figure 2.8). Normally, molecular weight should decrease at higher temperatures because the activation energies for chain-transfer reactions are typically larger than those for propagation.[2.25]

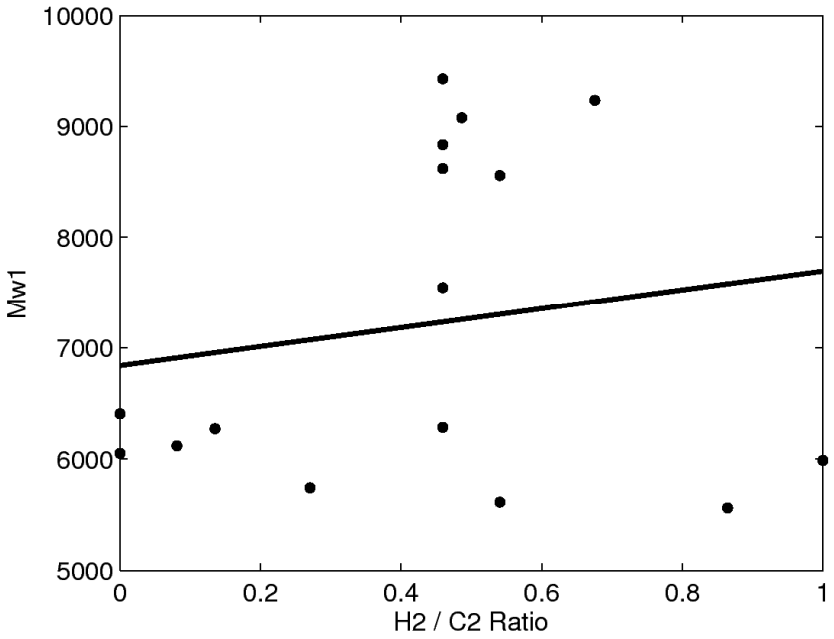

Figure 2.7 Scatter plot showing very little relationship between site 1 molecular weight and hydrogen-to-ethylene ratio.

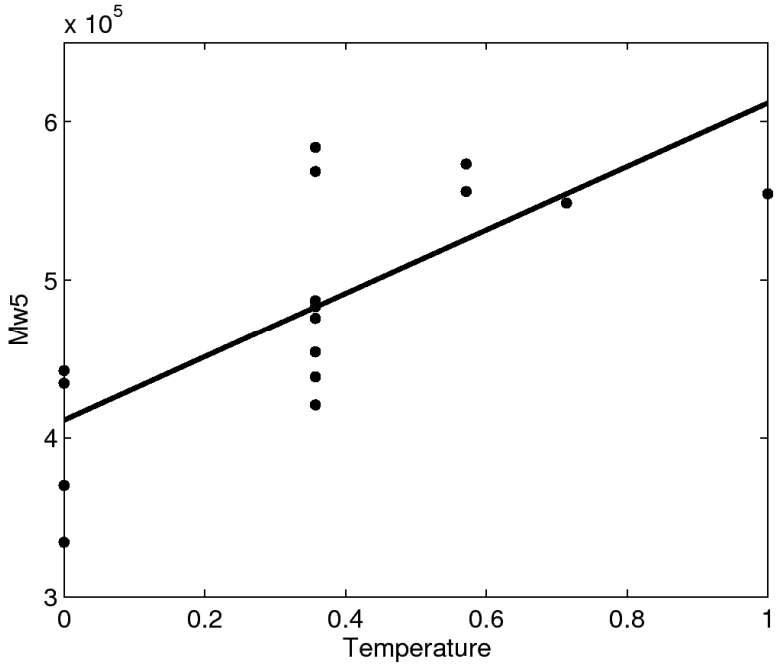

Figure 2.8 Scatter plot showing that site 5 molecular weight increases with temperature.

One possible explanation for the relationship shown in Figure 2.8 is that the reactor operating conditions were not chosen in an independent fashion. They were selected by engineers who wanted to make particular products, resulting in a negative correlation between temperature and the hydrogen-to-ethylene ratio (see Figure 2.9). A lower-molecular-weight product can be made by either increasing the temperature or by increasing the hydrogen-to-ethylene ratio. This type of relationship between reactor operating conditions can confuse matters. It is therefore important to realize that not all relationships shown in the scatter plots are necessarily causal.

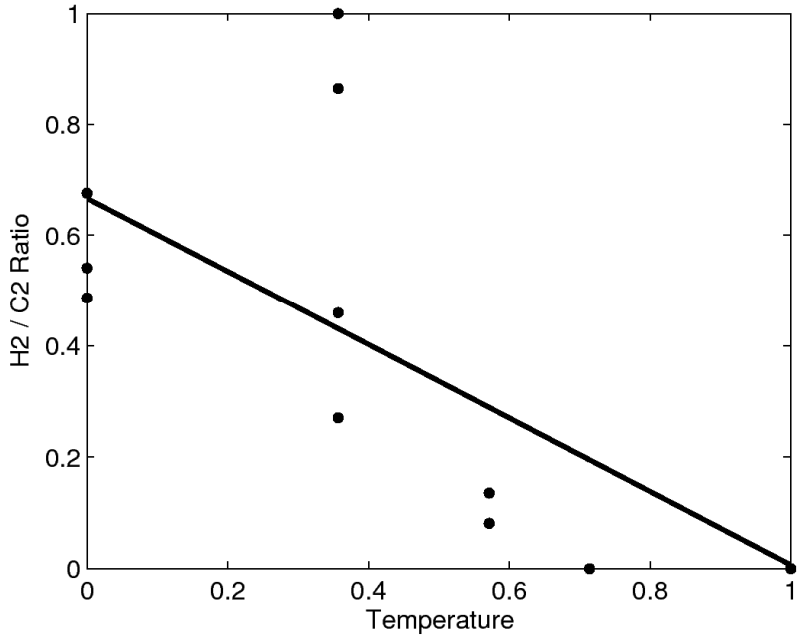

Figure 2.9 Scatter plot showing that temperature and hydrogen ratio appear to be negatively correlated.

Since there are five types of sites, with two deconvolution parameters per site, and there are four reactor operating variables for each polymer sample, a very large number of scatter plots

was generated. It was extremely difficult to determine by inspection which relationships are important, and how strong some relationships are. To help in judging the information on each scatter plot, correlation coefficients were calculated between each pair of variables to explore which operating variables influenced the copolymer molecular weights and mass fractions produced by the individual types of sites. For example, the correlation coefficient between the two variables shown in Figure 2.4, (m_2 and C_6/C_2 ratio) can be calculated as follows:

$$Corr(m_2, RC_6C_2) = \frac{\frac{1}{16-1}\sum_{i=1}^{16}\left(m_{2,i} - \overline{m}_2\right)\left(RC_6C_{2,i} - \overline{R}C_6C_2\right)}{s_{m2}s_{RC6C2}} = 0.53 \tag{2.4}$$

where $m_{2,i}$ and $RC_6C_{2,i}$ are the site-two mass fraction and hexene-to-ethylene ratio for the i^{th} polymer sample. The average of the site-two mass fractions for the 16 runs is $\overline{m}_2$=0.359 and the corresponding average of the hexene-to-ethylene ratios is $\overline{R}C_6C_2$=0.063. The respective standard deviations are s_{m2}=0.0536 and s_{RC6C2}=0.0524. All of the correlation coefficients are shown in Table 2.4, with the value of 0.53 (calculated above) appearing at the intersection of the 13^{th} row (RC_6C_2) and the 7^{th} column (m_2). The correlation between the hydrogen-to-ethylene ratio and the molecular weight of polymer produced at site 1 (shown in Figure 2.7) is 0.16, which is close to zero, indicating very little correlation between these two variables. We considered any correlation with an absolute value greater than 0.7 to be large, and we considered any correlation with an absolute value greater than 0.5 to be of interest. These thresholds are determined arbitrarily and a number of correlations with absolute values slightly less than these thresholds are still of interest.

As shown in Table 2.4, the ethylene partial pressure (PC_2) had small correlations with all of the deconvolution parameters, indicating that it had little influence on the MWD. As expected,

the hydrogen-to-ethylene ratio (RH_2C_2) in the gas phase of the reactor was negatively correlated with the average molecular weights of the polymer produced at most site types, but the correlation coefficients were small, ranging from -0.22 to -0.47 for sites 2 to 5. The hydrogen-to-ethylene ratio was slightly positively correlated with average molecular weight at site 1 (correlation coefficient of 0.16). Hydrogen-to-ethylene ratios were also positively correlated with the mass fraction of polymer produced at site 1 (correlation coefficient of 0.49); polymerization at the low-molecular-weight sites may be less inhibited by hydrogen than is polymerization at the high-molecular-weight sites. This is consistent with fast re-initiation of low-molecular-weight sites after chain-transfer-to-hydrogen reactions.[2.24, 2.25] The hexene-to-ethylene ratio (RC_6C_2) is negatively correlated with the molecular weight of polymer produced at all sites, except for the lowest-molecular-weight site (site 1). We believe that the negative correlation arises due to chain-transfer-to-hexene reactions. Hexene-to-ethylene ratios are also positively correlated with the mass fractions of copolymer being produced at lower-molecular-weight sites and negatively correlated with the mass fractions of polymer produced at high-molecular-weight sites. These correlations are consistent with the low-molecular-weight sites being more able to incorporate hexene, and with hexene reactivating the catalyst more rapidly (after chain transfer reactions) than ethylene does at these sites.[2.23]

Temperature was positively correlated with higher average molecular weights at some sites, which was unexpected, because increasing temperature is known to reduce the average molecular weight of polyethylene. As we described earlier, this peculiar type of result may arise because the temperature and the hydrogen-to-ethylene ratio are correlated (correlation coefficient = -0.64), indicating that the high temperature runs were conducted with low hydrogen-to-ethylene ratios. Caution should be exercised when interpreting the correlation coefficients in Table 2.4,

because correlation does not imply causation. There was little correlation between temperature and the mass fraction of polymer at each site. In general, correlations between reactor operating conditions (except for ethylene partial pressure) and the deconvolution parameters confirm that the effects of some factors (hydrogen-to-ethylene ratio, hexene-to-ethylene ratio, and temperature) should be included in fundamental models.

Table 2.4 Correlation coefficients for deconvolution parameters and reactor operating parameters from sixteen experimental runs.

	Mw_1	Mw_2	Mw_3	Mw_4	Mw_5	m_1	m_2	m_3	m_4	m_5	Temp	RH_2C_2	RC_6C_2	PC_2	Density
Mw_1	1	0.47	-0.11	-0.61	**-0.78**	-0.31	-0.46	**0.75**	0.11	0.31	-0.45	0.16	0.14	0.24	-0.06
Mw_2	0.47	1	**0.74**	0.20	0.07	**-0.86**	-0.50	0.65	0.44	0.50	0.38	-0.43	-0.48	0.03	0.44
Mw_3	-0.11	**0.74**	1	**0.77**	0.54	**-0.77**	-0.39	0.26	0.58	0.52	0.44	-0.38	-0.64	0.07	0.60
Mw_4	-0.61	0.20	**0.77**	1	**0.82**	-0.31	0.06	-0.29	0.29	0.10	0.42	-0.22	-0.45	-0.06	0.43
Mw_5	**-0.78**	0.07	0.54	**0.82**	1	-0.17	0.20	-0.42	0.15	-0.06	**0.73**	-0.47	-0.41	-0.37	0.33
m_1	-0.31	**-0.86**	**-0.77**	-0.31	-0.17	1	**0.71**	**-0.72**	**-0.75**	**-0.71**	-0.27	0.49	0.53	-0.10	-0.49
m_2	-0.46	-0.50	-0.39	0.06	0.20	**0.71**	1	**-0.88**	**-0.91**	**-0.95**	0.22	-0.05	0.53	-0.58	-0.59
m_3	**0.75**	0.65	0.26	-0.29	-0.42	**-0.72**	**-0.88**	1	0.66	**0.74**	-0.19	-0.02	-0.39	0.40	0.43
m_4	0.11	0.44	0.58	0.29	0.15	**-0.75**	**-0.91**	0.66	1	**0.94**	-0.05	-0.09	-0.61	0.52	0.65
m_5	0.31	0.50	0.52	0.10	-0.06	**-0.71**	**-0.95**	**0.74**	**0.94**	1	-0.16	0.00	-0.57	0.55	0.61
Temp	-0.45	0.38	0.44	0.42	**0.73**	-0.27	0.22	-0.19	-0.05	-0.16	1	-0.64	-0.45	-0.52	0.28
RH_2C_2	0.16	-0.43	-0.38	-0.22	-0.47	0.49	-0.05	-0.02	-0.09	0.00	-0.64	1	-0.07	0.66	0.22
RC_6C_2	0.14	-0.48	-0.64	-0.45	-0.41	0.53	0.53	-0.39	-0.61	-0.57	-0.45	-0.07	1	-0.35	**-0.97**
PC_2	0.24	0.03	0.07	-0.06	-0.37	-0.10	-0.58	0.40	0.52	0.55	-0.52	0.66	-0.35	1	0.49
Density	-0.06	0.44	0.60	0.43	0.33	-0.49	-0.59	0.43	0.65	0.61	0.28	0.22	**-0.97**	0.49	1

Of most interest from the correlation analysis in Table 2.4 are the correlation patterns among the deconvolution parameters themselves. If we look at only the upper left-hand corner of Table 2.4 (and ignore the reactor operating conditions for a moment) interesting patterns emerge. Correlations between the weight average molecular weights for most sites (sites 2 to 5) are positive, which is not surprising, because experimental conditions that lead one site to produce higher molecular weights likely induce other sites to also produce higher molecular weights. The

correlation coefficients for the lowest-molecular-weight site (site 1) do not follow this pattern, perhaps because this site produces very-low-molecular-weight waxy copolymer (so that high hexene operating conditions lead to more propagation with hexene and higher, rather than lower, molecular weight oligomers being produced at this site). Alternatively, perhaps because the amount of copolymer produced at this site is so small that the τ_1 and m_1 parameters and their associated correlations are so uncertain that they should not be trusted.

Correlations between the mass fractions at the various sites are also of interest. Operating conditions that increase the mass fraction of polymer produced by site 1 also increase the mass fraction of polymer produced by site 2 (correlation coefficient is 0.71). The mass fractions produced at the high-molecular-weight sites (sites 3, 4 and 5) also move up and down in concert with each other. Mass fractions of polymer produced at the high-molecular-weight sites are negatively correlated with mass fractions produced at the low-molecular-weight sites.

These trends in the deconvolution parameters provide information that may be useful for modeling and model simplification. Since all of the deconvolution parameters for the high-molecular-weight sites (sites 3, 4 and 5) have similar responses to the reactor operating conditions, perhaps some of the kinetic parameters for these sites can be assumed to be common among all three sites, thereby reducing the overall number of parameters to be estimated from limited available data. Furthermore, the correlations among the parameters for the high-molecular-weight sites suggest that there really are not five chemically distinct types of sites, but instead only two or three, with some of the breadth of the MWD arising from different types of catalyst-site/support interactions.[2.14] One chemical site (a combination of sites 3, 4, and 5 in our deconvolution analysis) could produce the high-molecular-weight low-hexene polymer. Another chemical site could produce most of the low-molecular-weight high-hexene copolymer (site 2).

The lowest-molecular-weight site, if it really is chemically distinct from site 2, produces waxy oligomer with very high hexene content. The idea that there are families of active sites that behave similarly and produce polymer with nearly the same average molecular weight was presented by Maschio et al.[2.15]

2.5 Conclusions

Deconvolution of MWDs for sixteen industrial ethylene-hexene copolymer samples and correlation analysis of deconvolution parameter estimates and operating conditions were used to explore the average molecular weight and mass fraction of polymer produced at different active sites of a heterogeneous Ziegler-Natta catalyst. The deconvolution parameter-estimation problem proved to be ill-conditioned, and the resulting mass-fraction and molecular-weight parameters were highly correlated. Constraints were implemented to prevent the deconvolution from converging to physically unrealistic values. Correlation analysis between the deconvolution parameters and the reactor operating conditions suggested that ethylene partial pressure had little influence on the MWD. As expected, high hydrogen-to-ethylene ratios were associated with lower molecular weights. High hexene-to-ethylene ratios were also associated with lower molecular weight, except, perhaps, for the waxy copolymer produced by the lowest-molecular-weight site. As a result, it will be important to include chain transfer attributable to hexene and to hydrogen in fundamental models to predict the MWD produced by this catalyst. High hexene-to-ethylene ratios were also associated with relatively more copolymer being produced at the low-molecular-weight sites and less copolymer being produced at the high-molecular-weight sites. Temperature was found to be correlated with higher average molecular weights, which was not expected since higher temperatures are generally associated with the production of lower molecular weight polymers. This somewhat peculiar result can be explained by high correlation

between the temperature and hydrogen-to-ethylene settings used to produce the sixteen polymer samples.

Correlations between the deconvolution parameters for the high-molecular-weight polymer sites are consistent with there being really only two or three chemically distinct types of sites, with additional broadening of the MWD resulting from other factors such as catalyst-site/support interactions. As a result, it may be possible to group some of the kinetic parameters for similar sites to simplify the model and reduce the number of parameters than need to be estimated during future model-development studies.

2.6 Acknowledgments

The authors wish to thank Innovene, NSERC, and Queen's University for their financial support, and Innovene for supplying experimental data.

2.7 References

[2.1] T. Y. Xie, K. B. McAuley, J. C. C. Hsu, D. W. Bacon, *Ind. Eng. Chem. Res.*, **1994**, *33*, 449.

[2.2] M. M. Kaus "UNIPOL PE Gas-Phase Process: Delivering Value to the PE Industry" In: *Handbook of Petrochemicals Production Processes*, R. A. Meyers, ED., McGraw-Hill, New York, **2005**, 14.113-14.130.

[2.3] J. Bicerano "*Prediction of Polymer Properties*", 2nd edition, Marcel Dekker Inc., **1996**.

[2.4] Y. V. Kissin, *Makromol. Chem., Macromol. Symp.*, **1993**, *66*, 83.

[2.5] K. S. Ha, K. Y. You, H. K. Rhee, *J. Appl. Polym. Sci.*, **2001**, *79*, 2480.

[2.6] B. M. Shaw., K. B. McAuley, D. W. Bacon, *Polym. React. Eng.*, **1998**, *6*, 113.

[2.7] T. Y. Xie, K. B. McAuley, J. C. C. Hsu, D. W. Bacon, *AIChE J.*, **1995**, *41*, 1251.

[2.8] K. B. McAuley, J. F. MacGregor, A. E. Hamielec, *AIChE J.*, **1990**, *36*, 837.

[2.9] K. Y. Choi, S. Tang, A. Sirohi, *Ind. Eng. Chem. Res.*, **1997**, *36*, 1095.

[2.10] V. V. Vickroy, H. Schneider, R. F. Abbott, *J. Appl. Polym. Sci.*, **1993**, *50*, 551.

[2.11] J. B. P. Soares, A. E. Hamielec, *Polymer*, **1995**, *36*, 2257.

[2.12] A. A. da Silva Filho, J. B. P. Soares, G. B. de Galland, *Macromol. Chem. Phys.*, **2000**, *201*, 1226.

[2.13] N. P. Khare, K. C. Seavey, Y. A. Liu, S. Ramanathan, S. Lingard, C. C. Chen, *Ind. Eng. Chem. Res.*, **2002**, *41*, 5601.

[2.14] J. B. P. Soares, *Polym. React. Eng.*, **1998**, *6*(3&4), 225.

[2.15] B. Maschio, C. Bruni, L. de Tullio, F. Ciardelli, *Macromol. Chem. Phys.*, **1998**, *199*, 415.

[2.16] T. Keii, *Macromol. Theory Simul.*, **1995**, *4*, 947-952.

[2.17] G. Maschio, C. Scali, *Macromol. Chem. Phys.*, **1999**, *200*, 1708.

[2.18] M. Fortuny, M. Nele, P. A. Melo, J. C. Pinto, *Macromol. Theory Simul.*, **2004**, *13*, 355.

[2.19] V. Matos, A. G. Neto, J. C. Pinto, *J. Appl. Polym. Sci.*, **2001**, *79*, 2076.

[2.20] V. Matos, A. G. M. Neto, M. Nele, J. C. Pinto, *J. Appl. Polym. Sci.*, **2002**, *86*, 3226.

[2.21] J. B. P. Soares, R. F. Abbott, J. N. Willis, X. Liu, *Macromol. Chem. Phys.*, **1996**, *197*, 3383.

[2.22] M. Nele, J. C. Pinto, *Macromol. Theory Simul.*, **2002**, *11*, 293.

[2.23] Y. V. Kissin, R. I. Mink, T. E. Nowlin, *J. Polym. Sci. Pol. Chem.*, **1999**, *37*, 4255.

[2.24] Y. V. Kissin, *Macromol. Theory and Simul.*, **2002**, *11*, 67.

[2.25] Y. V. Kissin, *J. Polym. Sci. Pol. Chem.*, **2001**, *39*, 1681.

[2.26] Y. V. Kissin, *J. Polym. Sci. Pol. Chem.*, **1995**, *33*, 227.

[2.27] Y. V. Kissin, *J. Polym. Sci. Pol. Chem.*, **2003**, *41*, 1745.

[2.28] Y. V. Kissin, *Macromol. Symp.*, **1995**, *89*, 113.

[2.29] Y. V. Kissin, R. I. Mink, T. E. Nowlin, A. J. Brandolini, *Top. Catal.*, **1999**, *7*, 69.

[2.30] J. G. Wang, W. B. Zhang, B. T. Huang, *Makromol. Chem. Macromol. Symp.*, **1992**, *63*, 245.

[2.31] Y. V. Kissin, R. I. Mink, T. E. Nowlin, A. J. Brandolini, *J. Polym. Sci. Pol. Chem.*, **1999**, *37*, 4281.

[2.32] D. C. Montgomery, G. C. Runger, "*Applied Statistics and Probability for Engineers*", 4th edition, John Wiley & Sons Inc., **2007**, 483-486.

2.8 Appendix: Derivation of differential Flory MWD expression

A MWD is naturally a discrete distribution. A Flory distribution gives the weight fraction of polymer produced at a certain chain-length, r.[2.11]

$$W(r) = \tau^2 r \exp(-\tau r) \tag{2.5}$$

If one wished to determine the weight fraction of polymer chains with lengths between 100 and 200, one could take the sum of the Flory distribution for each chain length between 100 and 200.

$$W(r = 100...200) = \sum_{r=100}^{200} \tau^2 r \exp(-\tau r)\Delta r \tag{2.6}$$

Δr is equal to one since chain length increases one unit at a time. It is easier to work with the distribution in continuous form than in discrete form. If r is treated as a continuous variable, one would integrate to find the weight fraction of polymer chains with lengths between 100 and 200.

$$W(r = 100...200) = \int_{100}^{200} \tau^2 r \exp(-\tau r) dr \tag{2.7}$$

In order to find the height of the MWD curve at any value of *r*, one must differentiate Equation 2.7 with respect to *r*.

$$\frac{dW}{dr} = \tau^2 r \exp(-\tau r) \tag{2.8}$$

MWDs are normally plotted as log molecular weight distributions, in which $\frac{dW}{d\log_{10} Mw}$ is plotted against $\log_{10} Mw$ As a result, an appropriate conversion factor is needed to convert between the Flory distribution expression in eq. 1 and the experimental log molecular weight distributions.

$$\frac{dW}{dr} \cdot \frac{dr}{d\log_{10} Mw} = \frac{dW}{d\log_{10} Mw} \tag{2.9}$$

Mw, the molecular weight of a polymer chain of length *r,* is 28r. Letting z = $\log_{10}$(28r) gives the following relationship between *r* and *z*:

$$\begin{aligned} 28\mathrm{r} &= 10^{z} = \left[e^{\ln(10)}\right]^{z} = e^{z\ln(10)} \\ \therefore \mathrm{r} &= \tfrac{1}{28} e^{z\ln(10)} \end{aligned} \tag{2.10}$$

Taking the derivative of Equation 2.10 yields $\frac{dr}{dz}$, which is the $\frac{dr}{d\log_{10} Mw}$ conversion factor required in Equation 2.9:

$$\begin{aligned}
&\frac{\mathrm{dr}}{\mathrm{dz}} = \tfrac{1}{28} e^{z \ln(10)} \cdot \ln(10) \\
&\therefore \frac{\mathrm{dr}}{\mathrm{d}\log_{10}(28r)} = \frac{e^{z \ln(10)} \cdot \ln(10)}{28} \\
&= \frac{\ln(10) \cdot 10^{z}}{28} = \frac{\ln(10) \cdot 10^{\log_{10}(28r)}}{28} \\
&= \frac{\ln(10) \cdot 28r}{28} = \mathrm{r}\ln(10)
\end{aligned} \tag{2.11}$$

Therefore, the desired conversion factor is r ln(10). Multiplying Equation 2.8 by the conversion factor gives the differential log molecular weight Flory distribution that we can plot.

$$\frac{dW}{d\log_{10} Mw} = \tau^2 \mathrm{r}^2 \ln(10) \cdot \exp(-\tau \cdot \mathrm{r}) \tag{2.12}$$

Chapter 3

A Simplified Model for Prediction of Molecular Weight Distributions in Ethylene-Hexene Copolymerization Using Ziegler-Natta Catalysts

Duncan E. Thompson, Kim B. McAuley*, and P. James McLellan

Department of Chemical Engineering, Queen's University, Kingston, ON, K7L 3N6, Canada

Fax: 1-613-533-6637 Email: mcauleyk@chee.queensu.ca

Keywords: copolymerization, molecular weight distribution, modeling, parameter estimation, Ziegler-Natta polymerization

3.1 Summary

A simplified steady-state model is developed to predict molecular weight distributions (MWDs) and average composition of ethylene-hexene copolymers produced using heterogeneous Ziegler-Natta (Z-N) catalysts in gas-phase reactors. The model uses a simplified reaction scheme to limit the number of parameters that must be estimated. The number of parameters is further reduced by assuming that different types of active sites share common rate constants for some reactions. Estimates of kinetic parameters are obtained using deconvolution analysis of industrial copolymer samples produced using a variety of isothermal steady-state operating conditions. The parameter estimates should prove useful as initial guesses for future parameter estimation in a non-isothermal model.

This work was originally published in *Macromolecular Reaction Engineering* in 2007.

3.2 Introduction

Engineers and industrial scientists would like to predict end-use properties, (e.g., tensile strength, impact strength, melting point, and Young's modulus) from reactor operating conditions so that they can optimize reactor performance and design new products. End-use properties are influenced by the MWD and the level of comonomer incorporation.[3.1] Fundamental model equations have previously been developed[3.2-3.8] to predict MWDs from reactor temperature, reactant concentrations, and catalyst properties, assuming that appropriate values of the model parameters are available. In addition, engineers can predict end-use properties from measured MWDs and copolymer composition information using empirical models.[3.9] Therefore, there are now significant opportunities for combining reactor models with product-property models so that end-use properties can be predicted directly from reactant concentrations, temperature, and catalyst information.

One of the main barriers in the development of such models is the difficulty associated with determining appropriate values for kinetic rate constants. Unfortunately, each different Z-N catalyst has its own set of kinetic parameters so that new parameters must be estimated for each new catalyst. Polymers produced using heterogeneous Z-N catalysts have broad MWDs (i.e., polydispersities ranging from 3 to 10, depending on the catalyst).[3.10] The predominant explanation for the large polydispersities is that Z-N catalysts have multiple types of active sites.[3.11] Under constant reactor conditions, each type of catalyst site produces polymer with a Flory distribution,[3.12] and the overall MWD for the polymer is the aggregate of the distributions produced at the different types of sites on the catalyst.

It is possible to separate a measured MWD into its component distributions using deconvolution. In the deconvolution method outlined by Soares and Hamielec,[3.13] two

parameters are estimated to characterize each component Flory distribution (see Figure 3.1). One parameter, τ_j, is the ratio of the rate of production of dead polymer chains to the rate of propagation at site type j.[3.13] τ_j determines the average molecular weight of polymer produced by that site. Large values of τ_j correspond to low number-average molecular weights. The other parameter, m_j, is the mass fraction of polymer produced by site-type j, which depends on the relative activities of the various sites. Deconvolution has been used by many authors to investigate the number of types of active sites on Z-N catalysts and also the different types of polymer (or copolymer) produced by each site.[3.11, 3.14-3.18]

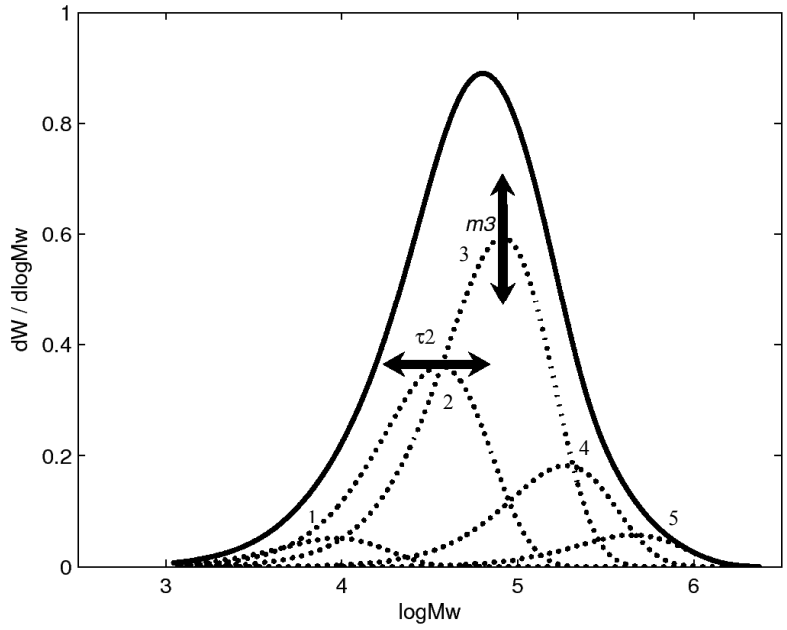

Figure 3.1 The effects of τ_j and m_j on overall Molecular Weight Distribution. MWDs generated by individual sites are dashed lines. The overall MWD is a solid line.

In our previous work,[3.14] deconvolution was used to examine how τ_j and m_j at various active sites were correlated with the reactor operating conditions used to produce industrial high-

density ethylene-hexene copolymers. We found that five types of sites were needed to adequately fit the shapes of the MWDs. The need for five sites is consistent with findings in the literature, particularly the work of Kissin[3.10, 3.11, 3.15] and Fan et al.,[3.19] for similar Ti-based Z-N catalysts. Our deconvolution analysis[3.14] suggested that the low-molecular-weight producing sites, (sites 1 and 2 in Figure 3.1) responded similarly to reactor operating conditions (e.g., relatively more polymer was produced at these sites when the hexene-to-ethylene concentration ratios in the reactor were high). The high-molecular-weight sites (sites 3, 4, and 5 in Figure 3.1) also responded in concert with each other. The high-molecular-weight sites produced relatively less polymer when high hexene-to-ethylene ratios were used. These observations support Kissin's suggestion[3.20] that hexene may be important for the initiation (and re-initiation) of low-molecular-weight sites, but not for high-molecular-weight sites.

Because of the multi-site nature of Z-N catalysts, models to predict MWDs of copolymers produced by heterogeneous Z-N catalysts have many kinetic parameters.[3.2-3.6] Most models make use of a reaction scheme that takes into account the formation, initiation and deactivation of active sites; propagation reactions; chain transfer to hydrogen, monomers, and organometallics; and β-hydride elimination. The combination of the large number of reactions and the large number of active site types results in a very large number of reaction rate constants, especially when temperature effects are considered. Some models also take into account diffusion limitations and heat-transfer resistances, thereby further increasing the complexity of the models and the number of parameters.[3.7, 3.21-3.24]

3.2.1 Estimating Model Parameters

Because of the difficulties associated with parameter estimation, many modellers obtain approximate values from the literature, or are forced to assume arbitrary values.[3.6, 3.8, 3.25, 3.26]

Sometimes a few key parameters are adjusted to match experimental or industrial observations.[3.5, 3.16, 3.18, 3.27, 3.28] To simplify the parameter estimation problem, modellers often assume only one, two, or three types of active sites.[3.5, 3.6, 3.8, 3.18, 3.21, 3.25, 3.27-3.33] This approach usually involves fitting the number and weight average molecular weights (or polydispersity) of a polymer sample, rather than the shape of the entire MWD curve.

Some efforts have been made to estimate parameters in multi-site olefin polymerization models. Choi et al.[3.26] and Chakravarti et al.[3.34] estimated propagation rate constants, reactivity ratios, deactivation rate constants and activation energies using monomer consumption and copolymer composition data. No attempts were made to predict MWD.

Matos et al.[3.18, 3.35] developed a methodology for estimating kinetic parameters in nonisothermal models for propylene polymerization, using gel permeation chromatography (GPC) measurements of the MWD, and nuclear magnetic resonance (NMR) data to provide stereotactic sequence information. They conducted a series of designed experiments to ensure that their product property data would be informative. Deconvolution analysis was used to decompose the MWDs. Fortunately, the MWDs of the polypropylene samples produced by their Z-N catalysts were quite narrow (i.e., polydispersities near 2.5) so that only two types of active sites were required to fit the MWDs. Ratios of influential kinetic parameters were estimated from the resulting τ_j and m_j values. Their parameter estimates resulted in quite good predictions of MWDs for several samples that were not used to fit the parameters; the modes of measured and predicted MWD curves matched well, but the tails of the distributions were not as well predicted. The same group (Mattos Neto et al.[3.29]) used measured polymerization rate profiles and MWD deconvolution results to estimate important kinetic parameters in a simplified model for ethylene/butene copolymerization using a Phillips catalyst. Mattos Neto et al.[3.29] used three

types of active sites to fit their MWDs, but it would appear that better fits of the tails of the MWDs could have been obtained if more sites were used. The authors selected three sites, to keep the number of kinetic parameters manageable.

Khare et al.[3.16, 3.36] developed a detailed methodology for estimating parameters in simplified isothermal models of steady-state and dynamic HDPE[3.16] and polypropylene[3.36] production processes. First, they adjusted the parameters in a single-site model to match number-average molecular weight, polymerization rate, and monomer and comonomer conversion. They then used deconvolution to find out how many sites were needed (they used five for their catalyst) and adjusted the chain-transfer to hydrogen and to monomer rate constants for each site, so as to match the average molecular weight for that site. The propagation rate constants were adjusted to match the weight fractions of polymer produced by the various sites to the deconvolution results. Khare's models were able to match average molecular weights, polydispersity, production rate, and copolymer composition. They were not used to fit or predict the shape of the entire MWD.

Kou et al.[3.37, 3.38] estimated a subset of the parameters in dynamic models for ethylene homopolymerization[3.37] and ethylene-hexene copolymerization[3.38] using a supported metallocene catalyst. Two site types were required to match the breadth of the MWD. Activation energies were estimated so that temperature effects could be predicted. Model equations were simplified to reduce the number of kinetic parameters. Number-average and weight-average molecular weight data, but not the whole MWD, were used to estimate the parameters.

D'Agnillo et al.[3.33] estimated kinetic rate constants in a two-site model of vanadium-catalyzed copolymerization and terpolymerization of ethylene, propylene, and dienes using production rate data and deconvolution data. Rate data were used to estimate coordination and propagation rate constants. Chain transfer and β-hydride elimination rate constants were

estimated using deconvolution results. The authors did not show how well their model was able to predict MWDs.

3.2.2 Reaction Schemes and Numbers of Model Parameters

If one were to take a standard reaction scheme such as the one presented by de Carvalho et al.[3.2], there would be about 20 reactions for an ethylene-hexene copolymerization at each type of active site. De Carvalho's scheme includes site formation; initiation; propagation; β-hydride elimination; chain transfer to monomers, organometallics, and hydrogen (with reinitiation); and site deactivation. This type of reaction scheme (i.e., terminal model) also takes into account end-group effects. If we assume that one rate constant is needed for each of these 20 reactions at each of five site types, 100 rate constants would be needed in an isothermal model to predict MWD, copolymer composition, and polymerization rate. If temperature effects are also considered, then activation energy estimates are also required, bringing the total number of kinetic parameters to 200. Estimating this large number of parameters, and obtaining the data required to do so, is an overwhelming task. For this reason, simplified reaction schemes are often used to predict MWD and other product properties.[3.2-3.6, 3.16, 3.22, 3.25, 3.37]

The literature reveals that parameter estimation in multi-site models is a very difficult problem. Deconvolution analysis can aid in simplifying the parameter estimation problem, as can using simplified reaction schemes. The present work presents a reaction scheme, which is used to develop a simplified kinetic model that predicts MWDs and copolymer content. In this simplified model, kinetic rate constants are grouped into ratios, reducing the number of parameters that require estimation. Deconvolution results from our previous work are used to fit the model parameters.[3.14] More precise parameter estimates are obtained when the correlations among the estimated deconvolution parameters (the τ_j's and m_j's) are accounted for during parameter

estimation. In future, the parameter estimates obtained will provide useful initial guesses for nonlinear least-squares parameter estimation in a more complex multi-site non-isothermal model.

3.3 Model Development

In the present work, we develop a simplified model, which has 39 parameters, to predict MWDs of ethylene-hexene copolymers, and then we further reduce the model to 18 parameters, based on the results of our parameter estimation. Our long-term goal is to produce a model for predicting the breadth and shape of the MWD from steady-state reactor operating conditions. We envision that MWD predictions from our model will be used as input to an empirical industrial model that predicts physical end-use properties of the copolymer. Together, the two models will predict end-use properties from reactor conditions.

We consider eight experimental HDPE samples produced at a common temperature. These samples are part of a larger set of industrial data containing sixteen samples produced at a variety of temperatures and steady-state reactor operating conditions.[3.14] The eight isothermal runs were produced using a variety of hydrogen-to-ethylene ratios and hexene-to-ethylene ratios, as can be seen in Figure 3.2. Note that the gas concentration ratios have been scaled between zero and one to protect the company's proprietary information. Note also that a scaled value of zero for the hexene-to-ethylene ratio corresponds to a nearly zero hexene concentration in the reactor, but that when the scaled hydrogen-to-ethylene ratio is zero, there are still substantial quantities of hydrogen in the reactor. Although scaled values are displayed, the un-scaled values were used in the model development and parameter estimation.

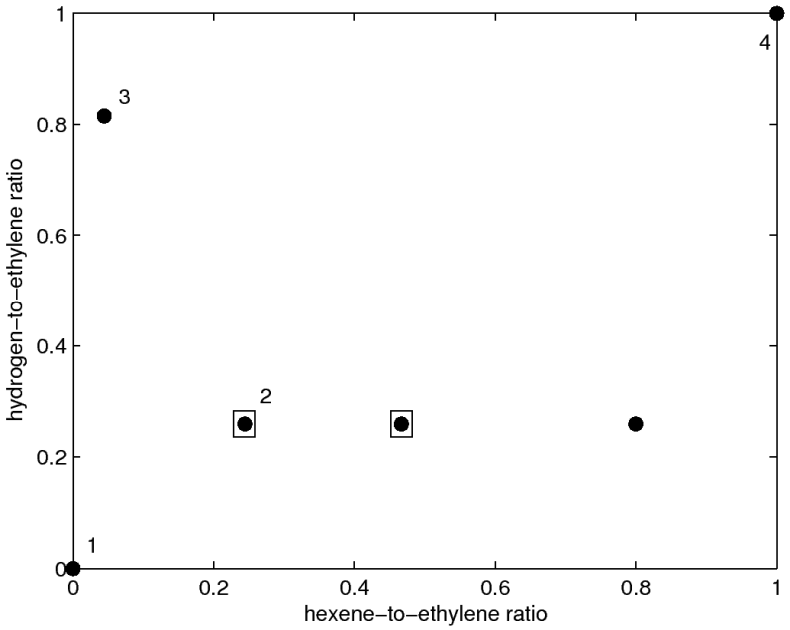

Figure 3.2 Scaled gas-phase concentration ratios used to produce HDPE sample. MWDs for samples labeled 1 to 4 are shown in Figure 3.3. 1 corresponds to the sample with the lowest melt index and the highest average molecular weight (*MI*=1.07) and 4 corresponds to the sample with the highest melt index (*MI*=9.24). The points in boxes indicate replicated experiments. Note that the measured gas concentration ratios were scaled between zero and one, so that point 1 appears at (0,0) and point 4 appears at (1,1). Small amounts of hydrogen and hexene were present in the reactor at experimental condition 1.

After examining measured MWDs for four of the industrial copolymer samples (with melt indexes ranging from 1.07 to 9.24 dg min^{-1}), shown in Figure 3.3, we are concerned that very good predictions of the entire MWD curves (including the tails) will be required. These four MWD curves correspond to the points at (0,0), (0.25,0.25), (0.04,0.81), and (1,1) in Figure 3.2. There is considerable overlap between the four MWD curves, even though MWDs for very different polymer grades, with different types of commercial applications are shown.

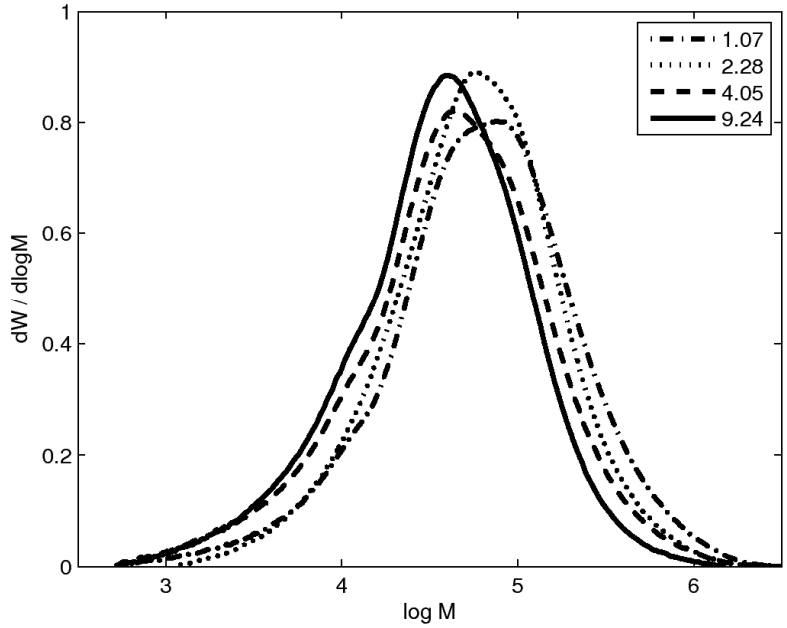

Figure 3.3 MWDs shift slightly to the left as the melt index increases. There is considerable overlap of the MWDs between very different grades.

The reactions included in the simplified steady-state isothermal model are outlined in Reaction Scheme 1. In this scheme, $Y_{j,n}$ is a growing copolymer chain of length n at a site of type j, and Y_{jD} is a temporarily dormant site of type j. These dormant sites, which are produced by chain transfer to hydrogen, are slowly reinitiated by reactions with ethylene and hexene.[3.5, 3.12, 3.15, 3.20] Dormant sites are tracked in the simplified model so that we can account for the effects of hydrogen-induced reduction in polymerization rate, which influences the mass fractions of polymer produced at the various sites. Note that no terminal group effects are taken into account in this simplified model. It is assumed that most of the terminal monomer groups are ethylene and that the difference in kinetics for the small portion of hexene end-groups can be ignored since prediction of MWDs, (rather than sequence length information) is the main purpose of the model.

As a result, rather than having four propagation reactions, only two are included, so that the model should only be applied to low-hexene content copolymers. The model includes propagation with ethylene and hexene; chain transfer to hydrogen, hexene, ethylene, and impurities; β-hydride elimination; and catalyst reinitiation with ethylene and hexene. No long-chain branching is produced by the Ziegler-Natta catalyst. In our isothermal steady-state model, we assume that the relative numbers of potential sites of different types, (Y_j + Y_{jD}) are constant and do not depend on reactor operating conditions. As a result, the simplified reaction scheme does not include any catalyst activation or deactivation reactions.

Scheme 3.1 Simplified Reaction Scheme.

Propagation with ethylene	$Y_{j,n} + \mathrm{C}_2 \xrightarrow{k_{pj}^E} Y_{j,n+1}$
Propagation with comonomer (hexene)	$Y_{j,n} + \mathrm{C}_6 \xrightarrow{k_{pj}^C} Y_{j,n+1}$
Chain transfer to hydrogen	$Y_{j,n} + \mathrm{H}_2 \xrightarrow{k_{tj}^H} Y_{jD}$
Chain transfer to ethylene	$Y_{j,n} + \mathrm{C}_2 \xrightarrow{k_{tj}^E} Y_{j,1}$
Chain transfer to hexene	$Y_{j,n} + \mathrm{C}_6 \xrightarrow{k_{tj}^C} Y_{j,1}$
Chain transfer to cocatalyst & other impurities	$Y_{j,n} + \mathrm{I} \xrightarrow{k_{tj}^I} Y_{j,1}$
Spontaneous chain transfer (β-hydride elimination)	$Y_{j,n} \xrightarrow{k_{tj}^\beta} Y_{j,1}$

Reinitiation with ethylene	$Y_{jD} + \mathrm{C}_2 \xrightarrow{k_{ij}^E} Y_{j,1}$
Reinitiation with hexene	$Y_{jD} + \mathrm{C}_6 \xrightarrow{k_{ij}^C} Y_{j,1}$

The model, which is intended for use with industrial gas-phase reactors, assumes that reaction rates are kinetically, rather than diffusionally, controlled and that the amorphous polymer in contact with the active sites is in phase equilibrium with the gas. We assume that phase equilibria for hydrogen, ethylene, and hexene are governed by Henry's law. The rate constants in Scheme 1 relate the gas-phase concentrations to reaction rates, eliminating the need for Henry's law constants to appear explicitly in the model.[3.5] It is also assumed that residence time does not have a significant impact on the MWD or composition of copolymer produced, and therefore residence time is not included in the model.

MWDs are usually plotted with the base 10 logarithm of the molecular weight as the abscissa and dMw/dlogMw as the ordinate, so that areas under the curve are proportional to the fraction of polymer in a given molecular weight range (see Figure 3.1). The MWD for each component Flory distribution is given by:

$$\frac{dW}{d\log_{10} Mw} = \tau^2 \mathrm{r}^2 \ln(10) \cdot \exp(-\tau \cdot \mathrm{r}) \tag{3.1}$$

where r is the chain length. The chain length is proportional to the number-average molecular weight, Mn, and the weight-average molecular weight, Mw. When computing molecular weights from r, we assume that all monomers have the molecular weight of ethylene, because the amount of hexene incorporated in the high-density polyethylene is small.[3.39]

By taking the ratio of the rates of chain terminating reactions and chain-propagating reactions, and assuming that the rate of propagation with hexene is small compared with the rate of propagation with ethylene, an expression for τ_j (see Equation 3.2, in which $Y_j = \sum_{n=1}^{\infty} Y_{j,n}$ is the number of moles of active sites of type *j* in the reactor) can derived:

$$\begin{aligned}\tau_j &= \frac{R_{tj}}{R_{pj}} = \frac{\left\{k_{tj}^H[\mathrm{H_2}] + k_{tj}^E[\mathrm{C_2}] + k_{tj}^C[\mathrm{C_6}] + k_{tj}^\beta + k_{tj}^I[\mathrm{I}]\right\}Y_j}{\left\{k_{pj}^E[\mathrm{C_2}] + k_{pj}^M[\mathrm{C_6}]\right\}Y_j} \\ &\cong \frac{k_{tj}^H[\mathrm{H_2}] + k_{tj}^E[\mathrm{C_2}] + k_{tj}^C[\mathrm{C_6}] + k_{tj}^\beta + k_{tj}^I[\mathrm{I}]}{k_{pj}^E[\mathrm{C_2}]}\end{aligned} \tag{3.2}$$

A rearranged version of this expression appears as Equation 3.1.1 in Table 3.1.

Table 3.1 Kinetic model equations.

$\tau_j = \frac{k_{tj}^H}{k_{pj}^E}\frac{[\mathrm{H_2}]}{[\mathrm{C_2}]} + \frac{k_{tj}^C}{k_{pj}^E}\frac{[\mathrm{C_6}]}{[\mathrm{C_2}]} + \frac{k_{tj}^E}{k_{pj}^E} + \frac{\left(k_{tj}^\beta + k_{tj}^I[\mathrm{I}]\right)}{k_{pj}^E}\frac{1}{[\mathrm{C_2}]}$	(3.1.1)
$\frac{dW}{d\log_{10} Mw} = m_1\left[r^2\ln(10)\cdot\tau_1^2\cdot\exp(-\tau_1 r)\right] + m_2\left[r^2\ln(10)\cdot\tau_2^2\cdot\exp(-\tau_2 r)\right] + m_3\left[r^2\ln(10)\cdot\tau_3^2\cdot\exp(-\tau_3 r)\right] + m_4\left[r^2\ln(10)\cdot\tau_4^2\cdot\exp(-\tau_4 r)\right] + m_5\left[r^2\ln(10)\cdot\tau_5^2\cdot\exp(-\tau_5 r)\right]$	(3.1.2)
$m_j = \frac{N_j}{\sum_{j=1}^{5} N_j}$	(3.1.3)
$N_1 = \left(\frac{k_{p1}^E\beta_1}{k_{p2}^E} + \frac{k_{p1}^C\beta_1}{k_{p2}^E}\frac{[\mathrm{C_6}]}{[\mathrm{C_2}]}\right)\left(1+\frac{k_{t2}^H[\mathrm{H_2}]}{k_{i2}^E[\mathrm{C_2}]+k_{i2}^C[\mathrm{C_6}]}\right)\left(1+\frac{k_{t3}^H[\mathrm{H_2}]}{k_{i3}^E[\mathrm{C_2}]+k_{i3}^C[\mathrm{C_6}]}\right)\left(1+\frac{k_{t4}^H[\mathrm{H_2}]}{k_{i4}^E[\mathrm{C_2}]+k_{i4}^C[\mathrm{C_6}]}\right)\left(1+\frac{k_{t5}^H[\mathrm{H_2}]}{k_{i5}^E[\mathrm{C_2}]+k_{i5}^C[\mathrm{C_6}]}\right)$	(3.1.4)
$N_2 = \left(1+\frac{k_{p2}^C}{k_{p2}^E}\frac{[\mathrm{C_6}]}{[\mathrm{C_2}]}\right)\left(1+\frac{k_{t1}^H[\mathrm{H_2}]}{k_{i1}^E[\mathrm{C_2}]+k_{i1}^C[\mathrm{C_6}]}\right)\left(1+\frac{k_{t3}^H[\mathrm{H_2}]}{k_{i3}^E[\mathrm{C_2}]+k_{i3}^C[\mathrm{C_6}]}\right)\left(1+\frac{k_{t4}^H[\mathrm{H_2}]}{k_{i4}^E[\mathrm{C_2}]+k_{i4}^C[\mathrm{C_6}]}\right)\left(1+\frac{k_{t5}^H[\mathrm{H_2}]}{k_{i5}^E[\mathrm{C_2}]+k_{i5}^C[\mathrm{C_6}]}\right)$	(3.1.5)

$N_3 = \left(\frac{k_{p3}^E \beta_3}{k_{p2}^E} + \frac{k_{p3}^C \beta_3}{k_{p2}^E}\frac{[C_6]}{[C_2]}\right)\left(1+\frac{k_{t1}^H[H_2]}{k_{i1}^E[C_2]+k_{i1}^C[C_6]}\right)\left(1+\frac{k_{t2}^H[H_2]}{k_{i2}^E[C_2]+k_{i2}^C[C_6]}\right)\left(1+\frac{k_{t4}^H[H_2]}{k_{i4}^E[C_2]+k_{i4}^C[C_6]}\right)\left(1+\frac{k_{t5}^H[H_2]}{k_{i5}^E[C_2]+k_{i5}^C[C_6]}\right)$	(3.1.6)
$N_4 = \left(\frac{k_{p4}^E \beta_4}{k_{p2}^E} + \frac{k_{p4}^C \beta_4}{k_{p2}^E}\frac{[C_6]}{[C_2]}\right)\left(1+\frac{k_{t1}^H[H_2]}{k_{i1}^E[C_2]+k_{i1}^C[C_6]}\right)\left(1+\frac{k_{t2}^H[H_2]}{k_{i2}^E[C_2]+k_{i2}^C[C_6]}\right)\left(1+\frac{k_{t3}^H[H_2]}{k_{i3}^E[C_2]+k_{i3}^C[C_6]}\right)\left(1+\frac{k_{t5}^H[H_2]}{k_{i5}^E[C_2]+k_{i5}^C[C_6]}\right)$	(3.1.7)
$N_5 = \left(\frac{k_{p5}^E \beta_5}{k_{p2}^E} + \frac{k_{p5}^C \beta_5}{k_{p2}^E}\frac{[C_6]}{[C_2]}\right)\left(1+\frac{k_{t1}^H[H_2]}{k_{i1}^E[C_2]+k_{i1}^C[C_6]}\right)\left(1+\frac{k_{t2}^H[H_2]}{k_{i2}^E[C_2]+k_{i2}^C[C_6]}\right)\left(1+\frac{k_{t3}^H[H_2]}{k_{i3}^E[C_2]+k_{i3}^C[C_6]}\right)\left(1+\frac{k_{t4}^H[H_2]}{k_{i4}^E[C_2]+k_{i4}^C[C_6]}\right)$	(3.1.8)

The overall MWDs for our ethylene-hexene copolymer samples can be modeled using a weighted sum of the single-site Flory distributions (Equation 3.1), as shown in Equation 3.1.2 in Table 3.1.

If we knew all of the rate constants in Scheme 1, we could calculate τ_1 to τ_5. Additional model equations that account for the rates of copolymer production at each site type are required to predict the mass fractions of polymer produced at each site type. To illustrate how the mass fraction equations (using 5 sites) in Table 3.1 were developed, while keeping the model equations as simple as possible, we first consider a two-site catalyst. R_{p1} is the production rate, (in moles of monomers consumed per unit time) at site 1, and R_{p2} is that for site two:

$$R_{p1} = k_{p1}^E[C_2]Y_1 + k_{p1}^C[C_6]Y_1 \tag{3.3}$$

$$R_{p2} = k_{p2}^E[C_2]Y_2 + k_{p2}^C[C_6]Y_2 \tag{3.4}$$

These rate equations lead to expressions for the mass fractions produced by the two sites; if we neglect the differences in the molar masses of ethylene and hexene:

$$m_1 = \frac{R_{p1}}{R_{p1}+R_{p2}} = \frac{k_{p1}^E[C_2]Y_1 + k_{p1}^C[C_6]Y_1}{k_{p1}^E[C_2]Y_1 + k_{p1}^C[C_6]Y_1 + k_{p2}^E[C_2]Y_2 + k_{p2}^C[C_6]Y_2} \tag{3.5}$$

$$m_2 = \frac{R_{p2}}{R_{p1} + R_{p2}} = \frac{k_{p2}^{E}[\mathrm{C}_2]Y_2 + k_{p2}^{C}[\mathrm{C}_6]Y_2}{k_{p1}^{E}[\mathrm{C}_2]Y_1 + k_{p1}^{C}[\mathrm{C}_6]Y_1 + k_{p2}^{E}[\mathrm{C}_2]Y_2 + k_{p2}^{C}[\mathrm{C}_6]Y_2} \tag{3.6}$$

Determining the fraction of each type of site that is dormant is important for predicting the relative amounts of polymer produced by the different sites. The presence of hydrogen in the reactor can reduce the rates of polymerization at the various types of active sites to different degrees, because chain transfer to hydrogen leads to dormant catalyst sites that need to be reinitiated by a reaction with monomer before propagation can continue (See Scheme 1). At steady state, the rate of production of dormant sites will be equal to the rate of reinitiation. As a result, the number of moles of dormant sites, Y_{jD}, is related to Y_j, the number of moles of living sites available for propagation reactions. For site 1:

$$\begin{aligned} k_{t1}^{H}[\mathrm{H}_2]Y_1 &= k_{i1}^{E}[\mathrm{C}_2]Y_{1D} + k_{i1}^{C}[\mathrm{C}_6]Y_{1D} \\ \therefore Y_{1D} &= Y_1 \frac{k_{t1}^{H}[\mathrm{H}_2]}{k_{i1}^{E}[\mathrm{C}_2] + k_{i1}^{C}[\mathrm{C}_6]} \end{aligned} \tag{3.7}$$

Similarly, for site 2:

$$\therefore Y_{2D} = Y_2 \frac{k_{t2}^{H}[\mathrm{H}_2]}{k_{i2}^{E}[\mathrm{C}_2] + k_{i2}^{C}[\mathrm{C}_6]} \tag{3.8}$$

Since the number of moles of catalyst sites of each type is not easily determined, it is advantageous to develop a model in which the Y_j's are eliminated. We define a parameter β_j, which is the ratio of potential sites of type j (growing chains plus dormant sites), on the catalyst to potential sites of type 2. We choose site type 2, quite arbitrarily, as our reference site, so that β_2=1. We assume that the ratio of the number of potential sites is a property of the catalyst, and is therefore not influenced by the operating conditions in our isothermal model. For site type 1:

$$\beta_1 = \frac{Y_1 + Y_{1D}}{Y_2 + Y_{2D}} \tag{3.9}$$

Substituting for Y_{2D}, and Y_{1D} from Equation 3.7 and 3.8 and solving for Y_1 gives:

$$\begin{aligned}
\beta_1\left(Y_2 + Y_{2D}\right) &= Y_1 + Y_{1D} \\
\beta_1\left(Y_2 + Y_2\frac{k_{t2}^H[\mathrm{H}_2]}{k_{i2}^E[\mathrm{C}_2]+k_{i2}^C[\mathrm{C}_6]}\right) &= Y_1 + Y_1\frac{k_{t1}^H[\mathrm{H}_2]}{k_{i1}^E[\mathrm{C}_2]+k_{i1}^C[\mathrm{C}_6]} \\
\beta_1 Y_2\left(1+\frac{k_{t2}^H[\mathrm{H}_2]}{k_{i2}^E[\mathrm{C}_2]+k_{i2}^C[\mathrm{C}_6]}\right) &= Y_1\left(1+\frac{k_{t1}^H[\mathrm{H}_2]}{k_{i1}^E[\mathrm{C}_2]+k_{i1}^C[\mathrm{C}_6]}\right) \\
Y_1 &= \beta_1 Y_2\frac{1+\dfrac{k_{t2}^H[\mathrm{H}_2]}{k_{i2}^E[\mathrm{C}_2]+k_{i2}^C[\mathrm{C}_6]}}{1+\dfrac{k_{t1}^H[\mathrm{H}_2]}{k_{i1}^E[\mathrm{C}_2]+k_{i1}^C[\mathrm{C}_6]}}
\end{aligned} \tag{3.10}$$

Substituting the expression for Y_1 into the expression for m_2 in Equation 3.6 gives:

$$m_2 = \frac{k_{p2}^E[\mathrm{C}_2]Y_2 + k_{p2}^C[\mathrm{C}_6]Y_2}{k_{p2}^E[\mathrm{C}_2]Y_2 + k_{p2}^C[\mathrm{C}_6]Y_2 + k_{p1}^E[\mathrm{C}_2]\beta_1 Y_2\dfrac{\left(1+\dfrac{k_{t2}^H[\mathrm{H}_2]}{k_{i2}^E[\mathrm{C}_2]+k_{i2}^C[\mathrm{C}_6]}\right)}{\left(1+\dfrac{k_{t1}^H[\mathrm{H}_2]}{k_{i1}^E[\mathrm{C}_2]+k_{i1}^C[\mathrm{C}_6]}\right)} + k_{p2}^C[\mathrm{C}_6]\beta_1 Y_2\dfrac{\left(1+\dfrac{k_{t2}^H[\mathrm{H}_2]}{k_{i2}^E[\mathrm{C}_2]+k_{i2}^C[\mathrm{C}_6]}\right)}{\left(1+\dfrac{k_{t1}^H[\mathrm{H}_2]}{k_{i1}^E[\mathrm{C}_2]+k_{i1}^C[\mathrm{C}_6]}\right)}} \tag{3.11}$$

Multiplying the numerator and denominator by $\dfrac{1+\dfrac{k_{t1}^H[\mathrm{H}_2]}{k_{i1}^E[\mathrm{C}_2]+k_{i1}^C[\mathrm{C}_6]}}{k_{p2}^E[\mathrm{C}_2]Y_2}$ gives:

$$m_2 = \frac{\left(1+\dfrac{k_{p2}^C}{k_{p2}^E}\dfrac{[\mathrm{C}_6]}{[\mathrm{C}_2]}\right)\left(1+\dfrac{k_{t1}^H[\mathrm{H}_2]}{k_{i1}^E[\mathrm{C}_2]+k_{i1}^C[\mathrm{C}_6]}\right)}{\left(1+\dfrac{k_{p2}^C}{k_{p2}^E}\dfrac{[\mathrm{C}_6]}{[\mathrm{C}_2]}\right)\left(1+\dfrac{k_{t1}^H[\mathrm{H}_2]}{k_{i1}^E[\mathrm{C}_2]+k_{i1}^C[\mathrm{C}_6]}\right)+\left(\dfrac{k_{p1}^E\beta_1}{k_{p2}^E}+\dfrac{k_{p1}^C\beta_1}{k_{p2}^E}\dfrac{[\mathrm{C}_6]}{[\mathrm{C}_2]}\right)\left(1+\dfrac{k_{t2}^H[\mathrm{H}_2]}{k_{i2}^E[\mathrm{C}_2]+k_{i2}^C[\mathrm{C}_6]}\right)} \tag{3.12}$$

Similarly:

$$m_1 = \frac{\left(\frac{k_{p1}^E \beta_1}{k_{p2}^E} + \frac{k_{p1}^C \beta_1}{k_{p2}^E}\frac{[C_6]}{[C_2]}\right)\left(1 + \frac{k_{t2}^H [H_2]}{k_{i2}^E [C_2] + k_{i2}^C [C_6]}\right)}{\left(1 + \frac{k_{p2}^C}{k_{p2}^E}\frac{[C_6]}{[C_2]}\right)\left(1 + \frac{k_{t1}^H [H_2]}{k_{i1}^E [C_2] + k_{i1}^C [C_6]}\right) + \left(\frac{k_{p1}^E \beta_1}{k_{p2}^E} + \frac{k_{p1}^C \beta_1}{k_{p2}^E}\frac{[C_6]}{[C_2]}\right)\left(1 + \frac{k_{t2}^H [H_2]}{k_{i2}^E [C_2] + k_{i2}^C [C_6]}\right)} \quad (3.13)$$

Note that Equations 3.12 and 3.13 do not contain Y_1 or Y_2, but only their ratio, β_1. The expression for each site has a unique numerator, but both sites share the same denominator. This is also true for the five site model, (Equation 3.1.3 in Table 3.1) but the expressions are more complicated. Expressions for the numerators in the five site model are given in Equations 3.1.4-3.1.8 in Table 3.1.

In the expressions in Table 3.1, the kinetic rate constants appear in ratios. As a result, rather than estimating each of the individual rate constants (e.g. k^H_{tj} and k^E_{pj}), (which is impossible using MWD data without polymerization rate data) we focus on estimating the required ratios at the various sites (e.g. k^H_{tj} / k^E_{pj}). To simplify the notation, the model equations were expressed in terms of lumped ratio parameters (in Table 3.2), which contain rate constant ratios and β parameters. Note that the expressions in Table 3.1 do not require information about the number of moles of active catalyst sites in the reactor (i.e., the model has been simplified to remove Y_j s). Estimates of Y_j values and the corresponding propagation rate constants (i.e., k^E_{pj} and k^E_{pj}) would be required if the modeller wanted to predict the overall polymerization rate (see Equations 3.3 and 3.4) in addition to the MWD.

The simplified model equations in Table 3.3 are expressed in terms of the lumped ratio parameters defined in Table 3.2. Note that the expression for α_{22}, as defined by Equation 3.2.6 (in Table 3.2), would be equal to 1, so this parameter does not appear in Equation 3.3.4 (in Table 3.3). The concentration of impurities [I] in the reactor is unknown, but we assume that [I] is

similar for all operating conditions in a particular reactor. With [I] held constant, we lumped the kinetic rate constants for chain transfer to impurities (and cocatalyst) and for β-hydride elimination together in the K_{4j} parameter in Table 3.2. Note that the rates of β-hydride elimination and chain-transfer to cocatalyst are expected to be very small[3.15] so that it is not important to obtain good estimates for the influence of these reactions on the MWD. Reactions with impurities, however, may have an important influence on molecular weight, depending on the type and concentration of impurities that are present in the ethylene and hexene feed streams. If this MWD model were to be used to predict MWDs of copolymers made in different reactors, it might be appropriate to use different values of K_{4j} as a tuning parameter. For example, small pilot-scale reactors with higher impurity levels could have substantially larger values of K_{4j} than when the same catalyst is used in commercial reactors with lower impurity levels.

Table 3.2 Lumped parameter definitions.

$K_{1j} = \frac{k_{tj}^{H}}{k_{pj}^{E}}$	(3.2.1)
$K_{2j} = \frac{k_{tj}^{C}}{k_{pj}^{E}}$	(3.2.2)
$K_{3j} = \frac{k_{tj}^{E}}{k_{pj}^{E}}$	(3.2.3)
$K_{4j} = \frac{\left(k_{tj}^{\beta} + k_{tj}^{I}[\mathrm{I}]\right)}{k_{pj}^{E}}$	(3.2.4)
$\alpha_{1j} = \frac{k_{tj}^{H}}{k_{ij}^{E}}$	(3.2.5)
$\alpha_{2j} = \frac{k_{Pj}^{E}\beta_{j}}{k_{P2}^{E}}$	(3.2.6)
$\alpha_{3j} = \frac{k_{pj}^{C}\beta_{j}}{k_{p2}^{E}}$	(3.2.7)
$\alpha_{4j} = \frac{k_{ij}^{C}}{k_{ij}^{E}}$	(3.2.8)

Table 3.3 Parameterized model equations to predict MWD and comonomer incorporation.

$\tau_j = K_1 \frac{[H_2]}{[C_2]} + K_2 \frac{[C_6]}{[C_2]} + K_3 + K_4 \frac{1}{[C_2]}$	(3.3.1)
$\frac{dW}{d\log_{10} Mw} = m_1\left[r^2 \ln(10)\cdot\tau_1^2\cdot\exp(-\tau_1 r)\right] + m_2\left[r^2 \ln(10)\cdot\tau_2^2\cdot\exp(-\tau_2 r)\right] + m_3\left[r^2 \ln(10)\cdot\tau_3^2\cdot\exp(-\tau_3 r)\right] + m_4\left[r^2 \ln(10)\cdot\tau_4^2\cdot\exp(-\tau_4 r)\right] + m_5\left[r^2 \ln(10)\cdot\tau_5^2\cdot\exp(-\tau_5 r)\right]$	(3.3.2)
$m_j = \frac{N_j}{\sum_{j=1}^{5} N_j}$	(3.3.3)
$N_1 = \left(\alpha_{21} + \alpha_{31}\frac{[C_6]}{[C_2]}\right)\left(1+\alpha_{12}\frac{[H_2]}{[C_2]+\alpha_{42}[C_6]}\right)\left(1+\alpha_{13}\frac{[H_2]}{[C_2]+\alpha_{43}[C_6]}\right)\left(1+\alpha_{14}\frac{[H_2]}{[C_2]+\alpha_{44}[C_6]}\right)\left(1+\alpha_{15}\frac{[H_2]}{[C_2]+\alpha_{45}[C_6]}\right)$	(3.3.4)
$N_2 = \left(1+\alpha_{32}\frac{[C_6]}{[C_2]}\right)\left(1+\alpha_{11}\frac{[H_2]}{[C_2]+\alpha_{41}[C_6]}\right)\left(1+\alpha_{13}\frac{[H_2]}{[C_2]+\alpha_{43}[C_6]}\right)\left(1+\alpha_{14}\frac{[H_2]}{[C_2]+\alpha_{44}[C_6]}\right)\left(1+\alpha_{15}\frac{[H_2]}{[C_2]+\alpha_{45}[C_6]}\right)$	(3.3.5)
$N_3 = \left(\alpha_{23} + \alpha_{33}\frac{[C_6]}{[C_2]}\right)\left(1+\alpha_{11}\frac{[H_2]}{[C_2]+\alpha_{41}[C_6]}\right)\left(1+\alpha_{12}\frac{[H_2]}{[C_2]+\alpha_{42}[C_6]}\right)\left(1+\alpha_{14}\frac{[H_2]}{[C_2]+\alpha_{44}[C_6]}\right)\left(1+\alpha_{15}\frac{[H_2]}{[C_2]+\alpha_{45}[C_6]}\right)$	(3.3.6)
$N_4 = \left(\alpha_{24} + \alpha_{34}\frac{[C_6]}{[C_2]}\right)\left(1+\alpha_{11}\frac{[H_2]}{[C_2]+\alpha_{41}[C_6]}\right)\left(1+\alpha_{12}\frac{[H_2]}{[C_2]+\alpha_{42}[C_6]}\right)\left(1+\alpha_{13}\frac{[H_2]}{[C_2]+\alpha_{43}[C_6]}\right)\left(1+\alpha_{15}\frac{[H_2]}{[C_2]+\alpha_{45}[C_6]}\right)$	(3.3.7)
$N_5 = \left(\alpha_{25} + \alpha_{35}\frac{[C_6]}{[C_2]}\right)\left(1+\alpha_{11}\frac{[H_2]}{[C_2]+\alpha_{41}[C_6]}\right)\left(1+\alpha_{12}\frac{[H_2]}{[C_2]+\alpha_{42}[C_6]}\right)\left(1+\alpha_{13}\frac{[H_2]}{[C_2]+\alpha_{43}[C_6]}\right)\left(1+\alpha_{14}\frac{[H_2]}{[C_2]+\alpha_{44}[C_6]}\right)$	(3.3.8)
$f_j = \frac{1}{1+\frac{\alpha_{2j}}{\alpha_{3j}}\frac{1}{\frac{[C_6]}{[C_2]}}}$	(3.3.9)

In addition to predicting MWD, predictions of hexene content in the copolymer can also be made using the simplified model without using any additional parameters. The mole fraction of hexene in the copolymer produced by site *j* is:

$$f_j = \frac{R_{pj}^C}{R_{pj}} = \frac{k_{pj}^C [\mathrm{C}_6] Y_j}{k_{pj}^C [\mathrm{C}_6] Y_j + k_{pj}^E [\mathrm{C}_2] Y_j} \tag{3.14}$$

which simplifies to the following expression:

$$f_j = \frac{1}{1 + \frac{k_{pj}^E}{k_{pj}^C} \frac{1}{\frac{[\mathrm{C}_6]}{[\mathrm{C}_2]}}} \tag{3.15}$$

which relates hexene incorporation in the copolymer the $[C_6]$ to $[C_2]$ ratio in the gas phase. Equation 3.15 can be parameterised using the parameters α_{2j} and α_{3j}, as defined in Table 3.2, to give Equation 3.3.9 in Table 3.3.

$$\frac{\alpha_{2j}}{\alpha_{3j}} = \frac{k_{pj}^E \beta_j}{k_{p2}^E} \cdot \frac{k_{p2}^E}{k_{pj}^C \beta_j} = \frac{k_{pj}^E}{k_{pj}^C} \tag{3.16}$$

Parameter Estimation

From the deconvolution analysis,[3.14] values for τ_j and m_j were obtained from the eight HDPE samples produced at a common temperature. The comonomer content of the samples was calculated from density measurements using an empirical industrial correlation specific to the catalyst. To obtain initial estimates of the model parameters, the parameters were fitted using the τ_j, and m_j deconvolution results (and the comonomer incorporation values) as response variables. The *K* parameters (appearing in Equation 3.3.1) were fitted using the τ values. The α parameters (appearing in Equations 3.3.3-3.3.9) were fitted using the *m* values and the comonomer incorporation *f*. To ensure that the parameter estimates were physically realistic, they were

constrained to positive values. The resulting estimates of the K parameters (obtained by linear regression) are shown in Table 3.4. Unfortunately, none of these parameter estimates are statistically significantly different from zero at the 95% confidence level, and therefore they may be unreliable as initial guesses for future model development. Further model simplification was used to reduce the number of parameters and to obtain the estimates in Table 3.5. The bold parameter values shown in the table are statistically significant.

Table 3.4 Parameter estimates obtained using standard linear least-squares regression.

Parameter	Site 1	Site 2	Site 3	Site 4	Site 5
K_{1j}	0.00777	0.00092	0.00021	0	0
K_{2j}	0	0	0.00019	0.00013	0.00029
K_{3j}	0.00427	0.00106	0.00050	0.00022	0.00007
K_{4j}	0	0.00126	0.00078	0.00054	0.00034

Not all of the ordinary least-squares regression assumptions are satisfied in this situation. Specifically, the assumption that there is no error in the input variables is not satisfied. An error-in-variables approach[3.40] could be used to address this problem if one wished to obtain the best possible results. However, since the goal of this work is to obtain initial parameter guesses it is not necessary to add the additional complexity of using an error-in-variables approach.

Kissin[3.20] showed, for a similar Z-N catalyst, that chain transfer to hexene is not an important reaction. It seems hexene increases melt index (and hence reduces average molecular weight) in industrial reactors, because it causes relatively more polymer to be produced at low-molecular-weight sites than at high-molecular-weight sites.[3.14] To simplify the model by removing chain-transfer-to-hexene reactions, the K_{2j} parameters (defined in Equation 3.2.2) were

set to zero and the other parameters were re-estimated. This still did not result in significant parameter estimates. Our reaction scheme (Scheme 1) contains both chain transfer to ethylene and β-hydride elimination. Since β-hydride elimination is a more important chain-stopping mechanism than chain transfer to monomer, the K_{3j} parameters (defined in Equation 3.2.3) were also set to zero. In addition, a common K_4 parameter which accounts for β-hydride elimination (and chain transfer to impurities as well as cocatalyst) was used for all sites. The parameters were re-estimated (see first column of estimates in Table 3.5). Only two of the parameters were significantly different from zero.

An important problem associated with using the deconvolution parameters τ_j as response variables for estimating the K parameters is that there is a large amount of uncertainty and correlation among the τ_j estimates. Unfortunately, standard linear regression does not take this situation into account. Fortunately, however, information about the uncertainty and the correlations is available in the covariance matrix for the τ_j estimates obtained by deconvolution.[3.14] To properly account for the covariance information, a generalized least-squares estimation[3.41] was conducted using the covariance matrices of the τ_j's from the deconvolutions. The resulting parameter estimates are shown in the second column of Table 3.5. Note that K_{15} tended to become negative (indicating that chain transfer to hydrogen is very slow at the highest-molecular-weight site) and was constrained at zero. We are pleased that the parameter estimates are physically realistic.

Table 3.5 Parameter estimates for K_{ij} and $K_4$with K_{2j}, K_{3j} and K_{15} set to zero. **Bold** parameter values are statistically significant at the 95% confidence level.

Parameter	Standard Least-Squares Estimation	Generalized Least-Squares Estimation
K_{11}	**0.01579**	**0.01489**
K_{12}	**0.00284**	**0.00303**
K_{13}	0.00089	**0.00115**
K_{14}	0.000064	**0.00034**
K_{15}	0	0
K_4	0.00208	**0.00092**

The mass-fraction parameters were estimated using m_j values and the comonomer content, f, as response variables. Unfortunately, when we attempted to estimate the α parameters defined in Table 3.2, none of the estimated parameters were significantly different from zero. We opted to further simplify the model to reduce the number of parameters. We assumed that ratio of the rate of propagation with ethylene to the rate of reinitiation with ethylene (see Scheme 1) is the same at the two low-molecular-weight sites, so that $\theta_L = k_{p1}^E / k_{i1}^E = k_{p2}^E / k_{i2}^E$. We also made a similar assumption for the three high-molecular-weight sites, so that $\theta_H = k_{p3}^E / k_{i3}^E = k_{p4}^E / k_{i4}^E = k_{p5}^E / k_{i5}^E$. Because Kissin[3.20] found that reinitiation reactions with hexene are important at low-molecular-weight sites, but not at high-molecular-weight sites, we also assumed that $\alpha_{43} = \alpha_{44} = \alpha_{45} = 0$ and that $\alpha_{41} = \alpha_{42} = \alpha_4$. The simplified model equations using these assumptions about the parameters are shown in Table 3.6. Note that the equations in Table 3.6 include the parameter K_{1j} because $\alpha_{1j} = \theta_j K_{1j}$. The generalized-least-

squares estimates of K_{1j} (obtained from the τ_j responses) were used directly in the mass fraction part of the model and were not re-estimated. The simplifying assumptions reduced the number of mass-fraction-related parameters from 19 to 12.

Table 3.6 Simplified mass fraction numerators.

$N_1 = \left(\alpha_{21} + \alpha_{31}\frac{[C_6]}{[C_2]}\right)\left(1+\theta_L K_{12}\frac{[H_2]}{[C_2]+\alpha_4[C_6]}\right)\left(1+\theta_H K_{13}\frac{[H_2]}{[C_2]}\right)\left(1+\theta_H K_{14}\frac{[H_2]}{[C_2]}\right)\left(1+\theta_H K_{15}\frac{[H_2]}{[C_2]}\right)$	(3.6.1)
$N_2 = \left(1+\alpha_{32}\frac{[C_6]}{[C_2]}\right)\left(1+\theta_L K_{11}\frac{[H_2]}{[C_2]+\alpha_4[C_6]}\right)\left(1+\theta_H K_{13}\frac{[H_2]}{[C_2]}\right)\left(1+\theta_H K_{14}\frac{[H_2]}{[C_2]}\right)\left(1+\theta_H K_{15}\frac{[H_2]}{[C_2]}\right)$	(3.6.2)
$N_3 = \left(\alpha_{23} + \alpha_{33}\frac{[C_6]}{[C_2]}\right)\left(1+\theta_L K_{11}\frac{[H_2]}{[C_2]+\alpha_4[C_6]}\right)\left(1+\theta_L K_{12}\frac{[H_2]}{[C_2]+\alpha_4[C_6]}\right)\left(1+\theta_H K_{14}\frac{[H_2]}{[C_2]}\right)\left(1+\theta_H K_{15}\frac{[H_2]}{[C_2]}\right)$	(3.6.3)
$N_4 = \left(\alpha_{24} + \alpha_{34}\frac{[C_6]}{[C_2]}\right)\left(1+\theta_L K_{11}\frac{[H_2]}{[C_2]+\alpha_4[C_6]}\right)\left(1+\theta_L K_{12}\frac{[H_2]}{[C_2]+\alpha_4[C_6]}\right)\left(1+\theta_H K_{13}\frac{[H_2]}{[C_2]}\right)\left(1+\theta_H K_{15}\frac{[H_2]}{[C_2]}\right)$	(3.6.4)
$N_5 = \left(\alpha_{25} + \alpha_{35}\frac{[C_6]}{[C_2]}\right)\left(1+\theta_L K_{11}\frac{[H_2]}{[C_2]+\alpha_4[C_6]}\right)\left(1+\theta_L K_{12}\frac{[H_2]}{[C_2]+\alpha_4[C_6]}\right)\left(1+\theta_H K_{13}\frac{[H_2]}{[C_2]}\right)\left(1+\theta_H K_{14}\frac{[H_2]}{[C_2]}\right)$	(3.6.5)

The mass-fraction-related parameters were re-estimated using two different methods:[3.41] weighted non-linear least-squares and generalized nonlinear least-squares. Weighted nonlinear least-squares regression accounts for the different levels of variability in the m_j and f response variables, but doesn't take into account covariances between the responses. The required variance estimates for the m_j and f responses were obtained by pooling information from the two sets of replicate MWDs (see Figure 3.2 and Figure 3.4). Generalized nonlinear least-squares regression accounts for the covariance among the m_j responses (obtained from deconvolution) and for the variance of the f responses (from replicates). Parameter estimates obtained using both weighted nonlinear least squares and generalized nonlinear least squares are shown in Table 3.7.

We are satisfied that the estimates are physically realistic, and we prefer the estimates obtained by generalized least squares because they account for the covariance matrix of the response variables. A correlation matrix for the parameter estimates obtained by generalized nonlinear regression is shown in Table 3.8. Many of the parameter estimates are highly correlated, particularly the α_{3j} and α_4 parameters, which account for propagation with hexene and reinitiation of low-molecular-weight sites by hexene.

Table 3.7 Parameter estimates for the simplified model in Table 3.6. **Bold** parameter values are statistically significant at the 95% confidence level.

Parameter	Weighted Non-linear Regression	Generalized Non-linear Regression
θ_L	**521.94**	**1325.75**
θ_H	**4882.61**	**3222.25**
α_{21}	**0.2849**	**0.4755**
α_{23}	**3.1525**	**1.9492**
α_{24}	**0.3514**	**0.3370**
α_{25}	**0.0998**	**0.0579**
α_{31}	**0.5560**	**0.8403**
α_{32}	$2.37*10^{-14}$	**0.0337**
α_{33}	**0.0579**	$4.06*10^{-13}$
α_{34}	$5.52*10^{-14}$	$1.73*10^{-9}$
α_{35}	$2.60*10^{-14}$	$7.33*10^{-7}$
α_4	**86.0593**	**49.0607**

Table 3.8 Correlation of parameter estimates. Correlations with magnitude larger than 0.7 are in **bold**.

	θ_L	θ_H	α_{21}	α_{23}	α_{24}	α_{25}	α_{31}	α_{32}	α_{33}	α_{34}	α_{35}	α_4
θ_L	**1**	0.53	**0.96**	**-0.73**	-0.64	-0.08	**0.79**	**0.85**	**0.86**	**-0.93**	**0.98**	**0.72**
θ_H	0.53	1	0.37	0.15	-0.27	-0.41	0.01	0.04	**0.87**	**-0.80**	0.68	**0.89**
α_{21}	**0.96**	0.37	1	**-0.81**	-0.48	0.18	**0.92**	**0.94**	**0.73**	**-0.83**	**0.92**	0.57
α_{23}	**-0.73**	0.15	**-0.81**	1	0.60	-0.18	**-0.86**	**-0.95**	-0.29	0.45	-0.60	-0.05
α_{24}	-0.64	-0.27	-0.48	0.60	1	0.63	-0.27	-0.50	-0.52	0.60	-0.59	-0.35
α_{25}	-0.08	-0.41	0.18	-0.18	0.63	1	0.47	0.28	-0.34	0.28	-0.13	-0.36
α_{31}	**0.79**	0.01	**0.92**	**-0.86**	-0.27	0.47	1	**0.96**	0.43	-0.55	**0.70**	0.28
α_{32}	**0.85**	0.04	**0.94**	**-0.95**	-0.50	0.28	**0.96**	1	0.47	-0.61	**0.75**	0.27
α_{33}	**0.86**	**0.87**	**0.73**	-0.29	-0.52	-0.34	0.43	0.47	1	**-0.98**	**0.93**	**0.96**
α_{34}	**-0.93**	**-0.80**	**-0.83**	0.45	0.60	0.28	-0.55	-0.61	**-0.98**	1	**-0.98**	**-0.89**
α_{35}	**0.98**	0.68	**0.92**	-0.60	-0.59	-0.13	**0.70**	**0.75**	**0.93**	**-0.98**	1	**0.81**
α_4	**0.72**	**0.89**	0.57	-0.05	-0.35	-0.36	0.28	0.27	**0.96**	**-0.89**	**0.81**	1

Using the generalized-least-squares values from Table 3.5 and Table 3.7, MWDs were predicted at the operating conditions shown in Figure 3.2. Figure 3.4 shows the fitted curve and the experimental data for the replicate experiments corresponding to point 2 in Figure 3.2. The model does a good job of matching these MWD data. Figure 3.5 compares predicted MWD curves and experimental data for points 1 and 4 from Figure 3.2 (with MI = 1.07 and 9.24, respectively. As expected, the predicted MWD curves shift to the left with increasing melt index (decreasing average molecular weight), but the model predictions are not as good as those in Figure 3.4. Fits to the comonomer incorporation data were very good, as shown in Figure 3.6.

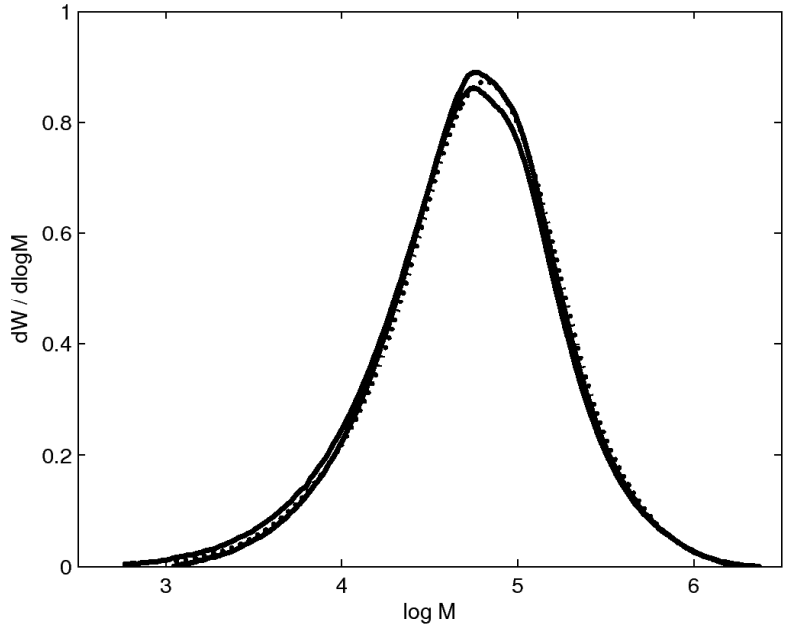

Figure 3.4 MWDs for two replicate runs (condition 2 from Figure 3.2). The solid lines are measured MWDs for the replicate experiments. The dotted line is a prediction obtained using the generalized-least-squares parameter estimates in Tables 3.5 and 3.7.

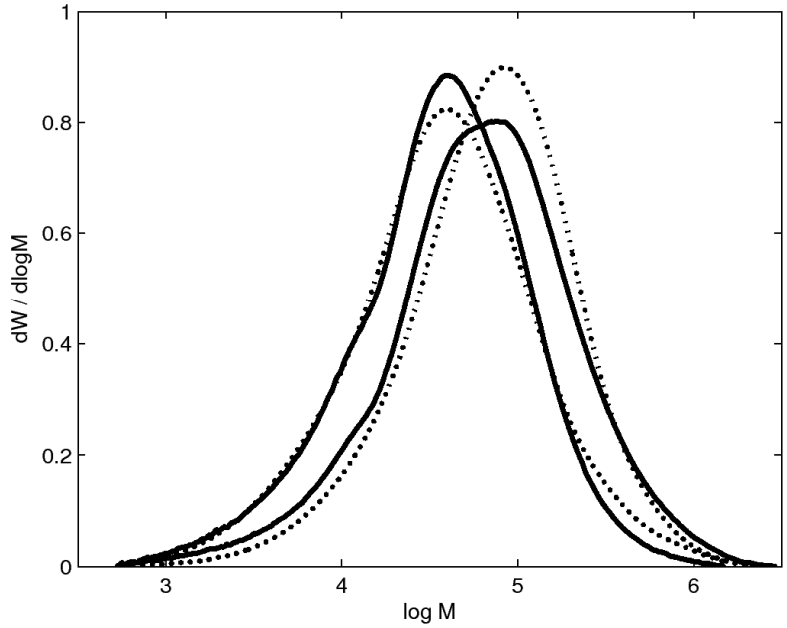

Figure 3.5 Measured and predicted MWDs for melt index values 9.24 and 1.07. The measured MWDs are shown with solid lines and the predictions with dotted lines. The higher melt index MWD is on the left, and corresponds to point 1 from Figure 3.2, the lower melt index MWD (point 4 from Figure 3.2) is on the right.

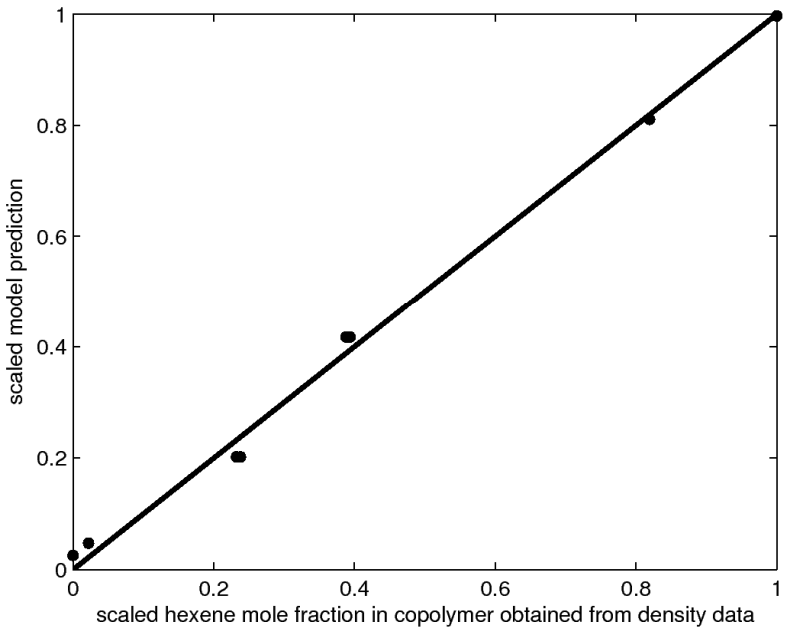

Figure 3.6 Comparison of comonomer content predicted using Equation 3.3.9 with comonomer content obtained from density data.

To investigate whether the parameter estimates in Tables 3.5 and 3.7 provide reasonable predictions for conditions not encountered in the data set, simulated results were generated when the hydrogen-to-ethylene and hexene-to-ethylene gas-concentration ratios were tripled, as shown in Figure 3.7 and Figure 3.8, respectively. In Figure 3.7, the predicted MWD shifts to the left when higher hydrogen concentrations are used, as would be expected. In Figure 3.8, relatively more copolymer is produced at sites 1 and 2, when higher hexene concentrations are used, causing a slight reduction in average molecular weight. We note that hexene has only a small predicted influence on the MWD, because only very small hexene concentrations are used to make the HDPE samples.

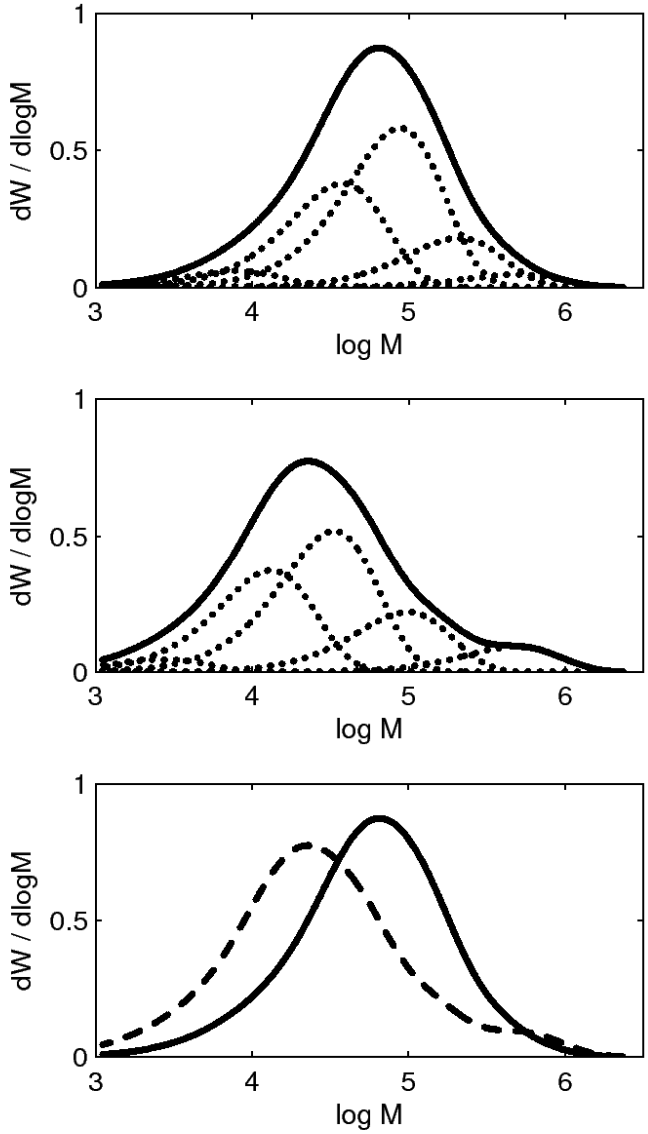

Figure 3.7 The effect of increasing the hydrogen to ethylene gas concentration ratio by a factor of 3. The top plot shows the model predictions at the original operating conditions. Dashed lines are MWDs produced by individual types of active sites. The solid line is the overall MWD. The middle plot shows the predictions at the new conditions. The bottom plot compares the simulated MWD produced using the higher hydrogen-to-ethylene ratio (dashed line) with that produced using the lower original hydrogen-to-ethylene ratio (solid line) produced using conditions labeled 2 on Figure 3.2. The predicted MWD shifts dramatically to the left as the hydrogen-to-ethylene ratio increases.

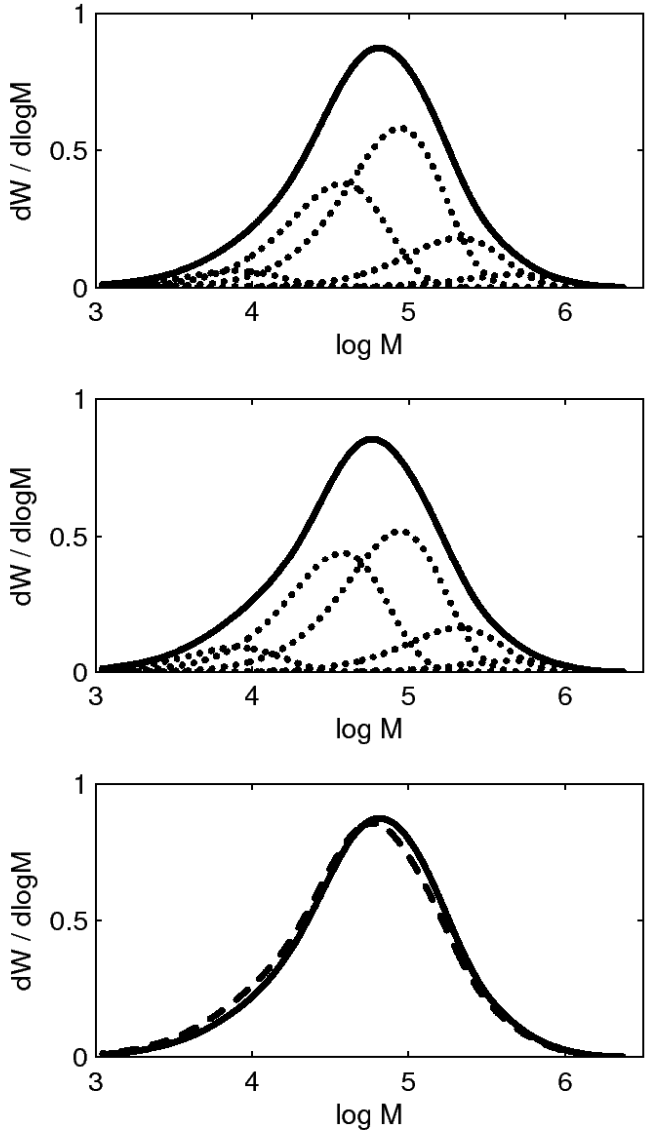

Figure 3.8 The effect of increasing the hexene-to-ethylene gas concentration ratio by a factor of 3. The top plot shows the model predictions at the original operating conditions. Dashed lines are MWDs produced by individual types of active sites. The solid line is the overall MWD. The middle plot shows the predictions at the new conditions. The bottom plot compares the simulated MWD produced using the higher hexene-to-ethylene ratio (dashed line) with that produced using the lower original hexene-to-ethylene ratio (solid line) produced using conditions labeled 2 on Figure 3.2. The predicted mass fraction of polymer produced at sites 1 and 2 are larger at slightly higher hexene concentrations.

These generalized-least-squares parameter estimates in Tables 3.5 and 3.7 seem to be good initial guesses for use in development of a non-isothermal model. We believe that improved parameter estimates might be obtained using the overall MWD curves as the responses, instead of the deconvolution parameters. Using the overall MWD curves will eliminate concerns about the uncertainty and correlation in the τ_j and m_j values obtained by deconvolution. Nonetheless, initial parameter guesses like those in Tables 3.5 and 3.7 are very important for tackling this type of complex nonlinear regression problem.

3.4 Conclusion

We have developed a simplified steady-state model to predict MWDs of ethylene/hexene copolymers produced using Ziegler-Natta catalysts in gas-phase industrial reactors at a fixed temperature. The simplified reaction scheme and sharing of rate constants between sites reduces the number of parameters that need to be estimated from approximately 100 to 18. The model predicts MWDs and comonomer incorporation directly from the gas-phase concentration ratios and ethylene partial pressure.

Comonomer incorporation data and results from MWD deconvolution analysis were used as the response variables for fitting the model parameters. These parameter estimates were obtained using generalized least squares regression, which takes into account covariance among the random errors in the MWD deconvolution responses, as well as different error levels in the comonomer incorporation data and deconvolution data. By simplifying the reaction scheme, it was possible to obtain statistically significant estimates for most of the parameters. Predictions using these parameter estimates show model behaviour that is consistent with expectations. We plan to further refine the parameter estimates using the overall MWD curves, instead of the

deconvolution parameters, as response variables. The parameter estimates that we have obtained will provide useful initial parameter guesses for use in development of a more complex non-isothermal model.

3.5 Acknowledgments

The authors wish to thank INEOS Technologies and Queen's University for their financial support and INEOS Technologies for supplying experimental data.

3.6 Notation

$[H_2]$	gas phase hydrogen concentration	bars
$[C_2]$	gas phase ethylene concentration	bars
$[C_6]$	gas phase hexene concentration	bars
$[I]$	gas phase impurities concentration	bars
α_{1j}	lumped parameter, ratio relating chain transfer to hydrogen to reinitiation with ethylene at site j	
α_{2j}	lumped parameter, ratio relating propagation with ethylene at site j to propagation with ethylene at site 2	
α_{3j}	lumped parameter, ratio relating propagation with hexene at site j to propagation with ethylene at site 2	
α_{4j}	lumped parameter, ratio relating reinitiation with hexene to reinitiation with ethylene at site j	
β_j	ratio of potential sites of type j to potential sites of type 1	
f_j	hexene mole fraction incorporated by site j	
K_{1j}	lumped parameter, ratio relating chain transfer to hydrogen to propagation with ethylene at site j	
K_{2j}	lumped parameter, ratio relating chain transfer to hexene to propagation with ethylene at site j	

K_{3j}	lumped parameter, ratio relating chain transfer to ethylene to propagation with ethylene at site *j*	
K_{4j}	lumped parameter, ratio relating spontaneous chain transfer and chain transfer to impurities to propagation with ethylene at site *j*	bars
k_{ij}^{E}	kinetic rate constant for reinitiation with ethylene at site *j*	$bars^{-1}\ s^{-1}$
k_{ij}^{C}	kinetic rate constant for reinitiation with hexene at site *j*	$bars^{-1}\ s^{-1}$
k_{pj}^{E}	kinetic rate constant for propagation with ethylene at site *j*	$bars^{-1}\ s^{-1}$
k_{pj}^{C}	kinetic rate constant for propagation with hexene at site *j*	$bars^{-1}\ s^{-1}$
k_{tj}^{H}	kinetic rate constant for chain transfer to hydrogen at site *j*	$bars^{-1}\ s^{-1}$
k_{tj}^{E}	kinetic rate constant for chain transfer to ethylene at site *j*	$bars^{-1}\ s^{-1}$
k_{tj}^{C}	kinetic rate constant for chain transfer to hexene at site *j*	$bars^{-1}\ s^{-1}$
k_{tj}^{β}	kinetic rate constant for spontaneous chain transfer at site *j*	s^{-1}
k_{tj}^{I}	kinetic rate constant for chain transfer to impurities at site *j*	$bars^{-1}\ s^{-1}$
m_j	mass fraction of polymer produced at site *j*	
R_{tj}	Rate of termination at site *j*	$bars\ s^{-1}$
R_{pj}	Rate of propagation at site *j*	$bars\ s^{-1}$
r	chain length	
θ_L	ratio of kinetic rate constants for propagation with ethylene and reinitiation with ethylene for sites 1 and 2	
θ_H	ratio of kinetic rate constants for propagation with ethylene and reinitiation with ethylene for sites 3, 4, and 5	
τ_j	inverse number-average molecular weight of site *j*	
$Y_{j,n}$	growing polymer chain of length *n* at site of type *j*	
Y_{jD}	temporarily dormant site of type *j*	

3.7 References

[3.1] J. Bicerano, "*Prediction of Polymer Properties, 2nd ed.*", Marcel Dekker Inc., New York 1996.

[3.2] A. B. de Carvalho, P. E. Gloor, A. E. Hamielec, *Polymer*, **1989**, *30*, 280.

[3.3] J. Villermaux, P. Lorenzini, P. Bertrand, J. Greffe, "Modelling of Polymerization of Ethylene by Ziegler-Natta Catalysis", in: *Polymer Reaction Engineering: Proceedings of the Third Berlin International Workshop on Polymer Reaction Engineering*, K.-H. Reichert, W. Geiseler, Eds, VCH Publishers, New York, **1989**, p. 350.

[3.4] P. Lorenzini, P. Bertrand, J. Villermaux, *Can. J. Chem. Eng.*, **1991**, *69*, 682.

[3.5] K. B. McAuley, J. F. MacGregor, A. E. Hamielec, *AIChE J.*, **1990**, *36* (6), 837.

[3.6] T. Xie, K. B. McAuley, J. C. C. Hsu, D. W. Bacon, *AIChE J.*, **1995**, *41* (5), 1251.

[3.7] E. J. Nagel, V. A. Kirllov, W. H. Ray, *Ind. Eng. Chem. Prod. Res. Dev.*, **1980**, *19*, 372.

[3.8] G. Dompazis, V. Kanellopoulos, C. Kiparissides, *Macromol. Mater. Eng.*, **2005**, *290*, 525.

[3.9] A. Latado, M. Embirucu, A.G. M. Neto, J. C. Pinto, *Polym. Test.*, **2001**, *20*, 419.

[3.10] Y. V. Kissin, T. E. Nowlin, R. I. Mink, *Macromolecules*, **1993**, *26*, 2151.

[3.11] Y. V. Kissin, *Makromol. Chem.-M. Symp.*, **1993**, *66*, 83.

[3.12] Y. V. Kissin, "Isospecific Polymerization of Olefins with Heterogeneous Ziegler-Natta Catalysts", Springer-Verlag Inc., New York 1985.

[3.13] J. B. P. Soares, A. E. Hamielec, *Polymer*, **1995**, *36* (11), 2257.

[3.14] D. E. Thompson, K. B. McAuley, P. J. McLellan, *Macromol. React. Eng.*, **2007**, *1*, 264.

[3.15] Y. V. Kissin, *J. Polym. Sci., Part A: Pol. Chem.*, **2001**, *39*, 1681.

[3.16] N. P. Khare, K. C. Seavey, Y. A. Liu, S. Ramanathan, S. Lingard, C.-C. Chen, *Ind. Eng. Chem. Res.*, **2002**, *41*, 5601.

[3.17] J. B. P. Soares, R. F. Abbott, J. N. Willis, X. Liu, *Macromol. Chem. Phys.*, **1996**, *197*, 3383.

[3.18] V. Matos, A. G. Mattos Neto, J. C. Pinto, *J. Appl. Polym. Sci.*, **2001**, *79*, 2076.

[3.19] Z.-Q. Fan, L.-X. Feng, S.-L. Yang, *J. Polym. Sci., Part A: Pol. Chem.*, **1996**, *34*, 3329.

[3.20] Y. V. Kissin, R. I. Mink, T. E. Nowlin, *J. Polym. Sci., Part A: Pol. Chem.*, **1999**, *37*, 4255.

[3.21] R. Galvan, M. Tirrell, *Chem. Eng. Sci.*, **1986**, *41* (9), 2385.

[3.22] J. B. P. Soares, A. E. Hamielec, *Polym. React. Eng.*, **1995**, *3* (3), 261.

[3.23] R. A. Hutchinson, C. M. Chen, W. H. Ray, *J. Appl. Polym. Sci.*, **1992**, *44*, 1389.

[3.24] S. Floyd, K. Y. Choi, T. W. Taylor, W. H. Ray, *J. Appl. Polym. Sci.*, **1986**, *32*, 2935.

[3.25] B. M. Shaw, K. B. McAuley, D. W. Bacon, *Polym. React. Eng.*, **1998**, *6* (2), 113.

[3.26] K. Y. Choi, S. Tang, A. Sirohi, *Ind. Eng. Chem. Res.*, **1997**, *36*, 1095.

[3.27] M. Hamba, G. C. Han-Adebekun, W. H. Ray, *J. Polym. Sci., Part A: Pol. Chem.*, **1997**, *35*, 2075.

[3.28] Z. G. Xu, S. Chakravarti, W. H. Ray, *J. Appl. Polym. Sci.*, **2001**, *80*, 81.

[3.29] A. G. Mattos Neto, M. F. Freitas, M. Nele, J. C. Pinto, *Ind. Eng. Chem. Res.*, **2005**, *44*, 2697.

[3.30] G. B. Meier, G. Weickert, W. P. M. van Swaaij, *J. Polym. Sci., Part A: Pol. Chem.*, **2001**, *39*, 500.

[3.31] J. J. C. Samson, B. van Middelkoop, G. Weickert, K. R. Westerterp, *AIChE J.*, **1999**, *45* (7), 1548.

[3.32] M. R. Pourhossaini, E. Vasheghani-Farahani, M. Gholamian, M. Gholamian, *J. Appl. Polym. Sci.*, **2006**, *100*, 3101.

[3.33] L. D'Agnillo, J. B. P. Soares, G. H. J. van Doremaele, *Macromol. Mater. Eng.*, **2005**, *290*, 256.

[3.34] S. Chakravarti, W. H. Ray, S. X. Zhang, *J. Appl. Polym. Sci.*, **2001**, *81*, 1451.

[3.35] V. Matos, A. G. Mattos Neto, M. Nele, J. C. Pinto, *J. Appl. Polym. Sci.*, **2002**, *86*, 3226.

[3.36] N. P. Khare, B. Lucas, K. C. Seavey, Y. A. Liu, A. Sirohi, S. Ramanathan, S. Lingard, Y. Song, C. C. Chen, *Ind. Eng. Chem. Res.*, **2004**, *43*, 884.

[3.37] B. Kou, K. B. McAuley, C. C. Hsu, K. Z. Yao, *Ind. Eng. Chem. Res.*, **2005**, *44*, 2428.

[3.38] B. Kou, K. B. McAuley, C. C. Hsu, D. W. Bacon, K. Z. Yao, *Ind. Eng. Chem. Res.*, **2005**, *44*, 2443.

[3.39] J. C. J. F. Tacx, H. N. Linssen, A. L. German, *J. Polym. Sci., Part A: Pol. Chem.*, **1988**, *26*, 61.

[3.40] J. J. Jitjareonchai, P. M. Reilly, T. A. Duever, D. B. Chambers, *Can. J. Chem. Eng.*, **2006**, *84*, 125.

[3.41] G. A. Seber, C. J. Wild, "*Nonlinear Regression*" John Wiley & Sons, New York 1989.

Chapter 4

Parameter Estimation in a Simplified Molecular Weight Distribution Model for HDPE Produced by Ziegler-Natta Catalyst

Duncan E. Thompson, Kim B. McAuley*, and P. James McLellan

Department of Chemical Engineering, Queen's University, Kingston, ON, K7L 3N6, Canada

Fax: 1-613-533-6637 Email: kim.mcauley@chee.queensu.ca

Keywords: Parameter estimation, modeling, Ziegler-Natta polymerization, molecular weight distribution, identifiability

4.1 Summary

A simplified steady-state model to predict molecular weight distributions of ethylene-butene and ethylene-hexene copolymers produced industrially using heterogeneous Ziegler-Natta (Z-N) catalysts is developed. Estimability analysis is used to guide model simplification and to determine which parameters can be estimated using the available data. Scaling of response variables and parameters using information about their uncertainties ensures that appropriate results are obtained from the estimability analysis. Parameter estimates are obtained to provide good predictions of the measured molecular weight distributions. Although the parameter values obtained are specific to the Z-N catalyst of our industrial sponsor, the methodology should be useful for parameter estimation and model simplification in other catalytic polymerization systems.

This work has been accepted for publication in *Macromolecular Reaction Engineering*.

4.2 Introduction

Engineers want to predict end-use properties of polyolefins from reactor operating conditions so that they can optimize reactor operations and design new products. In our previous work,[4.1] we developed a simplified mathematical model to predict molecular weight distributions (MWDs) of ethylene-hexene copolymers, and used industrial data to obtain parameter estimates. This simplified model predicts MWD from reactor operating conditions (hydrogen concentration, ethylene partial pressure, hexene concentration) but does not account for temperature effects. In this work we include temperature effects, and we extend the model to include both butene and hexene comonomers. Many end-use properties of high density polyethylene (HDPE), such as tensile strength, impact strength, melting point, and Young's modulus, are influenced by the MWD. The model proposed in this paper predicts MWD, and can be used in combination with other models[4.2] to predict end-use properties from reactor operating conditions.

The extended non-isothermal model has many more parameters than the original isothermal model,[4.1] and not all of these parameters can be readily estimated using the available industrial data set.[4.3] Estimability analysis[4.4-4.6] is used to determine which parameters can be estimated from the available data. The unestimable parameters are either left at their initial guesses, or are removed from the model by further simplification. In deciding which parameters can be estimated, the estimability analysis technique accounts for the model structure, for correlated effects of model parameters, and for the level of uncertainty in each of the initial parameter guesses. The algorithm produces a list of model parameters, ranked from most to least estimable. A revised version of the estimability algorithm, which was originally described by Yao et al.[4.6] and by Kou et al.[4.4], is provided in the Appendix 4.10. Recently, Lund and Foss[4.7]

presented a similar parameter-ranking technique that produces equivalent results to those from the method of Kou et al., using more computationally complex calculations.

This paper begins by describing the extension of the original isothermal copolymerization model to account for butene incorporation and for temperature effects. Next, the estimability ranking is determined. Some inestimable parameters are removed from the model by assuming similar reaction rates (and similar activation energies) at different types of catalyst sites. The parameter estimation approach is described and the results are assessed for physical consistency. The final parameter estimates obtained are physically reasonable and will provide a useful starting point for designing new experiments to further improve parameter estimates and model predictions.

4.3 Model Extension

The extended simplified model, which accounts for temperature effects and for incorporation of both butene and hexene comonomers, is shown in Table 4.1.

Table 4.1 Kinetic model equations for predicting MWD.

$$\frac{dW}{d\log_{10} Mw} = m_1\left[r^2 \ln(10)\cdot\tau_1^2\cdot\exp(-\tau_1 r)\right] + m_2\left[r^2 \ln(10)\cdot\tau_2^2\cdot\exp(-\tau_2 r)\right] + m_3\left[r^2 \ln(10)\cdot\tau_3^2\cdot\exp(-\tau_3 r)\right] + m_4\left[r^2 \ln(10)\cdot\tau_4^2\cdot\exp(-\tau_4 r)\right] + m_5\left[r^2 \ln(10)\cdot\tau_5^2\cdot\exp(-\tau_5 r)\right]$$	(4.1.1)
$$\tau_j = \frac{k_{tj0}^H \exp\left(\frac{-E_{tj}^H}{R}\left(\frac{1}{\mathrm{T}}-\frac{1}{T_0}\right)\right)}{k_{pj0}^E \exp\left(\frac{-E_{pj}^E}{R}\left(\frac{1}{\mathrm{T}}-\frac{1}{T_0}\right)\right)}\frac{[\mathrm{H_2}]}{[\mathrm{C_2}]} + \frac{\left(k_{tj}^\beta + k_{tj}^I[\mathrm{I}]\right)}{k_{pj}^E}\frac{1}{[\mathrm{C_2}]}$$	(4.1.2)
$$m_j = \frac{N_j}{\sum_{j=1}^{5} N_j}$$	(4.1.3)

$$N_1=\left(\frac{k^{E}_{p1_0}\exp\left(\frac{-E^{E}_{p1}}{R}\left(\frac{1}{\mathrm{T}}-\frac{1}{T_0}\right)\right)\beta_1}{k^{E}_{p2_0}\exp\left(\frac{-E^{E}_{p2}}{R}\left(\frac{1}{\mathrm{T}}-\frac{1}{T_0}\right)\right)}+\frac{k^{But}_{p1_0}\exp\left(\frac{-E^{But}_{p1}}{R}\left(\frac{1}{\mathrm{T}}-\frac{1}{T_0}\right)\right)\beta_1}{k^{E}_{p2_0}\exp\left(\frac{-E^{E}_{p2}}{R}\left(\frac{1}{\mathrm{T}}-\frac{1}{T_0}\right)\right)}\frac{[\mathrm{C}_4]}{[\mathrm{C}_2]}+\frac{k^{Hex}_{p1_0}\exp\left(\frac{-E^{Hex}_{p1}}{R}\left(\frac{1}{\mathrm{T}}-\frac{1}{T_0}\right)\right)\beta_1}{k^{E}_{p2_0}\exp\left(\frac{-E^{E}_{p2}}{R}\left(\frac{1}{\mathrm{T}}-\frac{1}{T_0}\right)\right)}\frac{[\mathrm{C}_6]}{[\mathrm{C}_2]}\right)$$
$$\left(1+\frac{k^{H}_{t2_0}\exp\left(\frac{-E^{H}_{t2}}{R}\left(\frac{1}{\mathrm{T}}-\frac{1}{T_0}\right)\right)[\mathrm{H}_2]}{k^{E}_{i2_0}\exp\left(\frac{-E^{E}_{ij}}{R}\left(\frac{1}{\mathrm{T}}-\frac{1}{T_0}\right)\right)[\mathrm{C}_2]+k^{But}_{i2_0}\exp\left(\frac{-E^{But}_{i2}}{R}\left(\frac{1}{\mathrm{T}}-\frac{1}{T_0}\right)\right)[\mathrm{C}_4]+k^{Hex}_{i2_0}\exp\left(\frac{-E^{Hex}_{i2}}{R}\left(\frac{1}{\mathrm{T}}-\frac{1}{T_0}\right)\right)[\mathrm{C}_6]}\right)$$
$$\prod_{j=3,4,5}\left(1+\frac{k^{H}_{tj_0}\exp\left(\frac{-E^{H}_{tj}}{R}\left(\frac{1}{\mathrm{T}}-\frac{1}{T_0}\right)\right)[\mathrm{H}_2]}{k^{E}_{ij_0}\exp\left(\frac{-E^{E}_{ij}}{R}\left(\frac{1}{\mathrm{T}}-\frac{1}{T_0}\right)\right)[\mathrm{C}_2]}\right) \qquad (4.1.4)$$

$$N_2=\left(1+\frac{k^{But}_{p2_0}\exp\left(\frac{-E^{But}_{p2}}{R}\left(\frac{1}{\mathrm{T}}-\frac{1}{T_0}\right)\right)}{k^{E}_{p2_0}\exp\left(\frac{-E^{E}_{p2}}{R}\left(\frac{1}{\mathrm{T}}-\frac{1}{T_0}\right)\right)}\frac{[\mathrm{C}_4]}{[\mathrm{C}_2]}+\frac{k^{Hex}_{p2_0}\exp\left(\frac{-E^{Hex}_{p2}}{R}\left(\frac{1}{\mathrm{T}}-\frac{1}{T_0}\right)\right)}{k^{E}_{p2_0}\exp\left(\frac{-E^{E}_{p2}}{R}\left(\frac{1}{\mathrm{T}}-\frac{1}{T_0}\right)\right)}\frac{[\mathrm{C}_6]}{[\mathrm{C}_2]}\right)$$
$$\left(1+\frac{k^{H}_{t1_0}\exp\left(\frac{-E^{H}_{t1}}{R}\left(\frac{1}{\mathrm{T}}-\frac{1}{T_0}\right)\right)[\mathrm{H}_2]}{k^{E}_{i1_0}\exp\left(\frac{-E^{E}_{i1}}{R}\left(\frac{1}{\mathrm{T}}-\frac{1}{T_0}\right)\right)[\mathrm{C}_2]+k^{But}_{i1_0}\exp\left(\frac{-E^{But}_{i1}}{R}\left(\frac{1}{\mathrm{T}}-\frac{1}{T_0}\right)\right)[\mathrm{C}_4]+k^{Hex}_{i1_0}\exp\left(\frac{-E^{Hex}_{i1}}{R}\left(\frac{1}{\mathrm{T}}-\frac{1}{T_0}\right)\right)[\mathrm{C}_6]}\right)$$
$$\prod_{j=3,4,5}\left(1+\frac{k^{H}_{tj_0}\exp\left(\frac{-E^{H}_{tj}}{R}\left(\frac{1}{\mathrm{T}}-\frac{1}{T_0}\right)\right)[\mathrm{H}_2]}{k^{E}_{ij_0}\exp\left(\frac{-E^{E}_{ij}}{R}\left(\frac{1}{\mathrm{T}}-\frac{1}{T_0}\right)\right)[\mathrm{C}_2]}\right) \qquad (4.1.5)$$

$$N_3=\left(\frac{k^{E}_{p3_0}\exp\left(\frac{-E^{E}_{p3}}{R}\left(\frac{1}{\mathrm{T}}-\frac{1}{T_0}\right)\right)\beta_3}{k^{E}_{p2_0}\exp\left(\frac{-E^{E}_{p2}}{R}\left(\frac{1}{\mathrm{T}}-\frac{1}{T_0}\right)\right)}+\frac{k^{But}_{p3_0}\exp\left(\frac{-E^{But}_{p3}}{R}\left(\frac{1}{\mathrm{T}}-\frac{1}{T_0}\right)\right)\beta_3}{k^{E}_{p2_0}\exp\left(\frac{-E^{E}_{p2}}{R}\left(\frac{1}{\mathrm{T}}-\frac{1}{T_0}\right)\right)}\frac{[\mathrm{C}_4]}{[\mathrm{C}_2]}+\frac{k^{Hex}_{p3_0}\exp\left(\frac{-E^{Hex}_{p3}}{R}\left(\frac{1}{\mathrm{T}}-\frac{1}{T_0}\right)\right)\beta_3}{k^{E}_{p2_0}\exp\left(\frac{-E^{E}_{p2}}{R}\left(\frac{1}{\mathrm{T}}-\frac{1}{T_0}\right)\right)}\frac{[\mathrm{C}_6]}{[\mathrm{C}_2]}\right)$$
$$\prod_{j=1,2}\left(1+\frac{k^{H}_{tj_0}\exp\left(\frac{-E^{H}_{tj}}{R}\left(\frac{1}{\mathrm{T}}-\frac{1}{T_0}\right)\right)[\mathrm{H}_2]}{k^{E}_{ij_0}\exp\left(\frac{-E^{E}_{ij}}{R}\left(\frac{1}{\mathrm{T}}-\frac{1}{T_0}\right)\right)[\mathrm{C}_2]+k^{But}_{ij_0}\exp\left(\frac{-E^{But}_{ij}}{R}\left(\frac{1}{\mathrm{T}}-\frac{1}{T_0}\right)\right)[\mathrm{C}_4]+k^{Hex}_{ij_0}\exp\left(\frac{-E^{Hex}_{ij}}{R}\left(\frac{1}{\mathrm{T}}-\frac{1}{T_0}\right)\right)[\mathrm{C}_6]}\right)$$
$$\prod_{j=4,5}\left(1+\frac{k^{H}_{tj_0}\exp\left(\frac{-E^{H}_{tj}}{R}\left(\frac{1}{\mathrm{T}}-\frac{1}{T_0}\right)\right)[\mathrm{H}_2]}{k^{E}_{ij_0}\exp\left(\frac{-E^{E}_{ij}}{R}\left(\frac{1}{\mathrm{T}}-\frac{1}{T_0}\right)\right)[\mathrm{C}_2]}\right) \qquad (4.1.6)$$

$$N_4 = \left(\frac{k_{p4_0}^E \exp\left(\frac{-E_{p4}^E}{R}\left(\frac{1}{\mathrm{T}}-\frac{1}{T_0}\right)\right)\beta_4}{k_{p2_0}^E \exp\left(\frac{-E_{p2}^E}{R}\left(\frac{1}{\mathrm{T}}-\frac{1}{T_0}\right)\right)} + \frac{k_{p4_0}^{But} \exp\left(\frac{-E_{p4}^{But}}{R}\left(\frac{1}{\mathrm{T}}-\frac{1}{T_0}\right)\right)\beta_4}{k_{p2_0}^E \exp\left(\frac{-E_{p2}^E}{R}\left(\frac{1}{\mathrm{T}}-\frac{1}{T_0}\right)\right)} \frac{[\mathrm{C}_4]}{[\mathrm{C}_2]} + \frac{k_{p4_0}^{Hex} \exp\left(\frac{-E_{p4}^{Hex}}{R}\left(\frac{1}{\mathrm{T}}-\frac{1}{T_0}\right)\right)\beta_4}{k_{p2_0}^E \exp\left(\frac{-E_{p2}^E}{R}\left(\frac{1}{\mathrm{T}}-\frac{1}{T_0}\right)\right)} \frac{[\mathrm{C}_6]}{[\mathrm{C}_2]} \right)$$
$$\prod_{j=1,2} \left(1 + \frac{k_{tj_0}^H \exp\left(\frac{-E_{tj}^H}{R}\left(\frac{1}{\mathrm{T}}-\frac{1}{T_0}\right)\right)[\mathrm{H}_2]}{k_{ij_0}^E \exp\left(\frac{-E_{ij}^E}{R}\left(\frac{1}{\mathrm{T}}-\frac{1}{T_0}\right)\right)[\mathrm{C}_2] + k_{ij_0}^{But} \exp\left(\frac{-E_{ij}^{But}}{R}\left(\frac{1}{\mathrm{T}}-\frac{1}{T_0}\right)\right)[\mathrm{C}_4] + k_{ij_0}^{Hex} \exp\left(\frac{-E_{ij}^{Hex}}{R}\left(\frac{1}{\mathrm{T}}-\frac{1}{T_0}\right)\right)[\mathrm{C}_6]} \right)$$
$$\prod_{j=3,5} \left(1 + \frac{k_{tj_0}^H \exp\left(\frac{-E_{tj}^H}{R}\left(\frac{1}{\mathrm{T}}-\frac{1}{T_0}\right)\right)[\mathrm{H}_2]}{k_{ij_0}^E \exp\left(\frac{-E_{ij}^E}{R}\left(\frac{1}{\mathrm{T}}-\frac{1}{T_0}\right)\right)[\mathrm{C}_2]} \right) \qquad (4.1.7)$$

$$N_5 = \left(\frac{k_{p5_0}^E \exp\left(\frac{-E_{p5}^E}{R}\left(\frac{1}{\mathrm{T}}-\frac{1}{T_0}\right)\right)\beta_5}{k_{p2_0}^E \exp\left(\frac{-E_{p2}^E}{R}\left(\frac{1}{\mathrm{T}}-\frac{1}{T_0}\right)\right)} + \frac{k_{p5_0}^{But} \exp\left(\frac{-E_{p5}^{But}}{R}\left(\frac{1}{\mathrm{T}}-\frac{1}{T_0}\right)\right)\beta_5}{k_{p2_0}^E \exp\left(\frac{-E_{p2}^E}{R}\left(\frac{1}{\mathrm{T}}-\frac{1}{T_0}\right)\right)} \frac{[\mathrm{C}_4]}{[\mathrm{C}_2]} + \frac{k_{p5_0}^{Hex} \exp\left(\frac{-E_{p5}^{Hex}}{R}\left(\frac{1}{\mathrm{T}}-\frac{1}{T_0}\right)\right)\beta_5}{k_{p2_0}^E \exp\left(\frac{-E_{p2}^E}{R}\left(\frac{1}{\mathrm{T}}-\frac{1}{T_0}\right)\right)} \frac{[\mathrm{C}_6]}{[\mathrm{C}_2]} \right)$$
$$\prod_{j=1,2} \left(1 + \frac{k_{tj_0}^H \exp\left(\frac{-E_{tj}^H}{R}\left(\frac{1}{\mathrm{T}}-\frac{1}{T_0}\right)\right)[\mathrm{H}_2]}{k_{ij_0}^E \exp\left(\frac{-E_{ij}^E}{R}\left(\frac{1}{\mathrm{T}}-\frac{1}{T_0}\right)\right)[\mathrm{C}_2] + k_{ij_0}^{But} \exp\left(\frac{-E_{ij}^{But}}{R}\left(\frac{1}{\mathrm{T}}-\frac{1}{T_0}\right)\right)[\mathrm{C}_4] + k_{ij_0}^{Hex} \exp\left(\frac{-E_{ij}^{Hex}}{R}\left(\frac{1}{\mathrm{T}}-\frac{1}{T_0}\right)\right)[\mathrm{C}_6]} \right)$$
$$\prod_{j=3,4} \left(1 + \frac{k_{tj_0}^H \exp\left(\frac{-E_{tj}^H}{R}\left(\frac{1}{\mathrm{T}}-\frac{1}{T_0}\right)\right)[\mathrm{H}_2]}{k_{ij_0}^E \exp\left(\frac{-E_{ij}^E}{R}\left(\frac{1}{\mathrm{T}}-\frac{1}{T_0}\right)\right)[\mathrm{C}_2]} \right) \qquad (4.1.8)$$

As shown in Figure 4.1, Equation 4.1.1 uses the sum of five Flory distributions to predict points on the MWD curve obtained using steady-state reactor operating conditions.[4.3] m_j is the mass fraction of copolymer produced at the j^{th} type of active site, τ_j is the ratio of the rate of chain-stopping to chain-propagating events at the j^{th} type of active site and r is the chain length. The expression for τ_j in Equation 4.1.2 is different from that in the original simplified model because it includes Arrhenius expressions to account for the temperature dependence of reaction rates. $k_{tj_0}^H$ is the rate constant for chain transfer to hydrogen at the reference temperature, T_0, and $k_{pj_0}^E$ is

the rate constant for propagation with ethylene at the same reference temperature. Note that chain propagation with butene and hexene are ignored in Equation 4.1.2. This is a reasonable assumption for HDPE copolymers, because the mole fraction of butene or hexene incorporated is small. k_{tj}^{β} and k_{tj}^{I} are rate constants for β-hydride elimination and for chain transfer to impurities, respectively. Note that no temperature effects are included in the second term of Equation 4.1.2. The concentration of impurities in the reactor is unknown, so the overall coefficient involving k_{tj}^{β} and k_{tj}^{I} is lumped into a single parameter for estimation. Also note that chain transfer to comonomers is neglected in Equation 1.2 because these reactions are negligible compared to other chain-stopping reactions.[4.1, 4.8]

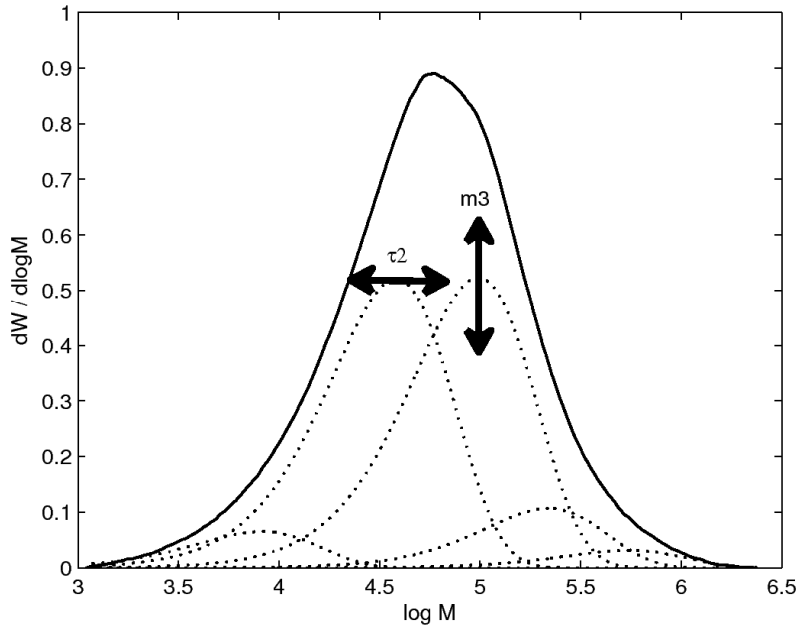

Figure 4.1 The predicted MWD is the sum of the five component Flory distributions.

Equation 4.1.3 shows that the mass fraction of copolymer produced at site j can be determined from a numerator term, N_j, divided by the sum of the numerators for all sites. The expression for N_1 in Equation 4.1.4 was derived in an analogous fashion to the expression for N_1 in our earlier isothermal hexene copolymerization model.[4.1] Activation energies appear in this extended model to account for temperature effects, and additional additive terms account for butene incorporation. Equation 4.1.4 contains the chain-transfer-to-hydrogen rate constant, $k_{tj_0}^H$, because we assume that sites are temporarily dormant after chain transfer to hydrogen,[4.1, 4.8] as shown in the mechanism in Table 4.2. Dormant sites are reinitiated by reactions with ethylene, butene, and hexene. Kissin[4.8] found that reinitiation reactions with comonomers are important at the low-molecular-weight sites, but not at the high-molecular-weight sites. Because of Kissin's findings, it is assumed that low-molecular-weight sites (sites 1 and 2) undergo reinitiation reactions with ethylene and comonomers, and that high-molecular-weight sites (sites 3 to 5) only reinitiate with ethylene.[4.1] Expressions for numerators N_2 to N_5 in Equations 4.1.5 to 4.1.8 are similar to Equation 4.1.4 for N_1. Note that site 2 was used as a reference site in the derivation of these expressions[4.1] and that β_j, which appears in Equations 4.1.4 and 4.1.6 to 4.1.8, is the ratio of the number of catalyst sites of type j (growing chains plus dormant sites) to catalyst sites of type 2. Since site 2 is the reference site, $\beta_2 = 1$.

Table 4.2 Reaction mechanism for ethylene α-olefin terpolymerization. Note that this simplified mechanism does not account for the influence of the monomer on reaction rates.

Propagation with ethylene	$Y_{j,n} + \mathrm{C}_2 \xrightarrow{k_{pj}^{E}} Y_{j,n+1}$
Propagation with comonomer (butene)	$Y_{j,n} + \mathrm{C}_4 \xrightarrow{k_{pj}^{But}} Y_{j,n+1}$
Propagation with comonomer (hexene)	$Y_{j,n} + \mathrm{C}_6 \xrightarrow{k_{pj}^{Hex}} Y_{j,n+1}$
Chain transfer to hydrogen	$Y_{j,n} + \mathrm{H}_2 \xrightarrow{k_{tj}^{H}} Y_{jD}$
Chain transfer to cocatalyst & other impurities	$Y_{j,n} + \mathrm{I} \xrightarrow{k_{tj}^{I}} Y_{j,1}$
Spontaneous chain transfer (β-hydride elimination)	$Y_{j,n} \xrightarrow{k_{tj}^{\beta}} Y_{j,1}$
Reinitiation with ethylene	$Y_{jD} + \mathrm{C}_2 \xrightarrow{k_{ij}^{E}} Y_{j,1}$
Reinitiation with butene	$Y_{jD} + \mathrm{C}_4 \xrightarrow{k_{ij}^{But}} Y_{j,1}$
Reinitiation with hexene	$Y_{jD} + \mathrm{C}_6 \xrightarrow{k_{ij}^{Hex}} Y_{j,1}$

Since the kinetic rate constants in the model always appear as ratios, it is impossible to estimate the individual rate constants independently. The model has been reparameterized, as shown in Table 4.3, to show the lumped parameters that we attempt to estimate. Definitions of these lumped parameters are provided in Table 4.4. Appendix 4.11 shows a sample derivation of an activation energy parameter. Parameters K_{1j} and K_4 defined in Equations 4.3.1 and 4.3.2

influence τ_j, whereas the α parameters in Table 4.4 are used to predict mass fractions, m_j. The ε parameters account for temperature effects.

Table 4.3 Re-parameterized model equations to predict MWD and comonomer incorporation.

$$\frac{dW}{d\log_{10} Mw} = m_1\left[r^2 \ln(10)\cdot\tau_1^2\cdot\exp(-\tau_1 r)\right] + m_2\left[r^2 \ln(10)\cdot\tau_2^2\cdot\exp(-\tau_2 r)\right] + m_3\left[r^2 \ln(10)\cdot\tau_3^2\cdot\exp(-\tau_3 r)\right] + m_4\left[r^2 \ln(10)\cdot\tau_4^2\cdot\exp(-\tau_4 r)\right] + m_5\left[r^2 \ln(10)\cdot\tau_5^2\cdot\exp(-\tau_5 r)\right]$$	(4.3.1)
$$\tau_j = K_{1j}\exp\left(\varepsilon_{K1j}\left(\frac{1}{\mathrm{T}}-\frac{1}{T_0}\right)\right)\frac{[\mathrm{H_2}]}{[\mathrm{C_2}]} + K_4\frac{1}{[\mathrm{C_2}]}$$	(4.3.2)
$$m_j = \frac{N_j}{\sum_{j=1}^{5} N_j}$$	(4.3.3)
$$N_1 = \left(\alpha_{21}\exp\left(\varepsilon_{\alpha 21}\left(\frac{1}{\mathrm{T}}-\frac{1}{T_0}\right)\right) + \alpha_{3Blow}\exp\left(\varepsilon_{\alpha 3Blow}\left(\frac{1}{\mathrm{T}}-\frac{1}{T_0}\right)\right)\frac{[\mathrm{C_4}]}{[\mathrm{C_2}]} + \alpha_{3Hlow}\exp\left(\varepsilon_{\alpha 3Hlow}\left(\frac{1}{\mathrm{T}}-\frac{1}{T_0}\right)\right)\frac{[\mathrm{C_6}]}{[\mathrm{C_2}]}\right) \left(1+\alpha_{1low}K_{12}\exp\left(\varepsilon_{K12}\left(\frac{1}{\mathrm{T}}-\frac{1}{T_0}\right)\right)\frac{[\mathrm{H_2}]}{[\mathrm{C_2}] + \alpha_{4B}\exp\left(\varepsilon_{\alpha 4B}\left(\frac{1}{\mathrm{T}}-\frac{1}{T_0}\right)\right)[\mathrm{C_4}] + \alpha_{4H}\exp\left(\varepsilon_{\alpha 4H}\left(\frac{1}{\mathrm{T}}-\frac{1}{T_0}\right)\right)[\mathrm{C_6}]}\right) \prod_{j=3,4,5}\left(1+\alpha_{1high}K_{1j}\exp\left(\varepsilon_{K1j}\left(\frac{1}{\mathrm{T}}-\frac{1}{T_0}\right)\right)\frac{[\mathrm{H_2}]}{[\mathrm{C_2}]}\right)$$	(4.3.4)
$$N_2 = \left(1+\alpha_{3Blow}\exp\left(\varepsilon_{\alpha 3Blow}\left(\frac{1}{\mathrm{T}}-\frac{1}{T_0}\right)\right)\frac{[\mathrm{C_4}]}{[\mathrm{C_2}]} + \alpha_{3Hlow}\exp\left(\varepsilon_{\alpha 3Hlow}\left(\frac{1}{\mathrm{T}}-\frac{1}{T_0}\right)\right)\frac{[\mathrm{C_6}]}{[\mathrm{C_2}]}\right) \left(1+\alpha_{1low}K_{11}\exp\left(\varepsilon_{K11}\left(\frac{1}{\mathrm{T}}-\frac{1}{T_0}\right)\right)\frac{[\mathrm{H_2}]}{[\mathrm{C_2}] + \alpha_{4B}\exp\left(\varepsilon_{\alpha 4B}\left(\frac{1}{\mathrm{T}}-\frac{1}{T_0}\right)\right)[\mathrm{C_4}] + \alpha_{4H}\exp\left(\varepsilon_{\alpha 4H}\left(\frac{1}{\mathrm{T}}-\frac{1}{T_0}\right)\right)[\mathrm{C_6}]}\right) \prod_{j=3,4,5}\left(1+\alpha_{1high}K_{1j}\exp\left(\varepsilon_{K1j}\left(\frac{1}{\mathrm{T}}-\frac{1}{T_0}\right)\right)\frac{[\mathrm{H_2}]}{[\mathrm{C_2}]}\right)$$	(4.3.5)

$$N_3 = \left(\alpha_{23}\exp\left(\varepsilon_{\alpha 23}\left(\frac{1}{\mathrm{T}}-\frac{1}{T_0}\right)\right)+\alpha_{3Bhigh}\exp\left(\varepsilon_{\alpha 3Bhigh}\left(\frac{1}{\mathrm{T}}-\frac{1}{T_0}\right)\right)\frac{[\mathrm{C}_4]}{[\mathrm{C}_2]}+\alpha_{3Hhigh}\exp\left(\varepsilon_{\alpha 3Hhigh}\left(\frac{1}{\mathrm{T}}-\frac{1}{T_0}\right)\right)\frac{[\mathrm{C}_6]}{[\mathrm{C}_2]}\right)$$
$$\prod_{j=1,2}\left(1+\alpha_{1low}K_{1j}\exp\left(\varepsilon_{K1j}\left(\frac{1}{\mathrm{T}}-\frac{1}{T_0}\right)\right)\frac{[\mathrm{H}_2]}{[\mathrm{C}_2]+\alpha_{4B}\exp\left(\varepsilon_{\alpha 4B}\left(\frac{1}{\mathrm{T}}-\frac{1}{T_0}\right)\right)[\mathrm{C}_4]+\alpha_{4H}\exp\left(\varepsilon_{\alpha 4H}\left(\frac{1}{\mathrm{T}}-\frac{1}{T_0}\right)\right)[\mathrm{C}_6]}\right)$$
$$\prod_{j=4,5}\left(1+\alpha_{1high}K_{1j}\exp\left(\varepsilon_{K1j}\left(\frac{1}{\mathrm{T}}-\frac{1}{T_0}\right)\right)\frac{[\mathrm{H}_2]}{[\mathrm{C}_2]}\right) \qquad (4.3.6)$$

$$N_4 = \left(\alpha_{24}\exp\left(\varepsilon_{\alpha 23}\left(\frac{1}{\mathrm{T}}-\frac{1}{T_0}\right)\right)+\alpha_{3Bhigh}\exp\left(\varepsilon_{\alpha 3Bhigh}\left(\frac{1}{\mathrm{T}}-\frac{1}{T_0}\right)\right)\frac{[\mathrm{C}_4]}{[\mathrm{C}_2]}+\alpha_{3Hhigh}\exp\left(\varepsilon_{\alpha 3Hhigh}\left(\frac{1}{\mathrm{T}}-\frac{1}{T_0}\right)\right)\frac{[\mathrm{C}_6]}{[\mathrm{C}_2]}\right)$$
$$\prod_{j=1,2}\left(1+\alpha_{1low}K_{1j}\exp\left(\varepsilon_{K1j}\left(\frac{1}{\mathrm{T}}-\frac{1}{T_0}\right)\right)\frac{[\mathrm{H}_2]}{[\mathrm{C}_2]+\alpha_{4B}\exp\left(\varepsilon_{\alpha 4B}\left(\frac{1}{\mathrm{T}}-\frac{1}{T_0}\right)\right)[\mathrm{C}_4]+\alpha_{4H}\exp\left(\varepsilon_{\alpha 4H}\left(\frac{1}{\mathrm{T}}-\frac{1}{T_0}\right)\right)[\mathrm{C}_6]}\right)$$
$$\prod_{j=3,5}\left(1+\alpha_{1high}K_{1j}\exp\left(\varepsilon_{K1j}\left(\frac{1}{\mathrm{T}}-\frac{1}{T_0}\right)\right)\frac{[\mathrm{H}_2]}{[\mathrm{C}_2]}\right) \qquad (4.3.7)$$

$$N_5 = \left(\alpha_{25}\exp\left(\varepsilon_{\alpha 25}\left(\frac{1}{\mathrm{T}}-\frac{1}{T_0}\right)\right)+\alpha_{3Bhigh}\exp\left(\varepsilon_{\alpha 3Bhigh}\left(\frac{1}{\mathrm{T}}-\frac{1}{T_0}\right)\right)\frac{[\mathrm{C}_4]}{[\mathrm{C}_2]}+\alpha_{3Hhigh}\exp\left(\varepsilon_{\alpha 3Hhigh}\left(\frac{1}{\mathrm{T}}-\frac{1}{T_0}\right)\right)\frac{[\mathrm{C}_6]}{[\mathrm{C}_2]}\right)$$
$$\prod_{j=1,2}\left(1+\alpha_{1low}K_{1j}\exp\left(\varepsilon_{K1j}\left(\frac{1}{\mathrm{T}}-\frac{1}{T_0}\right)\right)\frac{[\mathrm{H}_2]}{[\mathrm{C}_2]+\alpha_{4B}\exp\left(\varepsilon_{\alpha 4B}\left(\frac{1}{\mathrm{T}}-\frac{1}{T_0}\right)\right)[\mathrm{C}_4]+\alpha_{4H}\exp\left(\varepsilon_{\alpha 4H}\left(\frac{1}{\mathrm{T}}-\frac{1}{T_0}\right)\right)[\mathrm{C}_6]}\right)$$
$$\prod_{j=3,4}\left(1+\alpha_{1high}K_{1j}\exp\left(\varepsilon_{K1j}\left(\frac{1}{\mathrm{T}}-\frac{1}{T_0}\right)\right)\frac{[\mathrm{H}_2]}{[\mathrm{C}_2]}\right) \qquad (4.3.8)$$

$$f_{Bj} = \frac{1}{1+\dfrac{\alpha_{2j}\exp\left(\varepsilon_{\alpha 2j}\left(\dfrac{1}{\mathrm{T}}-\dfrac{1}{T_0}\right)\right)}{\alpha_{3Bj}\exp\left(\varepsilon_{\alpha 3Bj}\left(\dfrac{1}{\mathrm{T}}-\dfrac{1}{T_0}\right)\right)}\dfrac{1}{\dfrac{[\mathrm{C}_4]}{[\mathrm{C}_2]}}} \qquad (4.3.9a)$$

$$f_{Hj} = \frac{1}{1 + \frac{\alpha_{2j} \exp\left(\varepsilon_{\alpha 2j}\left(\frac{1}{\mathrm{T}} - \frac{1}{T_0}\right)\right)}{\alpha_{3Hj} \exp\left(\varepsilon_{\alpha 3Hj}\left(\frac{1}{\mathrm{T}} - \frac{1}{T_0}\right)\right)} \frac{1}{\frac{[\mathrm{C}_6]}{[\mathrm{C}_2]}}}$$	(4.3.9b)
$$m_B = \sum_{j=1-5} m_j \left(\frac{3 f_{Bj}}{1 + 2 f_{Bj}}\right)$$	(4.3.10a)
$$m_H = \sum_{j=1-5} m_j \left(\frac{3 f_{Hj}}{1 + 2 f_{Hj}}\right)$$	(4.3.10b)

Table 4.4 Lumped parameter definitions.

$$K_{1j} = \frac{k_{tj_0}^H}{k_{pj_0}^E}$$	(4.4.1)
$$K_{4j} = \frac{\left(k_{tj}^{\beta} + k_{tj}^I [\mathrm{I}]\right)}{k_{pj}^E}$$	(4.4.2)
$$\alpha_{1low} = \alpha_{11} = \alpha_{12} = \frac{k_{p1_0}^E}{k_{i1_0}^E} = \frac{k_{p2_0}^E}{k_{i2_0}^E}$$	(4.4.3)
$$\alpha_{1high} = \alpha_{13} = \alpha_{14} = \alpha_{15} = \frac{k_{p3_0}^E}{k_{i3_0}^E} = \frac{k_{p4_0}^E}{k_{i4_0}^E} = \frac{k_{p5_0}^E}{k_{i5_0}^E}$$	(4.4.4)
$$\alpha_{2j} = \frac{k_{pj_0}^E \beta_j}{k_{p2_0}^E}$$	(4.4.5)
$$\alpha_{3Blow} = \alpha_{3B1} = \alpha_{3B2} = \frac{k_{p1_0}^{But} \beta_1}{k_{p2_0}^E} = \frac{k_{p2_0}^{But}}{k_{p2_0}^E}$$	(4.4.6)

$\alpha_{3Bhigh} = \alpha_{3B3} = \alpha_{3B4} = \alpha_{3B5} \dfrac{k_{p3_0}^{But}\beta_3}{k_{p2_0}^{E}} = \dfrac{k_{p4_0}^{But}\beta_4}{k_{p2_0}^{E}} = \dfrac{k_{p5_0}^{But}\beta_5}{k_{p2_0}^{E}}$	(4.4.7)
$\alpha_{3Hlow} = \alpha_{3H1} = \alpha_{3H2} = \dfrac{k_{p1_0}^{Hex}\beta_1}{k_{p2_0}^{E}} = \dfrac{k_{p2_0}^{Hex}}{k_{p2_0}^{E}}$	(4.4.8)
$\alpha_{3Hhigh} = \alpha_{3H3} = \alpha_{3H4} = \alpha_{3H5} = \dfrac{k_{p3_0}^{Hex}\beta_3}{k_{p2_0}^{E}} = \dfrac{k_{p4_0}^{Hex}\beta_4}{k_{p2_0}^{E}} = \dfrac{k_{p5_0}^{Hex}\beta_5}{k_{p2_0}^{E}}$	(4.4.9)
$\alpha_{4B} = \dfrac{k_{i1_0}^{But}}{k_{i1_0}^{E}} = \dfrac{k_{i2_0}^{But}}{k_{i2_0}^{E}}$	(4.4.10)
$\alpha_{4H} = \dfrac{k_{i1_0}^{Hex}}{k_{i1_0}^{E}} = \dfrac{k_{i2_0}^{Hex}}{k_{i2_0}^{E}}$	(4.4.11)
$\varepsilon_{Kj} = \dfrac{E_{pj}^{E} - E_{tj}^{H}}{R}$	(4.4.12)
$\varepsilon_{\alpha 2j} = \dfrac{E_{p2}^{E} - E_{pj}^{E}}{R}$	(4.4.13)
$\varepsilon_{\alpha 3Blow} = \varepsilon_{\alpha 3B1} = \varepsilon_{\alpha 3B2} = \dfrac{E_{p2}^{E} - E_{p1}^{But}}{R} = \dfrac{E_{p2}^{E} - E_{p2}^{But}}{R}$	(4.4.14)
$\varepsilon_{\alpha 3Bhigh} = \varepsilon_{\alpha 3B3} = \varepsilon_{\alpha 3B4} = \varepsilon_{\alpha 3B5} = \dfrac{E_{p2}^{E} - E_{p3}^{But}}{R} = \dfrac{E_{p2}^{E} - E_{p4}^{But}}{R} = \dfrac{E_{p2}^{E} - E_{p5}^{But}}{R}$	(4.4.15)
$\varepsilon_{\alpha 3Hlow} = \varepsilon_{\alpha 3H1} = \varepsilon_{\alpha 3H2} = \dfrac{E_{p2}^{E} - E_{p1}^{Hex}}{R} = \dfrac{E_{p2}^{E} - E_{p2}^{Hex}}{R}$	(4.4.16)
$\varepsilon_{\alpha 3Hhigh} = \varepsilon_{\alpha 3H3} = \varepsilon_{\alpha 3H4} = \varepsilon_{\alpha 3H5} = \dfrac{E_{p2}^{E} - E_{p3}^{Hex}}{R} = \dfrac{E_{p2}^{E} - E_{p4}^{Hex}}{R} = \dfrac{E_{p2}^{E} - E_{p5}^{Hex}}{R}$	(4.4.17)
$\varepsilon_{\alpha 4B} = \dfrac{E_{i1}^{E} - E_{i1}^{But}}{R} = \dfrac{E_{i2}^{E} - E_{i2}^{But}}{R}$	(4.4.18)
$\varepsilon_{\alpha 4H} = \dfrac{E_{i1}^{E} - E_{i1}^{Hex}}{R} = \dfrac{E_{i2}^{E} - E_{i2}^{Hex}}{R}$	(4.4.19)

Deconvolution analysis[4.3] of the industrial MWD data revealed that sites 1 and 2 (the low-molecular-weight sites) tend to respond in a similar manner to changes in the reactor operating conditions, and that sites 3, 4, and 5 (the high-molecular-weight sites) also tend to respond together. This behaviour indicates that there may be only two chemically-distinct types of active sites on the Z-N catalyst and that broadening of the MWD may be due to catalyst-support interactions. Therefore, as shown in Table 4.4, some parameter values are shared between similar sites to reduce the number of parameters that appear in the model. For example, α_{1j}, the ratio of the propagation rate constant for ethylene to the reinitiation rate constant for ethylene, is assumed to be common to sites 1 and 2 (the low-molecular-weight sites) and a separate common value is used for the three high-molecular-weight sites (see Equations 4.4.3 and 4.4.4).

Based on the work of Kissin,[4.8] our previous deconvolution analysis,[4.3] and experience with estimating parameters in the original isothermal model,[4.1] further simplifying assumptions were made to reduce the number of new parameters included in the extended non-isothermal model shown in Table 4.3:

1. Since τ values do not appear to change with temperature in the absence of hydrogen,[4.8] we assume that K_4 is not temperature dependent.
2. α_1, the ratio of the rate constant for propagation with ethylene to the rate constant for reinitiation with ethylene, was assumed to be temperature independent, because this ratio was not very influential in the earlier isothermal model.

As shown in Table 4.5, initial guesses for parameters involving hexene and ethylene were obtained from the isothermal model.[4.1] Parameters involving butene were given the same initial

guesses as the corresponding hexene parameters. Initial values for the Arrhenius-type parameters were calculated from deconvolution results presented by Kissin.[4.8]

Table 4.5 Initial guesses, uncertainties and estimability ranking of the parameters in the model in Table 4.3.

Parameter	Initial Value	Scaling Value	Rank
K_{11}	0.0149	$6.209*10^{-3}$	27
K_{12}	0.0030	$9.0*10^{-4}$	25
K_{13}	0.0012	$5.57*10^{-4}$	17
K_{14}	0.0003	$5.39*10^{-4}$	23
K_{15}	0	$8.8781*10^{-3}$	3
i_4	$9.4*10^{-4}$	$1.3055*10^{-4}$	18
α_{1low}	1325.8	1893.7	4
α_{1high}	3222.2	5048.4	5
α_{21}	0.4755	0.2074	21
α_{23}	1.9492	1.0260	14
α_{24}	0.3370	0.2042	9
α_{25}	0.0579	0.0656	11
α_{3Blow}	0.4370	0.5	19
α_{3Bhigh}	$1.73*10^{-9}$	0.5	7
α_{3Hlow}	0.4370	0.5	22
α_{3Hhigh}	$1.73*10^{-9}$	0.5	8
α_{4B}	0.0491	51.3868	1
α_{4H}	0.0491	51.3868	2
ε_{K11}	-2828.7	-1414.4	15
ε_{K12}	-1603	-801.5	10
ε_{K13}	-2613.9	-1307	6
ε_{K14}	-3652	-1826	20
ε_{K15}	-3652	-1826	33
$\varepsilon_{\alpha 21}$	-3974	-1987.2	16
$\varepsilon_{\alpha 23}$	1439	719.4	24
$\varepsilon_{\alpha 24}$	6983	3491.4	12
$\varepsilon_{\alpha 25}$	10758	5379	13
$\varepsilon_{\alpha 3Blow}$	-3974.4	-3974.4	26
$\varepsilon_{\alpha 3Bhigh}$	6982.8	6982.8	31
$\varepsilon_{\alpha 3Hlow}$	-3974.4	-3974.4	28
$\varepsilon_{\alpha 3Hhigh}$	6982.8	6982.8	32
$\varepsilon_{\alpha 4B}$	0	1504.2	29
$\varepsilon_{\alpha 4H}$	0	1504.2	30

The initial parameter values in Table 4.5 can be used to predict comonomer incorporation (i.e., using Equations 4.3.9a to 4.3.10b in Table 4.3). Several simplifying assumptions were made in the development of these equations, so that the approximate level of comonomer incorporation could be predicted without including additional parameters in the model. The most problematic assumption required is that the rate of propagation is not influenced significantly by the terminal group (ethylene, butene or hexene) on the growing polymer chain.[4.1] The industrial data set[4.3] used for fitting the model parameters contains overall comonomer incorporation measurements and measured MWD curves. If detailed comonomer composition distribution or sequence length information were also available, then a more complex copolymerization model that properly accounts for reactivity ratios at the various type of sites could have been estimated. Nevertheless, the main objective of the current research is to develop a simplified model to predict the MWD curve from reactor operating conditions. Equation 4.3.10 is included in the model to ensure that the parameter values in the MWD model are consistent with observed overall levels of comonomer incorporation.

4.4 Estimability Analysis

The model parameters were ranked from most estimable to least estimable using the estimability ranking technique described in the Appendix. This parameter ranking technique uses a sensitivity matrix whose elements, $\partial y_i / \partial \theta_k$, are partial derivatives of each predicted model response, y_i, with respect to each of the parameters of interest, θ_k. The y_i values for each experimental run consist of 100 equally-spaced points (on the log scale) from the predicted MWD curve and a single comonomer incorporation (in mass fraction) value. Proper scaling of each element of the sensitivity matrix is required to ensure that the elements are dimensionally

consistent and that some parameters or predicted responses do not dominate the ranking due to their large numerical values. To address this concern, Kou et al. used initial guesses for parameters, and typical values for predicted responses as scaling factors.[4.4] The proposed algorithm in the Appendix uses an improved method for scaling that provides the modeller with an opportunity to include additional knowledge. As shown in the Appendix, each element of the sensitivity matrix is scaled using the uncertainty in the initial value for the corresponding parameter, $s_{\theta k}$, and the uncertainty in the corresponding measured response, s_{yi}. An appropriate value for $s_{\theta k}$ reflects how far the modeller is willing to allow the particular parameter to move away from its initial guess, and s_{yi} reflects the modeller's knowledge about the reproducibility of measurements for the different responses. Using the proposed scaling, the limited information in the data is used to estimate influential parameters whose values are not well-known. Less-influential parameters and parameters whose initial values are more certain rank lower on the list. Parameters that rank near the bottom of the list may be kept at their initial values, if there is insufficient information to estimate all of the parameters.

In the current work, a value of $s_{yi} = 0.0154$ is used for MWD responses, and $s_{yi} = 0.0143$ was used for comonomer incorporation responses. These scaling values were determined from pooled variance estimates determined from three pairs of replicate experiments (see Figure 4.5a) to c)). Scaling factors $s_{\theta k}$ and the corresponding initial guesses for all of the parameters are shown in Table 4.5. Note that some of the initial parameter values in Table 4.5 are parameter estimates obtained using the isothermal model.[4.1] For these parameters, the corresponding $s_{\theta k}$ values are the standard deviations of the parameter estimates from the isothermal model estimation. For other parameters that do not appear in the isothermal model, $s_{\theta k}$ values were selected based on how far we anticipated that the parameter could move away from the initial

guess before its value might become physically unreasonable. For example, the initial value of ε_{K11} = -2828.7 in Table 4.5 was calculated using data from a different Ziegler-Natta catalyst obtained at several temperatures.[4.8] A value of $s_{\theta k}$, which is half of this initial guess, was selected to reflect our expectation that the final estimate for ε_{K11} could be quite different from -2828.7 but should be similar in size. The objective function for parameter estimation for the non-isothermal models also uses the s_{yi} values to weight the molecular weight and comonomer incorporation terms:

$$J = \sum \left(\frac{y_{MWD} - \hat{y}_{MWD}}{s_{yMWD}} \right)^2 + \sum \left(\frac{y_{CI} - \hat{y}_{CI}}{s_{yCI}} \right)^2 \tag{4.1}$$

The estimability algorithm was able to rank the parameters in Table 4.5 from most estimable to least estimable. However, singularity problems were encountered when ranking the final two parameters. This result suggests that, at very most, 32 parameters could be simultaneously estimated using the available MWD and composition data, because estimating all 33 parameters would lead to severe numerical conditioning problems. The parameter estimability rankings are shown in the final column of Table 4.5. A low rank number indicates a parameter that should be easy to estimate because of the large amount of information in the available data (compared to the uncertainty, $s_{\theta k}$). A high rank number indicates a parameter that cannot be readily estimated due to a lack of parameter influence on the predicted responses or due to correlation with the effects of parameters that appear earlier in the ranked list.

4.5 Parameter Estimation

The estimability analysis indicates that at most 32 parameters could be estimated without encountering severe numerical difficulties during parameter estimation. However, better model

predictions may be obtained if fewer parameters are estimated. As a result, it is important to determine how many parameters should be estimated from the ranked list. Kou et al.,[4.4] suggested using a pre-specified cut-off value for the magnitude of columns in the residual sensitivity matrix. When the magnitudes of the residuals became smaller than this cut-off value, Kou et al. stopped the ranking procedure and the parameters that had been ranked were then estimated. Unfortunately, it is difficult to choose an appropriate cut-off value, making the number of estimated parameters somewhat arbitrary. An improved method for determining how many parameters to estimate is used in this article.

When too many parameters are estimated using limited data, the high levels of uncertainty associated with the parameter estimates result in large variances for the model predictions.[4.9, 4.10] When only a subset of the model parameters is estimated (while keeping the other parameters at their initial guesses), model predictions and parameter estimates are biased due to the incorrect values of the fixed parameters.[4.9] This bias decreases when additional parameters are estimated. The optimal number of parameters to estimate balances the trade-off between variance and bias to produce model predictions with the lowest mean-squared prediction error.[4.10] A straightforward way to examine this trade-off is to use cross-validation,[4.11] as described below. Cross-validation tests the predictive ability of a model by removing data from the available data set. Model parameters are then estimated and used to predict the removed data.

Cross-validation was performed by selecting four key runs from the complete set of the 31 experimental runs. These four runs correspond to very different points in the operating space. Two runs used butene comonomer and two used hexene. The four points covered a range of temperatures and hydrogen-to-ethylene ratios. Various numbers of parameters from the ranked list were then estimated four times. Each time, data from one of the selected experiments were

left out, and the remaining 30 runs were used to estimate the parameters. The estimated parameters were then used to predict the responses for their corresponding left-out run. This procedure was repeated for each of the four runs selected. The weighted sum of squared residuals (see Equation 4.1) was then calculated and added together for the four left-out runs (using the corresponding sets of parameter values). This cross-validation procedure was performed for different numbers of parameters being estimated, and the resulting values of this cross-validation objective function are plotted in Figure 4.2 vs. the number of parameters that were estimated from the ranked list. A low value of the objective function indicates good predictive ability of the model and the parameters. One benefit of the cross-validation approach is that it provides a measure of how well the model can predict data that were not used for estimation. Cross-validation also provides information about the sensitivity of parameter values to particular experimental data points. Note that four key runs were chosen for cross-validation, rather than using all 31 runs, because of the heavy computational load required to estimate the parameters.

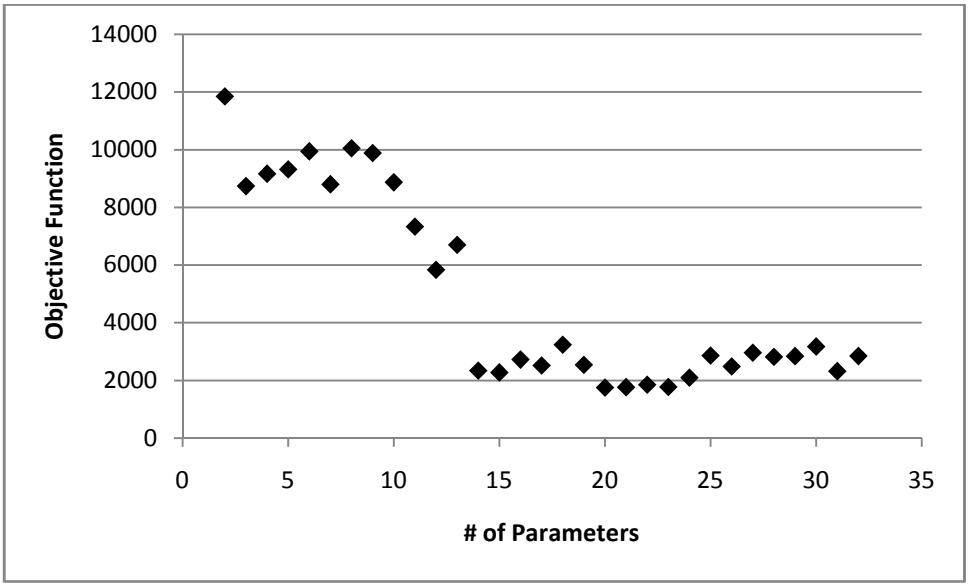

Figure 4.2 Influence of number of parameters estimated in the model in Table 4.3 on the cross-validation objective function.

The predictive ability of the model tended to improve as more parameters were estimated, up to approximately 14 parameters. Estimating additional parameters either had very little influence on the quality of the model predictions or resulted in worse predictions. The 14 highest-ranked parameters were then re-estimated using all 31 runs in the data set, and are reported in Table 4.6.

Table 4.6 Parameter estimates for the 14 most-estimable parameters from the model in Table 4.3. Parameter estimates that are statistically different from zero at the 95% confidence level are shown in **bold**. Approximate 95% confidence intervals, based on linearization, were used to determine whether parameters are significant.

Rank	Parameter	Estimate
1	α_{4B}	**7.3420**
2	α_{4H}	**26.9599**
3	K_{15}	$2.2222*10^{-14}$
4	α_{1low}	**2667.2**
5	α_{1high}	**544.7**
6	ε_{K13}	**-2924.1**
7	α_{3Bhigh}	$2.2246*10^{-14}$
8	α_{3Hhigh}	$2.2205*10^{-14}$
9	α_{24}	**0.0942**
10	ε_{K12}	**-2308.8**
11	α_{25}	**0.0159**
12	ε_{a24}	**2348.6**
13	ε_{a25}	1108.3
14	α_{23}	**0.3708**

The lower-ranked parameters that were not estimated tend to be activation energy parameters. The temperature effects of many kinetic rate constants may not be influential enough over the range of temperatures studied (80 to 115 °C) in order for separate activation energy parameters to estimated for individual types of active sites. To make the best possible use of the data, another round of model simplification was used. To further reduce the number of parameters in the model, it was assumed that sites 1 and 2 have common activation energy parameters, and

that sites 3, 4 and 5 share a different set of common values. We also assumed that, since there is little propagation with comonomers at the high-molecular-weight sites, it is reasonable to ignore the associated temperature effects (no activation energy parameter associated with α_{3Bhigh} and α_{3Hhigh}). These simplifications reduced the number of model parameters from 33 to 25. The re-parameterized model equations are shown in Table 4.7.

Table 4.7 Re-parameterized equations for computing MWD. This model was developed after making simplifying assumptions to reduce the number of unknown parameters to 25.

$$\frac{dW}{d\log_{10} Mw} = m_1\left[r^2 \ln(10)\cdot\tau_1^2\cdot\exp(-\tau_1 r)\right] + m_2\left[r^2 \ln(10)\cdot\tau_2^2\cdot\exp(-\tau_2 r)\right] + m_3\left[r^2 \ln(10)\cdot\tau_3^2\cdot\exp(-\tau_3 r)\right] + m_4\left[r^2 \ln(10)\cdot\tau_4^2\cdot\exp(-\tau_4 r)\right] + m_5\left[r^2 \ln(10)\cdot\tau_5^2\cdot\exp(-\tau_5 r)\right]$$	(4.7.1)
$$\tau_j = K_{1j}\exp\left(\varepsilon_{K1low}\left(\frac{1}{\mathrm{T}}-\frac{1}{T_0}\right)\right)\frac{[\mathrm{H_2}]}{[\mathrm{C_2}]} + K_4\frac{1}{[\mathrm{C_2}]} \quad \text{for } j = 1,2 \quad \text{OR}$$ $$\tau_j = K_{1j}\exp\left(\varepsilon_{K1high}\left(\frac{1}{\mathrm{T}}-\frac{1}{T_0}\right)\right)\frac{[\mathrm{H_2}]}{[\mathrm{C_2}]} + K_4\frac{1}{[\mathrm{C_2}]} \quad \text{for } j=3,4,5$$	(4.7.2)
$$m_j = \frac{N_j}{\sum_{j=1}^{5} N_j}$$	(4.7.3)
$$N_1 = \left(\alpha_{21}\exp\left(\varepsilon_{\alpha 21}\left(\frac{1}{\mathrm{T}}-\frac{1}{T_0}\right)\right) + \alpha_{3Blow}\exp\left(\varepsilon_{\alpha 3Blow}\left(\frac{1}{\mathrm{T}}-\frac{1}{T_0}\right)\right)\frac{[\mathrm{C_4}]}{[\mathrm{C_2}]} + \alpha_{3Hlow}\exp\left(\varepsilon_{\alpha 3Hlow}\left(\frac{1}{\mathrm{T}}-\frac{1}{T_0}\right)\right)\frac{[\mathrm{C_6}]}{[\mathrm{C_2}]}\right)$$ $$\left(1+\alpha_{1low}K_{12}\exp\left(\varepsilon_{Klow}\left(\frac{1}{\mathrm{T}}-\frac{1}{T_0}\right)\right)\frac{[\mathrm{H_2}]}{[\mathrm{C_2}] + \alpha_{4B}\exp\left(\varepsilon_{\alpha 4}\left(\frac{1}{\mathrm{T}}-\frac{1}{T_0}\right)\right)[\mathrm{C_4}] + \alpha_{4H}\exp\left(\varepsilon_{\alpha 4}\left(\frac{1}{\mathrm{T}}-\frac{1}{T_0}\right)\right)[\mathrm{C_6}]}\right)$$ $$\prod_{j=3,4,5}\left(1+\alpha_{1high}K_{1j}\exp\left(\varepsilon_{Khigh}\left(\frac{1}{\mathrm{T}}-\frac{1}{T_0}\right)\right)\frac{[\mathrm{H_2}]}{[\mathrm{C_2}]}\right)$$	(4.7.4)

$$N_2 = \left(1+\alpha_{3Blow}\exp\left(\varepsilon_{\alpha 3Blow}\left(\frac{1}{\mathrm{T}}-\frac{1}{T_0}\right)\right)\frac{[\mathrm{C}_4]}{[\mathrm{C}_2]}+\alpha_{3Hlow}\exp\left(\varepsilon_{\alpha 3Hlow}\left(\frac{1}{\mathrm{T}}-\frac{1}{T_0}\right)\right)\frac{[\mathrm{C}_6]}{[\mathrm{C}_2]}\right)$$ $$\left(1+\alpha_{1low}K_{11}\exp\left(\varepsilon_{Klow}\left(\frac{1}{\mathrm{T}}-\frac{1}{T_0}\right)\right)\frac{[\mathrm{H}_2]}{[\mathrm{C}_2]+\alpha_{4B}\exp\left(\varepsilon_{\alpha 4}\left(\frac{1}{\mathrm{T}}-\frac{1}{T_0}\right)\right)[\mathrm{C}_4]+\alpha_{4H}\exp\left(\varepsilon_{\alpha 4}\left(\frac{1}{\mathrm{T}}-\frac{1}{T_0}\right)\right)[\mathrm{C}_6]}\right)$$ $$\prod_{j=3,4,5}\left(1+\alpha_{1high}K_{1j}\exp\left(\varepsilon_{Khigh}\left(\frac{1}{\mathrm{T}}-\frac{1}{T_0}\right)\right)\frac{[\mathrm{H}_2]}{[\mathrm{C}_2]}\right)$$	(4.7.5)
$$N_3 = \left(\alpha_{23}\exp\left(\varepsilon_{\alpha 2high}\left(\frac{1}{\mathrm{T}}-\frac{1}{T_0}\right)\right)+\alpha_{3Bhigh}\frac{[\mathrm{C}_4]}{[\mathrm{C}_2]}+\alpha_{3Hhigh}\frac{[\mathrm{C}_6]}{[\mathrm{C}_2]}\right)$$ $$\prod_{j=1,2}\left(1+\alpha_{1low}K_{1j}\exp\left(\varepsilon_{Klow}\left(\frac{1}{\mathrm{T}}-\frac{1}{T_0}\right)\right)\frac{[\mathrm{H}_2]}{[\mathrm{C}_2]+\alpha_{4B}\exp\left(\varepsilon_{\alpha 4}\left(\frac{1}{\mathrm{T}}-\frac{1}{T_0}\right)\right)[\mathrm{C}_4]+\alpha_{4H}\exp\left(\varepsilon_{\alpha 4}\left(\frac{1}{\mathrm{T}}-\frac{1}{T_0}\right)\right)[\mathrm{C}_6]}\right)$$ $$\prod_{j=4,5}\left(1+\alpha_{1high}K_{1j}\exp\left(\varepsilon_{Khigh}\left(\frac{1}{\mathrm{T}}-\frac{1}{T_0}\right)\right)\frac{[\mathrm{H}_2]}{[\mathrm{C}_2]}\right)$$	(4.7.6)
$$N_4 = \left(\alpha_{24}\exp\left(\varepsilon_{\alpha 2high}\left(\frac{1}{\mathrm{T}}-\frac{1}{T_0}\right)\right)+\alpha_{3Bhigh}\frac{[\mathrm{C}_4]}{[\mathrm{C}_2]}+\alpha_{3Hhigh}\frac{[\mathrm{C}_6]}{[\mathrm{C}_2]}\right)$$ $$\prod_{j=1,2}\left(1+\alpha_{1low}K_{1j}\exp\left(\varepsilon_{Klow}\left(\frac{1}{\mathrm{T}}-\frac{1}{T_0}\right)\right)\frac{[\mathrm{H}_2]}{[\mathrm{C}_2]+\alpha_{4B}\exp\left(\varepsilon_{\alpha 4}\left(\frac{1}{\mathrm{T}}-\frac{1}{T_0}\right)\right)[\mathrm{C}_4]+\alpha_{4H}\exp\left(\varepsilon_{\alpha 4}\left(\frac{1}{\mathrm{T}}-\frac{1}{T_0}\right)\right)[\mathrm{C}_6]}\right)$$ $$\prod_{j=3,5}\left(1+\alpha_{1high}K_{1j}\exp\left(\varepsilon_{Khigh}\left(\frac{1}{\mathrm{T}}-\frac{1}{T_0}\right)\right)\frac{[\mathrm{H}_2]}{[\mathrm{C}_2]}\right)$$	(4.7.7)
$$N_5 = \left(\alpha_{25}\exp\left(\varepsilon_{\alpha 2high}\left(\frac{1}{\mathrm{T}}-\frac{1}{T_0}\right)\right)+\alpha_{3Bhigh}\frac{[\mathrm{C}_4]}{[\mathrm{C}_2]}+\alpha_{3Hhigh}\frac{[\mathrm{C}_6]}{[\mathrm{C}_2]}\right)$$ $$\prod_{j=1,2}\left(1+\alpha_{1low}K_{1j}\exp\left(\varepsilon_{Klow}\left(\frac{1}{\mathrm{T}}-\frac{1}{T_0}\right)\right)\frac{[\mathrm{H}_2]}{[\mathrm{C}_2]+\alpha_{4B}\exp\left(\varepsilon_{\alpha 4}\left(\frac{1}{\mathrm{T}}-\frac{1}{T_0}\right)\right)[\mathrm{C}_4]+\alpha_{4H}\exp\left(\varepsilon_{\alpha 4}\left(\frac{1}{\mathrm{T}}-\frac{1}{T_0}\right)\right)[\mathrm{C}_6]}\right)$$ $$\prod_{j=3,4}\left(1+\alpha_{1high}K_{1j}\exp\left(\varepsilon_{Khigh}\left(\frac{1}{\mathrm{T}}-\frac{1}{T_0}\right)\right)\frac{[\mathrm{H}_2]}{[\mathrm{C}_2]}\right)$$	(4.7.8)

With the model further simplified, a second round of estimability analysis was performed. The estimability rankings, along with the initial parameter estimates and the scaling

values, are shown in Table 4.8. This time, the estimability algorithm was able to rank all 25 model parameters.

Table 4.8 Estimability rankings for the simplified 25-parameter model that appears in Table 4.7.

Parameter	Initial Value	Scaling Value	Rank
K_{11}	0.0149	$6.209*10^{-3}$	21
K_{12}	0.0030	$9.0*10^{-4}$	23
K_{13}	0.0012	$5.57*10^{-4}$	13
K_{14}	0.0003	$5.39*10^{-4}$	19
K_{15}	0	$8.8781*10^{-3}$	3
K_4	$9.4*10^{-4}$	$1.3055*10^{-4}$	15
α_{1low}	1325.8	1893.7	4
α_{1high}	3222.2	5048.4	5
α_{21}	0.4755	0.2074	18
α_{23}	1.9492	1.0260	12
α_{24}	0.3370	0.2042	10
α_{25}	0.0579	0.0656	11
α_{3Blow}	0.4370	0.5	17
α_{3Bhigh}	$1.73*10^{-9}$	0.5	6
α_{3Hlow}	0.4370	0.5	20
α_{3Hhigh}	$1.73*10^{-9}$	0.5	8
α_{4B}	0.0491	51.3868	1
α_{4H}	0.0491	51.3868	2
ε_{Klow}	-2308.8	-801.5	16
ε_{Khigh}	-2924.1	-1307	7
$\varepsilon_{\alpha 21}$	-3974	-1987.2	14
$\varepsilon_{\alpha 2high}$	2348.6	3491.4	9
$\varepsilon_{\alpha 3Blow}$	-3974.4	-3874.4	22
$\varepsilon_{\alpha 3Hlow}$	-3974.4	-3974.4	24
$\varepsilon_{\alpha 4}$	0	1504.2	25

With the new estimability rankings in place, a new cross-validation plot (similar to Figure 4.2) was generated and is shown in Figure 4.3. This time, the objective function decreases until 16 parameters have been estimated. The MWD fits for the four runs used in cross-validation are shown in Figure 4.4a) to d), and the parameter estimates are shown in Table 4.9. The MWD model is able to match all four MWD curves very well. There is little difference between the final model predictions and the predictions obtained using the cross-validation parameters,

indicating that the model has good predictive capability for the four selected runs. The data set used for parameter estimation contains data from experimental runs that were replicated at three different sets of operating conditions. Model predictions and experimental data for these runs are shown in Figure 4.5a) to c). The small deviations between the model predictions and the data are similar in size to the deviations between the measured MWD curves.

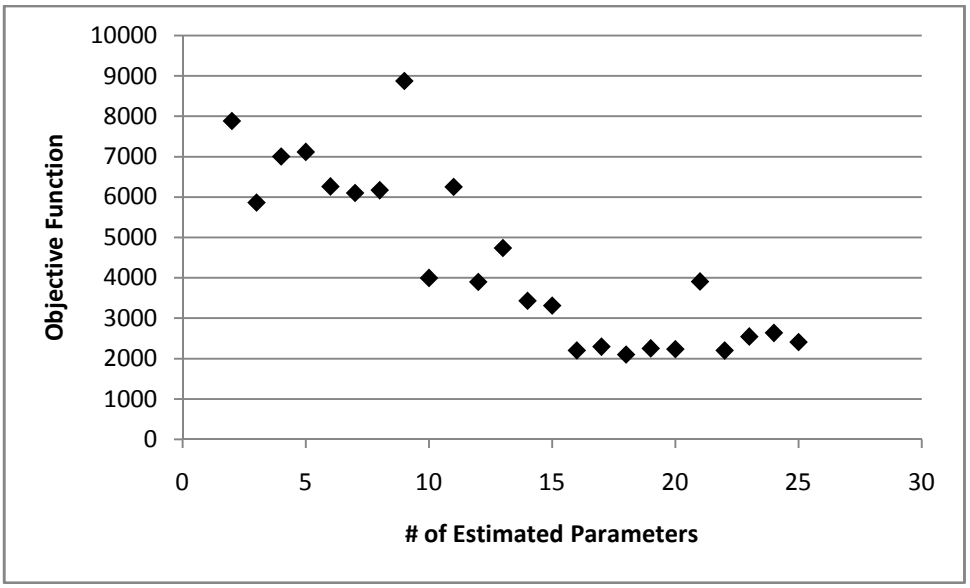

Figure 4.3 Influence of number of parameters estimated in the model in Table 4.7 on the cross-validation objective function.

a)

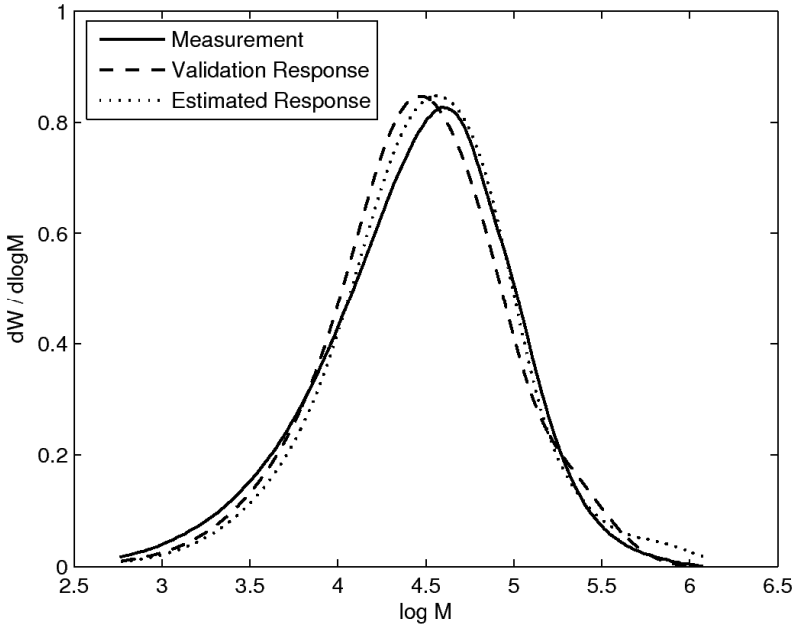
Measurement
Validation Response
Estimated Response
dW / dlogM
log M
0
0.2
0.4
0.6
0.8
1
2.5
3
3.5
4
4.5
5
5.5
6
6.5

b)

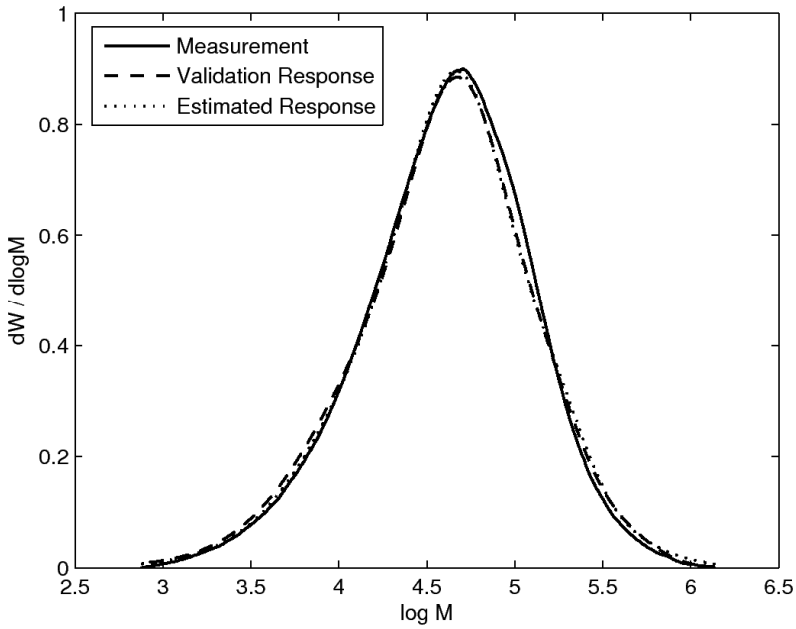
Measurement
Validation Response
Estimated Response
dW / dlogM
log M
0
0.2
0.4
0.6
0.8
1
2.5
3
3.5
4
4.5
5
5.5
6
6.5

c)

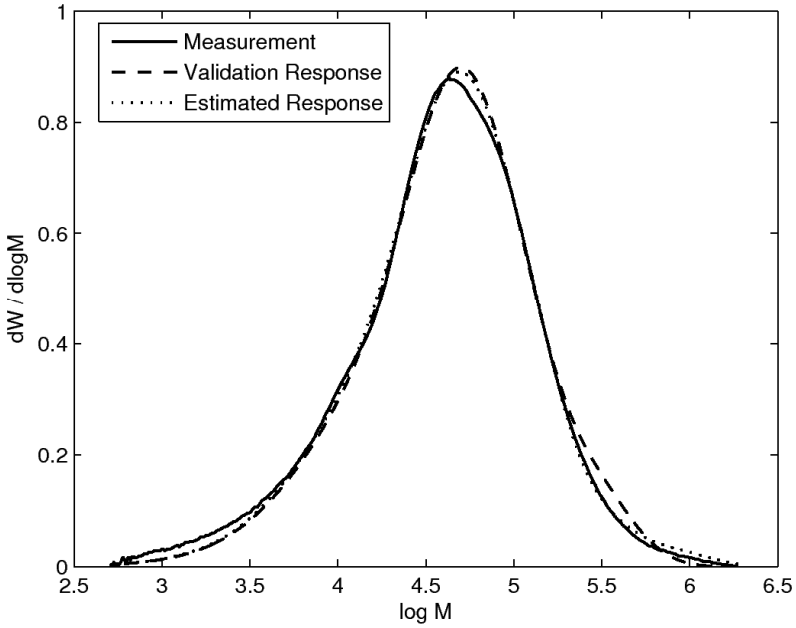

d)

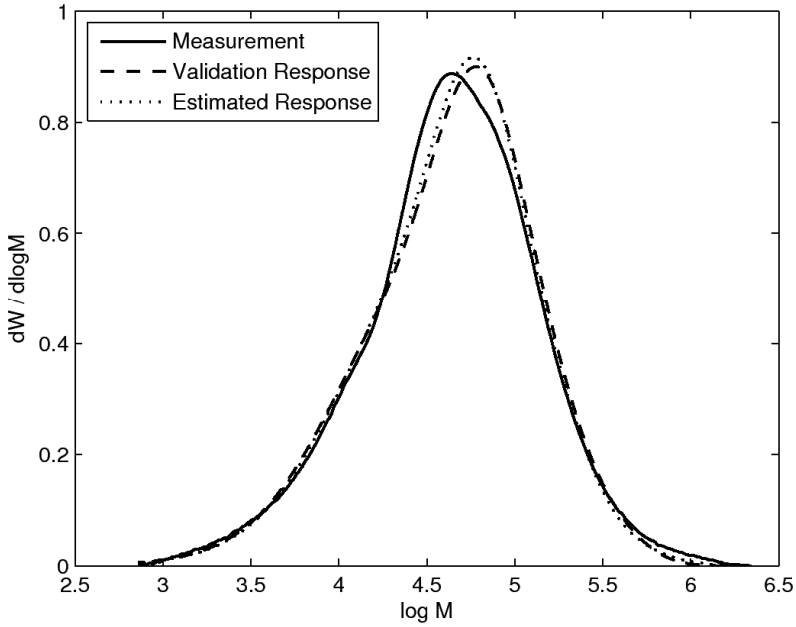

Figure 4.4 Predictions of MWD for runs used for cross validation. The solid line is the measured MWD, the dotted line is the fit with all runs included in the parameter estimation, and the dashed line is the prediction with this run left out of the parameter estimation. Run a) was conducted with butene at 90 °C. Run b) was conducted with hexene at 80 °C. Run c) was conducted with butene at 110 °C. Run d) was conducted with hexene at 100 °C.

a)

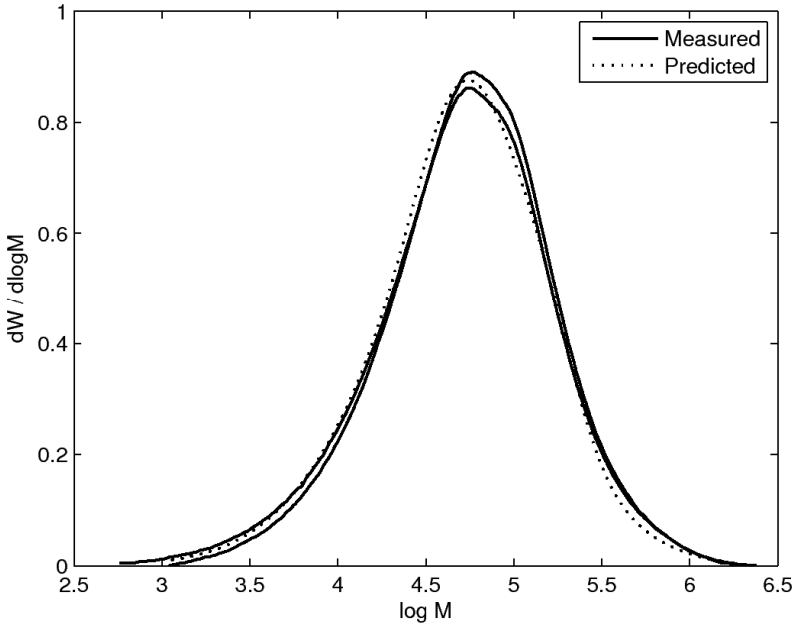
Measured
Predicted
dW / dlogM
log M
0
0.2
0.4
0.6
0.8
1
2.5
3
3.5
4
4.5
5
5.5
6
6.5

b)

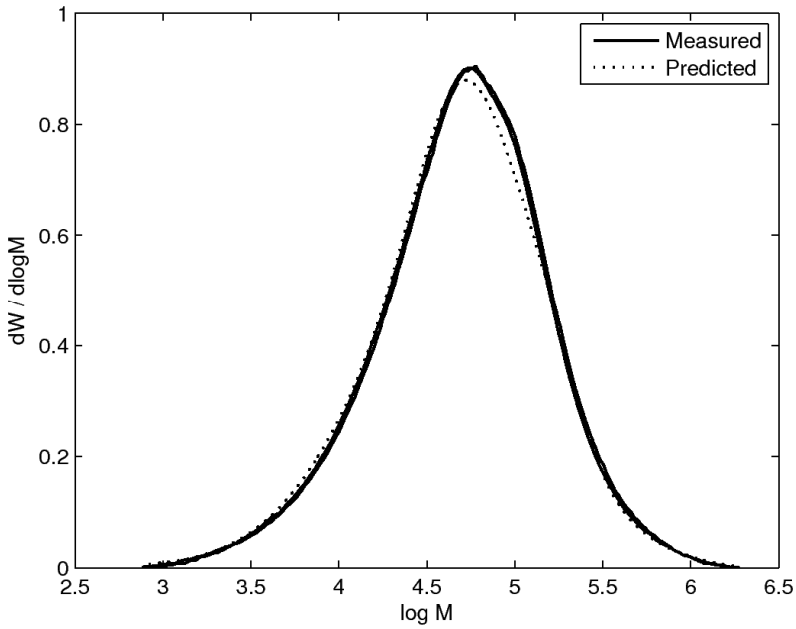
Measured
Predicted
dW / dlogM
log M
0
0.2
0.4
0.6
0.8
1
2.5
3
3.5
4
4.5
5
5.5
6
6.5

c)

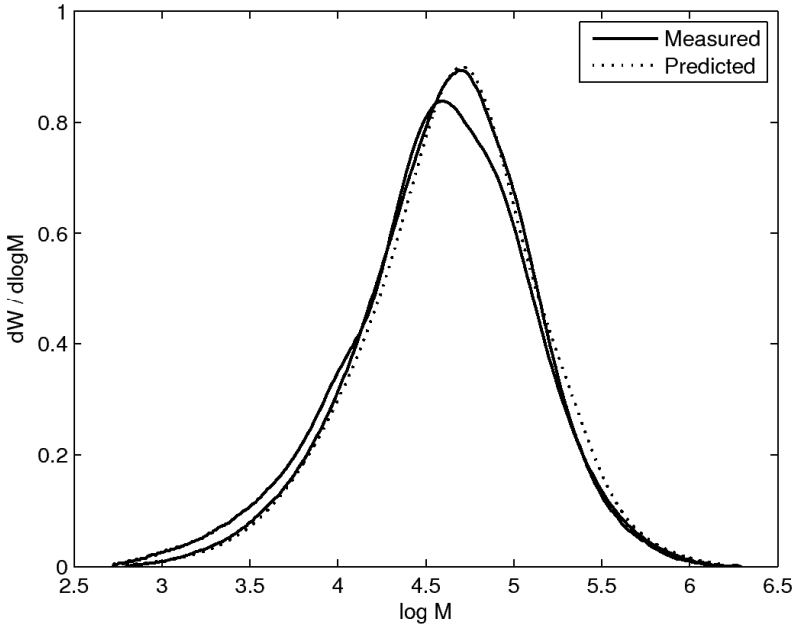

Figure 4.5 Predictions of three pairs of replicate runs. Runs a) and b) were conducted with hexene at 90 °C and run c) was conducted with hexene at 80 °C. Predictions were made using the model in Table 4.7 and the parameter estimates in Tables 4.8 and 4.9.

Table 4.9 Parameter estimates of the 16 most-estimable parameters in the 25-parameter model. Parameter estimates that are statistically different from zero at the 95% confidence interval are shown in **bold**. Approximate 95% confidence intervals, based on linearization, were used to determine whether parameters are significant.

Rank	Parameter	Estimate
1	α_{4B}	**6.72**
2	α_{4H}	**23.50**
3	K_{15}	$3.73*10^{-7}$
4	α_{1low}	**2423**
5	α_{1high}	**426.2**
6	α_{3Bhigh}	$4.3*10^{-13}$
7	ε_{Khigh}	**-3582**
8	α_{3Hhigh}	$8.3*10^{-13}$
9	$\varepsilon_{\alpha 2high}$	566.7
10	α_{24}	**0.06**
11	α_{25}	**0.017**
12	α_{23}	**0.34**
13	K_{13}	**0.001**
14	$\varepsilon_{\alpha 21}$	**-3385**
15	K_4	$\mathbf{8.18*10^{-4}}$
16	ε_{Klow}	**-2387**

Figure 4.6 shows the behaviour of the overall objective function for parameter estimation as additional parameters are estimated from the complete set of 31 runs. This figure confirms that the fit to the data cannot be improved significantly by estimating more than 16 parameters. The parameter estimates in Table 4.9 are consistent with the initial guesses and the scaling values from Table 4.8, indicating that none of the parameter estimates is physically or statistically unrealistic.

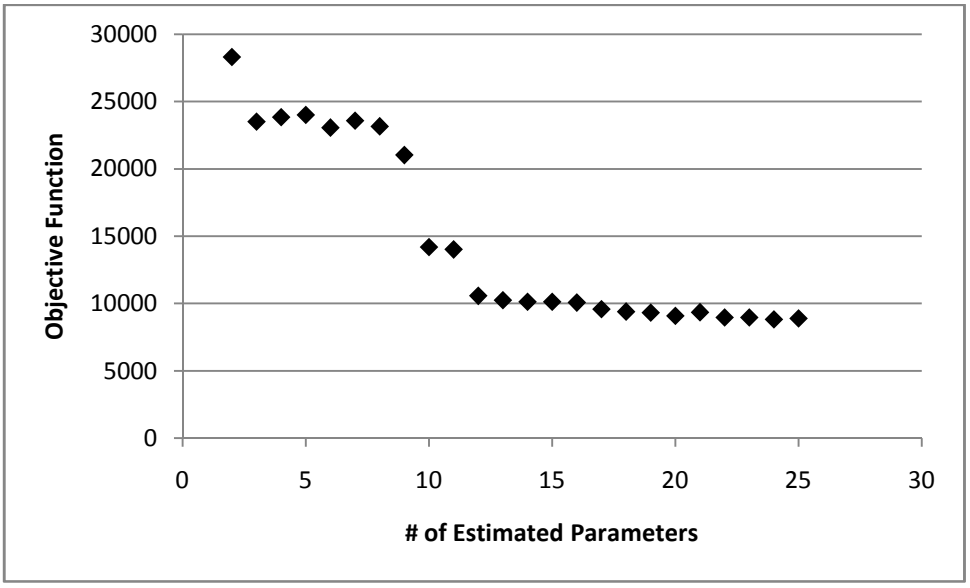

Figure 4.6 Parameter estimation objective function decreases as more parameters are added.

Unfortunately, comonomer incorporation is not as well predicted as the MWDs (see Figure 4.7). This is because the single comonomer incorporation data point from each run does not have much weight (compared to the 100 MWD points for each run) in the parameter-estimation objective function. The results in Figure 4.5 and Figure 4.7 may correspond to a local optimum in the parameter estimation surface. To fix this problem, another round of estimability analysis and parameter estimation was needed. In the first step, only the comonomer incorporation data were included and no MWD information was used in the estimability ranking or parameter estimation. Using the comonomer incorporation sensitivity coefficients, the eight most estimable parameters related directly to comonomer incorporation predictions were determined (i.e., α_{3Bhigh}, α_{3Hhigh}, α_{4B}, α_{4H}, $\varepsilon_{\alpha 3Blow}$, $\varepsilon_{\alpha 3Hlow}$, α_{3Blow}, α_{3Hlow}). These eight parameters were re-estimated starting from the values in Tables 4.8 and 4.9 to obtain an improved fit of the comonomer incorporation data. Next, the 16 parameters in Table 4.9 were re-estimated to fit both

the MWD and comonomer data, using the new values of the eight comonomer parameters as starting values (and fixed values). Parameters were successively re-estimated until further improvements in the objective function and comonomer incorporation fit were not observed. The new parameter values drastically improved the comonomer incorporation fit, as can be seen in Figure 4.8, with a small improvement in the MWD fits, as well (not shown). The complete set of final parameter estimates is provided in Table 4.10. The overall objective function, in Equation 4.1 was reduced from 10070 to 9457 when the parameters in Table 4.10 were used instead of those in Tables 4.8 and 4.9.

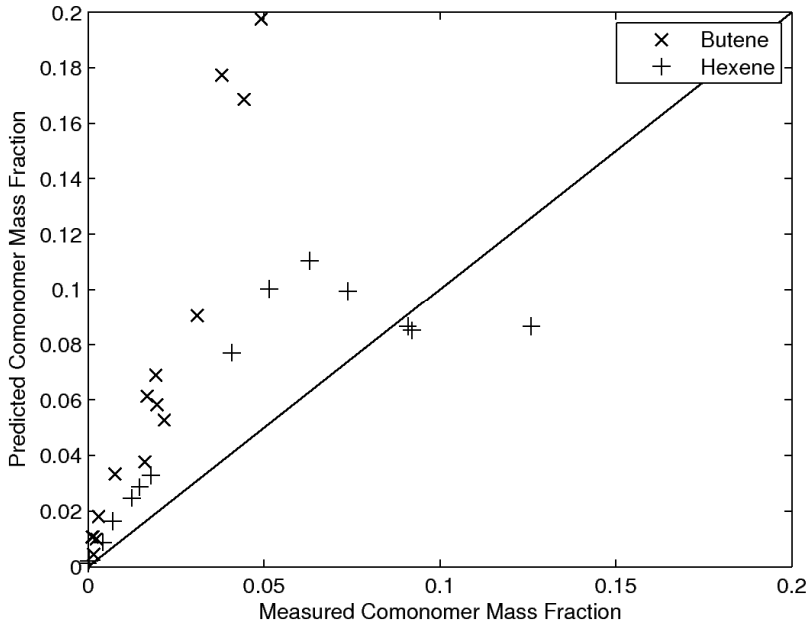

Figure 4.7 Comparison of predicted and measured comonomer incorporation using parameter values in Tables 4.8 and 4.9.

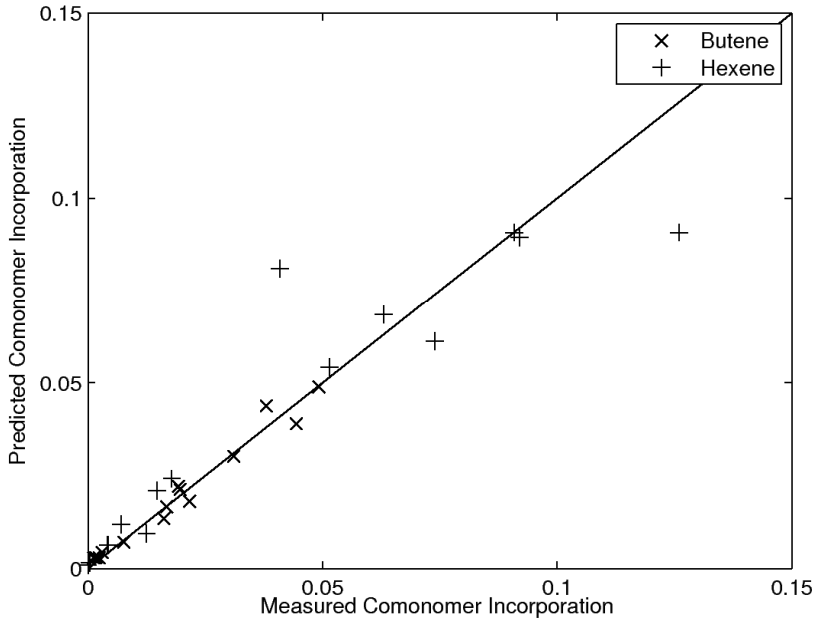

Figure 4.8 Comparison of predicted and measured comonomer incorporation using the final parameter values in Table 4.10.

Table 4.10 Final parameter values. The twenty bold values correspond to parameter that were estimated using the experimental data.

Parameter	Estimate
K_{11}	0.0149
K_{12}	0.0030
K_{13}	**0.0011**
K_{14}	0.0003
K_{15}	**$4.0*10^{-13}$**
K_4	**$7.9*10^{-4}$**
α_{1low}	**2431.6**
α_{1high}	**390.7**
α_{21}	0.4755
α_{23}	**0.3419**
α_{24}	**0.0671**
α_{25}	**0.0154**
α_{3Blow}	**0.0378**
α_{3Bhigh}	**0.0154**
α_{3Hlow}	**0.3065**
α_{3Hhigh}	**$4.44*10^{-9}$**
α_{4B}	**10.63**
α_{4H}	**28.84**
ε_{Klow}	**-3095**
ε_{Khigh}	**-4070**
$\varepsilon_{\alpha 21}$	**-2476**
$\varepsilon_{\alpha 2high}$	**-259.5**
$\varepsilon_{\alpha 3Blow}$	**-4377**
$\varepsilon_{\alpha 3Hlow}$	**495.6**
$\varepsilon_{\alpha 4}$	0

4.6 Conclusions

A simplified model has been developed to predict molecular weight distributions from ethylene-hexene and ethylene-butene copolymerization using a Ziegler-Natta catalyst. Estimability analysis and cross-validation were shown to be useful tools for deciding which parameters should be estimated using limited industrial data, and for guiding decisions about model simplification. Twenty of 25 parameters were estimated in the simplified model, which provides good predictions of MWD curves and comonomer incorporation. The small mismatch

between model predictions and experimental MWD results are similar in magnitude to deviations between MWD curves from replicate experimental runs. The parameter estimates from this study will be useful for designing experiments aimed at further model improvement, and the parameter estimation and model simplification strategy can be applied to other catalytic polymerization models.

4.7 Acknowledgments

Financial support, technical information, and data from INEOS Technologies are gratefully acknowledged, as is financial support from MITACS and scholarship support from the Province of Ontario and Queen's University.

4.8 Notation

$[H_2]$	gas phase hydrogen concentration	bars
$[C_2]$	gas phase ethylene concentration	bars
$[C_6]$	gas phase hexene concentration	bars
[I]	gas phase impurities concentration	bars
α_{1low}	lumped parameter, ratio relating chain transfer to hydrogen to reinitiation with ethylene at sites 1 and 2	
α_{1high}	lumped parameter, ratio relating chain transfer to hydrogen to reinitiation with ethylene at sites 3, 4, and 5	
α_{2j}	lumped parameter, ratio relating propagation with ethylene at site j to propagation with ethylene at site 2	
α_{3Blow}	lumped parameter, ratio relating propagation with butene at sites 1 and 2 to propagation with ethylene at site 2	
α_{3Bhigh}	lumped parameter, ratio relating propagation with butene at sites 3, 4, and 5 to propagation with ethylene at site 2	
α_{3Hlow}	lumped parameter, ratio relating propagation with hexene at sites 1 and 2 to propagation with ethylene at site 2	
α_{3Hhigh}	lumped parameter, ratio relating propagation with hexene at sites 3, 4, and 5 to propagation with ethylene at site 2	
α_{4B}	lumped parameter, ratio relating reinitiation with butene to reinitiation with ethylene at sites 1 and 2	
α_{4H}	lumped parameter, ratio relating reinitiation with hexene to reinitiation with ethylene at sites 1 and 2	
β_j	ratio of potential sites of type j to potential sites of type 2	

ε_{Kj}	lumped parameter, activation energies relating propagation with ethylene to chain transfer to hydrogen at site *j*	°K
$\varepsilon_{\alpha 2j}$	lumped parameter, activation energies relating propagation with ethylene at site *j* to propagation with ethylene site 2	°K
$\varepsilon_{\alpha 3Blow}$	lumped parameter, activation energies relating propagation with butene at sites 1 and 2 to propagation with ethylene site 2	°K
$\varepsilon_{\alpha 3Bhigh}$	lumped parameter, activation energies relating propagation with butene at sites 3, 4, and 5 to propagation with ethylene site 2	°K
$\varepsilon_{\alpha 3Hlow}$	lumped parameter, activation energies relating propagation with hexene at sites 1 and 2 to propagation with ethylene site 2	°K
$\varepsilon_{\alpha 3Hhigh}$	lumped parameter, activation energies relating propagation with hexene at sites 3, 4, and 5 to propagation with ethylene site 2	°K
$\varepsilon_{\alpha 4B}$	lumped parameter, activation energies relating reinitiation with ethylene to reinitiation with butene at sites 1 and 2	°K
$\varepsilon_{\alpha 4B}$	lumped parameter, activation energies relating reinitiation with ethylene to reinitiation with hexene at sites 1 and 2	°K
E_{tj}^{H}	activation energy for chain transfer to hydrogen at site *j*	J mol^{-1}
E_{pj}^{E}	activation energy for propagation with ethylene at site *j*	J mol^{-1}
E_{pj}^{But}	activation energy for propagation with butene at site *j*	J mol^{-1}
E_{pj}^{Hex}	activation energy for propagation with hexene at site *j*	J mol^{-1}
E_{ij}^{E}	activation energy for reinitiation with ethylene at site *j*	J mol^{-1}
E_{ij}^{But}	activation energy for reinitiation with butene at site *j*	J mol^{-1}
E_{ij}^{Hex}	activation energy for reinitiation with hexene at site *j*	J mol^{-1}
f_{Bj}	butene mole fraction incorporated by site *j*	
f_{Hj}	hexene mole fraction incorporated by site *j*	
J	objective function value	
K_{1j}	lumped parameter, ratio relating chain transfer to hydrogen to propagation with ethylene at site *j*	
K_4	lumped parameter, ratio relating spontaneous chain transfer and chain transfer to impurities to propagation with ethylene at all sites	bars
k_{ij0}^{E}	pre-exponential kinetic rate constant for reinitiation with ethylene at site *j*	bars^{-1} s^{-1}
k_{ij0}^{But}	pre-exponential kinetic rate constant for reinitiation with butene at site *j*	bars^{-1} s^{-1}
k_{ij0}^{Hex}	pre-exponential kinetic rate constant for reinitiation with hexene at site *j*	bars^{-1} s^{-1}
k_{pj0}^{E}	pre-exponential kinetic rate constant for propagation with ethylene at site *j*	bars^{-1} s^{-1}
k_{pj0}^{But}	pre-exponential kinetic rate constant for propagation with butene at site *j*	bars^{-1} s^{-1}
k_{pj0}^{Hex}	pre-exponential kinetic rate constant for propagation with hexene at site *j*	bars^{-1} s^{-1}

k_{tj0}^{H}	pre-exponential kinetic rate constant for chain transfer to hydrogen at site *j*	$bars^{-1}\ s^{-1}$
k_{tj}^{β}	kinetic rate constant for spontaneous chain transfer at site *j*	s^{-1}
k_{tj}^{I}	kinetic rate constant for chain transfer to impurities at site *j*	$bars^{-1}\ s^{-1}$
m_j	mass fraction of polymer produced at site *j*	
m_B	mass fraction of butene incorporation	
m_H	mass fraction of hexene incorporation	
N_j	mass fraction model numerator for site *j*	
R	gas constant	$J\ mol^{-1}\ K^{-1}$
r	chain length	
$s_{\theta k}$	parameter uncertainty in estimability analysis scaling	
s_{yi}	response uncertainty in estimability analysis scaling	
τ_j	inverse number-average molecular weight of site *j*	
θ_k	parameter *k* in estimability analysis	
T	reactor temperature	°K
T_0	reference temperature, T_0 = 363.15 °K	°K
y_i	response *i* in estimability analysis	
$Y_{j,n}$	growing polymer chain of length *n* at site of type *j*	
Y_{jD}	temporarily dormant site of type *j*	
Z	sensitivity matrix in estimability analysis	
$\hat{Z}_K$	least-squares prediction of *Z* in estimability analysis iteration *K*	

4.9 References

[4.1] D. E. Thompson, K. B. McAuley, P. J. McLellan, *Macromol. React. Eng.* **2007**, *1*, 523.

[4.2] A. Latado, M. Embirucu, A. G. M. Neto, J. C. Pinto, *Polym. Test.* **2001**, *20*, 419.

[4.3] D. E. Thompson, K. B. McAuley, P. J. McLellan, *Macromol. React. Eng.* **2007**, *1*, 264.

[4.4] B. Kou, K. B. McAuley, C. C. Hsu, D. W. Bacon, K. Z. Yao, *Ind. Eng. Chem. Res.* **2005**, *44*, 2428.

[4.5] B. Kou, K. B. McAuley, C. C. Hsu, D. W. Bacon, K. Z. Yao, *Ind. Eng. Chem. Res.* **2005**, *44*, 2443.

[4.6] K. Z. Yao, B. M. Shaw, B. Kou, K. B. McAuley, D. W. Bacon, *Polym. React. Eng.* **2003**, *11 (3)*, 563.

[4.7] B. F. Lund, B. A. Foss, *Automatica* **2008**, *44*, 278.

[4.8] Y. V. Kissin, *J. Polym. Sci., Par A: Pol. Chem.* **2001**, *39*, 1681.

[4.9] P. Rao, *Am. Stat.* **1971**, *25 (5)*, 37.

[4.10] S. Wu, T. J. Harris, K. B. McAuley, *Can. J. Chem. Eng.* **2007**, *85*, 386.

[4.11] M. Stone, *J. Roy. Stat. Soc. B Met.* **1974**, *36 (2)*, 111.

[4.12] R. Li, M. A. Henson, M. J. Kurtz, *IEEE T. Contr. Syst. T.* **2004**, *12 (3)*, 402.

[4.13] Y. Chu, J. Hahn, *AIChE J.* **2007**, *53 (11)*, 2858.

4.10 Appendix: Estimability Analysis Algorithm for Parameter Ranking

Estimability analysis is a tool for determining which parameters should be estimated when complex models contain too many parameters to be estimated using the available data. The estimability analysis algorithm used in this research is a simple and convenient tool, which was first proposed by Yao et al.[4.6] and then further developed by Kou et al.[4.4, 4.5] who studied olefin polymerization models with large numbers of parameters. Alternative tools, such as the approach of Li et al.[4.12], are less convenient to use. Li's method uses two separate measures, one that tests for parameter influence (magnitude of sensitivity coefficients) and a second that tests for linear independence. There is no easy way to combine the results from the two measures to decide which parameters should be estimated using the available data. Recently, Lund and Foss[4.7] proposed a method that produces identical results to the method of Kou et al., but Lund's method is more computationally complex. Chu and Hahn[4.13] have also suggested using an orthogonalization method to determine which parameters cannot be estimated together. Unfortunately, their method for parameter ranking uses a computationally-intensive genetic

algorithm to select parameters that should be estimated, using information from their orthogonalization results.

Estimability analysis uses sensitivity coefficients, which are the first-order partial derivatives of the response variables, y_i, with respect to the parameters, θ_k. A sensitivity matrix is constructed using these parametric sensitivity coefficients. Each column in the matrix contains partial derivatives with respect to a particular parameter, and each row corresponds to partial derivatives for a specific predicted response:

$$Z = \begin{bmatrix} \frac{\partial y_1}{\partial \theta_1} & \cdots & \frac{\partial y_1}{\partial \theta_k} \\ \vdots & \ddots & \vdots \\ \frac{\partial y_i}{\partial \theta_1} & \cdots & \frac{\partial y_i}{\partial \theta_k} \end{bmatrix} \tag{4.2}$$

The number of columns in Z is equal to the number of parameters in the model and the number of rows is equal to the total number of response values that will be used for parameter estimation. For example, the model in Table 4.3 has 33 unknown parameters and the data set available to estimate these parameters contains 31 MWD curves (with 100 points each) and 31 comonomer incorporation measurements. The resulting sensitivity matrix has dimensions of 3131 by 33. The sensitivity coefficients in Z should be properly scaled so that they are dimensionally consistent and can be meaningfully compared. To accomplish this objective, we propose that each coefficient should be multiplied by the uncertainty in the corresponding initial parameter guess, $s_{\theta k}$, and divided by the uncertainty in the particular measured response, s_{yi}, resulting in scaled sensitivity coefficients of the form:

$$\frac{\partial y_i}{\partial \theta_k} \frac{s_{\theta k}}{s_{yi}} \tag{4.3}$$

The relative influence of the various parameters can be found by examining the magnitudes of the entries in the columns of the sensitivity matrix. Parameters with large influence will correspond to columns with large (positive or negative) scaled sensitivity coefficients. To rank the parameters from most to least estimable, the following algorithm, which takes into account both the influence of the parameters and the correlations between their effects, is used:

1. Calculate the magnitude (sum of squares) of each column of the scaled sensitivity matrix, *Z*. Although analytical derivatives are used in the current research project, numerical derivatives could also be used.
2. Select the column with the largest magnitude. This column corresponds to the most estimable parameter.
3. Put the selected column into matrix X_K. When the first parameter is selected, $K=1$, and the matrix will contain only one column. When subsequent parameters are selected, the X_K matrix will contain K columns.
4. Calculate $\hat{Z}_K$, the least-squares prediction of the scaled sensitivity matrix, using the information in X_K.

$$\hat{Z}_K = X_K \left(X_K^T X_K \right)^{-1} X_K^T Z \tag{4.4}$$

5. Calculate the residual matrix R_K

$$R_K = Z - \hat{Z}_K \tag{4.5}$$

6. Calculate the magnitude of each column of R_K. The column with the largest magnitude corresponds to the next most estimable parameter.

7. Select the corresponding column in Z and augment the matrix X_K by including the new column. This augmented matrix is X_{K+1}.
8. Advance the iteration counter by 1 and repeat steps 4 to 7 until either all the parameters are ranked or singularity problems are encountered when inverting $X_K^T X_K$

4.11 Appendix: Sample Derivation of Activation Energy Parameters

The activation energy parameters presented in Table 4.4 are often defined as differences between activation energies. This appendix presents a sample derivation of one of the parameters, ε_{Kj}. The derivation begins with the isothermal model expression for τ (Equation 3.1.1)

$$\tau_j = \frac{k_{tj}^H}{k_{pj}^E}\frac{[\mathrm{H_2}]}{[\mathrm{C_2}]} + \frac{k_{tj}^C}{k_{pj}^E}\frac{[\mathrm{C_6}]}{[\mathrm{C_2}]} + \frac{k_{tj}^E}{k_{pj}^E} + \frac{\left(k_{tj}^\beta + k_{tj}^I[\mathrm{I}]\right)}{k_{pj}^E}\frac{1}{[\mathrm{C_2}]} \tag{3.1.1}$$

This sample derivation will focuses only on the term relating to chain transfer to hydrogen:

$$\frac{k_{tj}^H}{k_{pj}^E}\frac{[\mathrm{H_2}]}{[\mathrm{C_2}]} \tag{4.6}$$

First, Arrhenius expressions are added (see Equation 4.1.2):

$$\frac{k_{tj0}^H \exp\left(\frac{-E_{tj}^H}{R}\left(\frac{1}{\mathrm{T}}-\frac{1}{T_0}\right)\right)}{k_{pj0}^E \exp\left(\frac{-E_{pj}^E}{R}\left(\frac{1}{\mathrm{T}}-\frac{1}{T_0}\right)\right)}\frac{[\mathrm{H_2}]}{[\mathrm{C_2}]} \tag{4.7}$$

Next, the exponential expressions are combined:

$$\frac{k_{tj0}^H}{k_{pj0}^E}\exp\left(\frac{-E_{tj}^H}{R}\left(\frac{1}{\mathrm{T}}-\frac{1}{T_0}\right)-\frac{-E_{pj}^E}{R}\left(\frac{1}{\mathrm{T}}-\frac{1}{T_0}\right)\right)\frac{[\mathrm{H_2}]}{[\mathrm{C_2}]} \tag{4.8}$$

Then simplified:

$$\frac{k_{tj0}^{H}}{k_{pj0}^{E}}\exp\left(\frac{E_{pj}^{E}-E_{tj}^{H}}{R}\left(\frac{1}{\mathrm{T}}-\frac{1}{T_0}\right)\right)\frac{[\mathrm{H_2}]}{[\mathrm{C_2}]} \tag{4.9}$$

Finally, the parameters are lumped:

$$K_{1j}\exp\left(\varepsilon_{Kj}\left(\frac{1}{\mathrm{T}}-\frac{1}{T_0}\right)\right)\frac{[\mathrm{H_2}]}{[\mathrm{C_2}]} \tag{4.10}$$

The other activation energy parameters are derived in a similar manner.

Chapter 5

Design of Optimal Experiments to Improve Model Predictions

5.1 Summary

The quality of model predictions depends not only on having an appropriate model structure, but also on having good parameter estimates. For good parameter estimates to be achieved, it is important that the data used in parameter estimation are informative. Alphabet optimal experimental designs can be used to ensure that experiments conducted are as informative as possible. This work presents the development of D-, A-, and V-optimal sequential experimental designs to be used for improving the model predictions of a molecular-weight-distribution model for a Ziegler-Natta catalyst. Problems with local minima are addressed, and comparisons between the optimality criteria and resulting experimental designs are made.

5.2 Introduction

Owing to the multi-site nature of Ziegler-Natta catalysts, kinetic models of ethylene copolymerizations that use these catalysts tend to be very large, with many parameters that need to be estimated. Experimental runs on industrial reactors are expensive, especially when the required setpoints lie outside of the normal pattern of process operating conditions. Because of the difficulty of the parameter estimation problem and the expense of obtaining custom experimental data, it is important to design experiments and to use data as effectively as possible when building mathematical models. It is also important to extract all of the available information from prior experiments that may have been performed for other purposes.

Model simplification and estimability analysis are useful techniques to help with parameter estimation. However, these tools can only produce models with limited predictive capability when the data available for parameter estimation are of poor quality. Well-designed experiments ensure that the data that are collected are useful for parameter estimation and for improving model predictions. One common way of selecting appropriate experiments for parameter estimation is with an alphabet optimal design. Alphabet optimal designs use a number of different objective functions for determining optimal experimental designs. These objective functions typically focus on parameter precision or precision of predicted responses, or some combination of both. Although a large number of these designs have been proposed (e.g., A, D, E, G, I, L, T, V)[5.1-5.3] only a few are of interest in this work, where the goal is to obtain the best possible predictions from a simplified model. Note that considerable work has been done on selecting experimental runs for model discrimination,[5.2, 5.4-5.7] but this is beyond the focus of the current article.

D-optimal designs are the most commonly used of the alphabet-optimal designs.[5.1, 5.8-5.14] A D-optimal design is one that minimizes the volume of the parameter joint confidence region. Minimizing this volume is equivalent to minimizing the determinant of the variance-covariance matrix, or maximizing the determinant of the Fisher Information matrix, $Z^T Z$.[5.9] For nonlinear regression problems, the D-optimality objective function is:

$$J_D = \left| Z^T Z \right| \tag{5.1}$$

Z is the scaled parametric sensitivity matrix, which is the scaled Jacobian of the model predictions with respect to the model parameters:

$$Z = \begin{bmatrix} \frac{\partial y_{11}}{\partial \theta_1}\frac{s_{\theta 1}}{s_{y11}} & \cdots & \frac{\partial y_{11}}{\partial \theta_P}\frac{s_{\theta P}}{s_{y11}} \\ \vdots & \ddots & \vdots \\ \frac{\partial y_{Rn}}{\partial \theta_1}\frac{s_{\theta 1}}{s_{yRn}} & \cdots & \frac{\partial y_{Rn}}{\partial \theta_P}\frac{s_{\theta P}}{s_{yRn}} \end{bmatrix} \tag{5.2}$$

where y_{jk} is the predicted response at experimental condition j for variable k, θ_i is the i^{th} parameter, and $s_{\theta i}$ and s_{yjk} are appropriate scaling factors. Note that this experimental design is being developed for a multi-response estimation problem which has been formulated as a generalized least squares problem. The scaling factors take into account both prior information about the range and precision in which responses are measured and parameters are known, as well as taking into account the variances (and if necessary, covariances) of the responses as would be required in a GLS formulation.[5.15]

D-optimal designs have had considerable use in biological and chemical kinetic studies.[5.1] Van Derlinden et al.[5.14] used D-optimal designs in a study to determine parameter values for models relating temperature to microbial growth rates. Balsa-Canto et al.[5.16] used D-optimal experiments to estimate kinetic parameters for thermal degradation of nutrients in food.

Gueorguieva et al.[5.15] used D-optimal designs to improve parameter estimates in pharmacokinetic models, and Atkinson et al.[5.2] used D-optimal designs for parameter estimation of kinetics in reversible chemical reactions.

The D-optimality criterion is often used for sequential experimental designs.[5.17] Sequential designs are appealing because they offer the chance to change strategy after a first (or multiple) round of experiments has been completed[5.17] and new information is available. New experimental runs are selected after some runs have been completed. In sequential experimental design, the sensitivity coefficients for the prior experiments are included in the Z matrix, along with new rows corresponding to the new experimental run conditions that will be selected[5.18]. The Z matrix for the sequential design would therefore take the form:

$$Z = \begin{bmatrix} Z_{old} \\ Z_{new} \end{bmatrix} \tag{5.3}$$

where Z_{old} is the scaled sensitivity matrix for the pre-existing runs, and Z_{new} contains rows of scaled sensitivity coefficients corresponding to the new runs being selected. Given a set of initial parameter guesses, the coefficients in Z_{old} are fixed numerical values, and the coefficients in Z_{new} depend on the experimental settings for the proposed new runs. The new experimental settings constitute the decision variables for the D-optimal optimization problem. Many strategies have been developed for generation of D-optimal designs by sequentially adding runs to an existing design.[5.13, 5.17-5.22]

Criticisms of alphabet optimal designs in general, and of D-optimal designs in particular, centre mostly around sensitivity to model misspecification and poor initial parameter guesses.[5.10, 5.19, 5.23] Imperfect model structure and poor initial parameter guesses introduce bias into the design. In non-linear models, such as the ethylene copolymerization model in this work, the

elements of Z used in the design depend on the initial parameter guesses. As a result of these problems, some effort has focused on methods of experimental design that are more robust to model misspecification.

One approach taken to ensure model robustness is the use of Bayesian D-optimal designs. A Bayesian design allows the modeller to investigate additional parameters and effects that are believed to be unimportant for obtaining good model predictions.[5.24] These unimportant factors, which were likely not included in the initial model, make the experimental design more robust to model misspecification because the design can help to uncover poor initial assumptions. Ruggoo and Vandebroek[5.19] simulated a Bayesian D-optimal design, followed sequentially by a classical D-optimal design, for a linear regression model. They concluded that this combined approach produces superior results to either a Bayesian D-optimal design or a classical D-optimal design. Bayesian designs are more computationally intensive than standard optimal designs because they require numerical integration of probability density functions.[5.17] To our knowledge, the sequential Bayesian approach developed by Ruggoo and Vanderbroek[5.19] has not been used for mechanistic nonlinear models.

Myers[5.10, 5.17] provides a good review of approaches to ensure robustness in optimal experimental designs. In addition to the Bayesian approach, Myers also advocates sequential design, arguing again that sequential designs offer improved robustness against errors in initial guesses by allowing for parameter values to be corrected and for model structure adjustments to be made after an initial round of experiments.

Another type of optimal design is the A-optimal design, which minimizes the total parameter variance. The total parameter variance is obtained from the sum of the diagonal elements of the variance covariance matrix. Therefore, A-optimal designs minimize:

$$J_A = \text{trace}\left(\left(Z^T Z\right)^{-1}\right) \tag{5.4}$$

Although D-optimal designs are more commonly used, A-optimal designs are more computationally appealing[5.25] since they only use the diagonal elements of the matrix. Schittkowski used A-optimal designs for multiresponse ordinary-differential-equation and differential-algebraic-equation models that describe the dynamic behaviour of chemical processes.[5.25]

Model users often care more about the quality of the model predictions than about how well the parameters in the model are estimated. D-optimal and A-optimal designs focus primarily on improving the quality of the parameter estimates; however, it is sometimes possible to obtain good model predictions even though some of the less-important parameters may be poorly estimated. In keeping with this emphasis, V-optimal designs (also known as Q-optimal designs) can be used to select experiments to improve model predictions.[5.26] The information gained from a V-optimal design improves the estimates of the most important parameters more than the less-important parameters, whereas a D- or A-optimal design treats all parameters equally. Importance is judged by the impact of the parameters on the predictions at the points of interest. A V-optimal design is one that minimizes the average prediction variance over an operating region of interest. Thus, a V-optimal design minimizes:

$$J_V = \text{trace}\left(Z_{\text{int}}\left(Z^T Z\right)^{-1} Z_{\text{int}}^T\right) \tag{5.5}$$

where Z_{int} is a matrix of scaled sensitivity coefficients corresponding to a particular set of operating conditions of interest, where precise model predictions are desired by the model user. G-optimal designs, which are also focused on model prediction variance, minimize the maximum prediction variance over a domain of interest, which is equivalent to minimizing the *maximum* of

$\left(Z_{int}(Z^TZ)^{-1}Z_{int}^T\right)$. Since G-optimal designs involve solving a minimax problem, they are more likely to be computationally intensive than V-optimal designs.

In their classic paper Box and Draper[5.23, 5.27] provide 14 criteria for what constitutes a good experimental design. Of particular interest to this work is the criterion that a design should, "ensure that the fitted value at $\hat{y}(X)$ be as close as possible to the true value". In other words, the experimental design should ensure good model predictions. Box outlined his concerns about the suitability of alphabet optimal designs.[5.23] Of particular interest in the current work are his concerns about: 1) regions of experimental feasibility and modelling interest, and 2) acknowledging bias in experimental designs. When describing his first concern, Box asserts that the region of interest for making model predictions is usually much smaller than the region of feasible operation. He therefore reasons that designs that artificially constrain the design variables to the region of interest would not necessarily lead to the best predictions in that region of interest, since they do not take advantage of potential information that may be obtained by experimenting over a larger region. G- and V-optimal designs seem to address this concern very well; however, Box[5.23] indicates that G-optimality may not be practically desirable because of its minimax nature. He does not discuss V-optimality, perhaps because the V-optimal criterion was not widely used in 1982, but it would seem that V-optimality does not suffer from the same problems as G-optimality and so may be better suited for designing effective and practical experiments. It is not clear when V-optimality was first proposed; however, it appears to have evolved out of Box and Draper's idea of integrated variance.[5.3, 5.28-5.30] Welch[5.3] included V-optimality in a set of algorithms for computer-generated designs of experiments. Liu and Neudecker[5.31] used V-optimal designs in experiments with mixtures of several componenents.

François et al.[5.32] used V-optimal designs for selecting experiments to develop univariate nonlinear calibration models.

The second issue, bias in experimental design, is of concern in the current work because of the simplifying assumptions used in the model formulation. The model is a very simplified version of a complex system. The simplifying assumptions are included in the appendix. More complete and complex models reduce the bias, but this comes at the cost of increasing prediction variance[5.33, 5.34] because uncertainty in the model parameters propagates into uncertainty in predictions. Thus there is a trade-off between minimizing prediction variance and reducing bias. Traditional alphabet optimal designs, which assume that the model structure is correct, do not address this concern.

Some work has been done to include model imperfections and bias in the optimality criteria. Box and Draper[5.28] proposed a method that accounted for both variance and bias. In a polynomial model, they minimized the expected mean square error, which is the combination of the variance error and the bias error. Box and Draper noted that, in their example, the optimal design was very close to one which minimizes bias alone and ignores variance. Karson et al.[5.29] have done work with minimum bias designs. After they minimized the bias, they then proceeded to minimize the variance while ensuring minimum bias. Evans and Manson[5.30] have also done work with minimum bias estimation using the criterion outlined by Karson et al.[5.29] Evans and Manson[5.30] were able to select A-, D-, and V-optimal designs from within the set of experiments that minimized the bias in a two dimensional system. Draper and Sanders[5.35] have also used this approach to select rotatable designs. This minimum-bias approach is appealing, but it is difficult to apply to nonlinear mechanistic models where the bias cannot readily be assumed to be some function of higher order terms.

The objective of the current work is to select a small number of experimental runs that can be used to improve model predictions for our polyethylene MWD model. This model has been developed to have only as many parameters as are needed to explain the observed MWD curves and comonomer incorporation measurements from an industrial dataset.[5.36, 5.37]

5.3 Experimental Designs

Because of the multi-site nature of Ziegler-Natta catalysts, the associated olefin polymerization models tend to be very large and have many parameters. In this work, an attempt will be made to select new experimental runs to improve the predictions of the polyethylene copolymer MWD model.[5.37] An existing industrial data set was used to obtain the parameter estimates presented in the earlier work. Many of these parameter estimates have wide confidence intervals, and not all of the parameter estimates are statistically different from zero. Some less-important model parameters were never estimated and were left at their initial guesses.

Since data from 31 prior experimental runs have been obtained (15 with butene comonomer and 16 with hexene), it will be important to account for this prior information when planning the additional experiments. For each of these 31 experimental runs, a MWD curve and a comonomer incorporation measurement are available. The MWD curves can be discretized to give twenty equally-spaced (on a log scale) points per curve, with each of these points leading to a row in the sensitivity matrix, Z. Twenty points are sufficient to provide a reliable picture of the MWD curve from each run, without causing an undue computational load during sequential optimal design calculations. These twenty points correspond to 20 responses for each run condition. Additional rows in the Z matrix correspond to predictions of comonomer incorporation measurements (one row for each of the 31 experiments). As a result, Z_{old}, the sensitivity matrix resulting from the prior experiments has 31(20+1) = 651 rows (See Equation

5.3). Since the simplified model has 25 parameters, the overall sensitivity matrix Z has 25 columns, each containing derivatives with respect to a particular parameter. Note that each element in the sensitivity matrix is scaled appropriately as shown in Equation 5.2.[5.37] In the analysis that follows, assume that four additional runs can be selected. Each proposed experiment will provide 20 new values from the associated MWD curve (equally spaced between 2.7 and 6.6 on the log scale), along with a comonomer incorporation measurement. Thus, the proposed experiments will add 84 new rows to the Z matrix.

Since D-optimal designs are the most commonly used type of experimental design, a sensible starting point will be determining the D-optimal designs that arise from this sequential design problem. A D-optimal design is one that maximizes the determinant of the Fisher information matrix (i.e., that maximizes $|Z^T Z|$). The decision variables for this optimization problem are the following four reactor settings for each of the four proposed runs: reactor temperature (T), gas-phase hydrogen-to-ethylene ratio (H_2/C_2), the hexene-to-ethylene ratio (C_6/C_2), and the butene-to-ethylene ratio (C_4/C_2). Desired values of these reactor settings can be achieved and maintained using the available automatic control system of the pilot plant reactor. The gas-phase polyethylene reactor of interest can operate over a wide range of temperatures below the melting point of the ethylene copolymers.[5.38] High temperatures are desirable because they lead to high reaction rates and to higher yields per unit mass of catalyst. In this optimization problem, the temperature is constrained between 80 °C and 120 °C. Note that temperatures as low as 80 °C would not be desirable for industrial polymer production, but Box's advice[5.23] that the region of operation for designed experiments should be larger than the region of commercial interest where good predictions are desired has been heeded. The hydrogen-to-ethylene mole ratio is constrained between 0.1 and 0.6 to ensure that accurate MWD measurements can be

obtained, and the comonomer mole ratios are constrained between zero and 0.3. It is assumed that only one comonomer (either butene or hexene) can be used at a time. The following complementarity constraints are used to meet this requirement:[5.39]

$$\begin{aligned}\left(\mathrm{C}_4/\mathrm{C}_2\right)\left(\mathrm{C}_6/\mathrm{C}_2\right) &= 0\\ \left(\mathrm{C}_4/\mathrm{C}_2\right)+\left(\mathrm{C}_6/\mathrm{C}_2\right) &\geq 0\end{aligned} \tag{5.6}$$

Finally, to ensure that the reactor operating temperature remains safely below the melting point of the polymer, the following inequality constraint is used:

$$T \leq 122 - 81(C_X/C_2) \tag{5.7}$$

where T is the temperature in °C and C_X/C_2 is the comonomer (butene or hexene) to ethylene ratio. A minimum spacing constraint was also introduced to keep multiple experiments from being stacked at the same operating point:

$$\sqrt{\frac{\left(T_i-T_j\right)^2}{\left(T_{\max}-T_{\min}\right)^2}+\frac{\left(\left(H_2/C_2\right)_i-\left(H_2/C_2\right)_j\right)^2}{\left(\left(H_2/C_2\right)_{\max}-\left(H_2/C_2\right)_{\min}\right)^2}+\frac{\left(\left(C_4/C_2\right)_i-\left(C_4/C_2\right)_j\right)^2}{\left(\left(C_4/C_2\right)_{\max}-\left(C_4/C_2\right)_{\min}\right)^2}+\frac{\left(\left(C_6/C_2\right)_i-\left(C_6/C_2\right)_j\right)^2}{\left(\left(C_6/C_2\right)_{\max}-\left(C_6/C_2\right)_{\min}\right)^2}} \geq 0.5 \tag{5.8}$$

With the constraints in place, the optimization was performed using the fmincon routine in Matlab™, which can accommodate the required equality and inequality constraints. The algorithm in fmincon uses a sequential quadratic programming method. Expressions for analytical partial derivatives of the model equations with respect to the parameters (i.e., the elements of *Z*) were developed using Maple™. These partial derivatives are complicated expressions, because the model equations are complex. Note that Equation 4.7.1 (with 4.7.2 to 4.7.8 substituted) is used to predict MWD, and Equations 4.3.10a and 4.3.10b (with 4.7.3 to 4.7.8 and 4.3.9a and 4.3.9b substituted) are used to compute comonomer incorporation. Numerical values of the parameters in Table 4.10 were substituted into the partial derivative expressions, producing numerical values for the elements of Z_{old}. The elements of Z_{new} are analytical functions

of the decision variables for the four proposed experimental runs ((H_2/C_2), (C_4/C_2), (C_6/C_2), Temperature). The fmincon routine used these analytical expressions to calculate numerical derivatives of the various objective functions (Equations 5.6 to 5.8) with respect to the decision variables. Using fmincon, each optimization took between 15 to 40 minutes to solve. The optimizer generally stops when no further change occurs in the decision variables.

Six different sets of initial guesses were used for the decision variables. Unfortunately, several different local optima for the D-optimal design were obtained from the different initial guesses, as shown in Table 5.1. The value of the objective function $J = |Z^T Z|$ is reported for each of these local optima. The first set of initial guesses includes points of interest where good model predictions are desired. The resulting locally optimal runs, which are all at constraints, are reasonable since data collected over a wide operating range are often the most informative.[5.23] The second set of initial conditions is only slightly different from first the set, with each of the decision variables perturbed randomly up or down by a small amount. As expected, the resulting local optimum is the same as that obtained starting from the first initial guess.

The third set of initial guesses contains run conditions at extremes of the operating range. In this case, the resulting locally-optimal design points have not moved very far from the corresponding initial guesses. The fourth set of initial guesses has runs that are tightly grouped near the centre of the operating range. The resulting converged design points, which fall on constraints, have the highest objective function value among those obtained from the six attempts.

Table 5.1 D-optimal design of experiments. The most D-optimal design is shown in **bold**.

Set	J ($*10^{-6}$U)		Initial Conditions				D-optimal Runs			
		Run	Temp (°C)	H_2 / C_2	C_4 / C_2	C_6 / C_2	Temp (°C)	H_2 / C_2	C_4 / C_2	C_6 / C_2
1	3.6	1	100	0.4	0	0.15	100	0.6	0	0.27
		2	105	0.4	0.1	0	120	0.6	0	0
		3	115	0.2	0	0.01	120	0.1	0	0
		4	90	0.6	0.25	0	80	0.6	0.3	0
2	3.6	1	101	0.41	0	0.16	100	0.6	0	0.27
		2	106	0.39	0.09	0	120	0.6	0	0
		3	114	0.21	0	0.009	120	0.1	0	0
		4	91	0.59	0.24	0	80	0.6	0.3	0
3	2.73	1	80	0.1	0	0.01	80	0.1	0	0
		2	80	0.6	0	0.3	80	0.1	0	0.3
		3	120	0.1	0.01	0	120	0.1	0	0
		4	120	0.6	0.02	0	120	0.6	0	0
4	9.01	1	105	0.4	0	0.1	112.3	0.6	0	0.118
		2	105	0.4	0	0.15	97.5	0.1	0	0.3
		3	105	0.4	0.1	0	120	0.6	0	0
		4	105	0.4	0.15	0	112.1	0.6	0.12	0
5	1.27	1	100	0.4	0.15	0	119.4	0.6	0.03	0
		2	105	0.4	0.1	0	120	0.6	0	0
		3	115	0.2	0.01	0	120	0.1	0	0
		4	90	0.6	0.25	0	80	0.6	0.3	0
6	2.19	1	100	0.4	0	0.15	97.5	0.1	0	0.3
		2	105	0.4	0	0.1	120	0.6	0	0.023
		3	115	0.2	0	0.01	120	0.1	0	0
		4	90	0.6	0	0.25	80	0.6	0	0.3
7	**56.35**	**1**	**91.25**	**0.267**	**0.1**	**0**	**80**	**0.1**	**0.3**	**0**
		2	**97.07**	**0.4**	**0**	**0.2**	**120**	**0.6**	**0**	**0**
		3	**90**	**0.267**	**0**	**0.2**	**80**	**0.1**	**0**	**0.3**
		4	**90**	**0.4**	**0**	**0.2**	**105.2**	**0.1**	**0**	**0.205**
8	51.44	1	80	0.1	0.3	0	80	0.1	0.3	0
		2	97.55	0.5	0.3	0	120	0.6	0	0
		3	100	0.1	0	0.182	97.5	0.1	0	0.3
		4	100	0.5	0	0.182	114.1	0.6	0	0.096

It is disappointing, but not surprising, that numerous local minima were obtained from different starting points because of the nonlinearity of the system. Note that the optimizer never switched the comonomer that was used in any of the runs as the solution converged. Even when

all-butene or all-hexene designs (fifth and sixth set of initial conditions) are used as starting points, the optimizer does not change which comonomer is used in any of the runs, suggesting that the gradient-based optimizer in fmincon is not suitable for solving this design problem, possibly due to the complementarity constraints.

Several other optimization packages were considered, including the gradient-based interior-point optimizer IPOPT™[5.40] and the direct-search simplex optimizer simps™ in Matlab™. Using IPOPT™ proved to be impossible because AMPL™, which uses symbolic computation to provide analytical derivatives to IPOPT™, has no matrix algebra capabilities. Attempts were made to derive symbolic expressions for the required objective functions in Maple™, but they were too large to compute and caused memory overflow. Computation of the determinants and matrix inverses required in the objective functions was prohibitively difficult. Since simps uses Matlab™, matrix algebra is straightforward for this direct-search optimizer. However, simps does not readily accommodate some of the constraints (Equations 5.6 to 5.8). Perhaps the constraints could be reformulated using additional variables, but this option was not pursued. Instead, brute force optimization with fmincon was used, starting from a large number of initial guesses.

The existence of local optima makes it difficult to know whether the global optimum has been found. One way of addressing problems with local optima is to use a large number of initial guesses spread over a range of values. By moving the optimization starting point to different places, there is a better chance that the optimization will converge to the global optimum at least once. Using this strategy, 112 different sets of initial guesses were selected at well-spaced points throughout the operating region. Local D-optimal designs were determined from each of these starting points. Once all of the optimizations had converged, the best locally D-optimal

experimental design (among the results obtained) was determined and is reported as the 7th case in Table 5.1. Although the solver only converged on the optimal design once, there was another point that had nearly as good an objective value that was obtained five times and is reported as case 8 in Table 5.1. The fact that the design points lie along constraints is a positive outcome, since it is consistent with the notion of conducting experiments over a broader range of conditions to gain more insight and information.[5.23]

The A-optimal criterion was also used to design experiments. Again, several different starting points, the same as for the D-optimal designs, were used. The results are shown in Table 5.2. When the optimization was started from a large number of well-spaced starting points, the "best" design was selected with only butene comonomer and homopolymerization runs included (set 9 in Table 5.2). The objective function value for set 5 is nearly as good as for set 8, and these experiments were converged to from 11 of the 118 different initial guesses. The optimizer showed the same inability to switch between comonomers as was seen with the D-optimality calculations using the fmincon optimization code. It is somewhat surprising that the best run selected using the A-optimality criterion did not contain an experiment with hexene. This optimal design does have a homopolymerization run. Note that the D-optimal design (row 7 of Table 5.1) contains a homopolymerization run along with two hexene runs and a butene run.

Table 5.2 A-optimal design of experiments. The most A-optimal design is shown in **bold**.

Set	J		Initial Conditions				A-optimal Runs			
		Run	Temp (°C)	H_2 / C_2	C_4 / C_2	C_6 / C_2	Temp (°C)	H_2 / C_2	C_4 / C_2	C_6 / C_2
1	3.12	1	100	0.4	0	0.15	102.5	0.6	0	0.239
		2	105	0.4	0.1	0	110.8	0.1	0.136	0
		3	115	0.2	0	0.01	120	0.1	0	0
		4	90	0.6	0.25	0	80	0.1	0.3	0
2	3.12	1	101	0.41	0	0.16	102.5	0.6	0	0.239
		2	106	0.39	0.09	0	110.8	0.1	0.136	0
		3	114	0.21	0	0.009	120	0.1	0	0
		4	91	0.59	0.24	0	80	0.1	0.3	0
3	3	1	80	0.1	0	0.01	80	0.1	0	0
		2	80	0.6	0	0.3	80	0.1	0.3	0
		3	120	0.1	0.01	0	110.8	0.1	0.136	0
		4	120	0.6	0.02	0	120	0.6	0	0
4	4.72	1	105	0.4	0	0.1	119.2	0.6	0	0.032
		2	105	0.4	0	0.15	97.5	0.1	0	0.3
		3	105	0.4	0.1	0	112	0.6	0.122	0
		4	105	0.4	0.15	0	112.9	0.1	0.111	0
5	2.81	1	100	0.4	0.15	0	120	0.6	0	0
		2	105	0.4	0.1	0	110.8	0.1	0.136	0
		3	115	0.2	0.01	0	111.8	0.6	0.125	0
		4	90	0.6	0.25	0	80	0.1	0.3	0
6	10.54	1	100	0.4	0	0.15	105.7	0.6	0	0.2
		2	105	0.4	0	0.1	120	0.6	0	0
		3	115	0.2	0	0.01	120	0.1	0	0
		4	90	0.6	0	0.25	84.6	0.1	0	0.3
9	**2.71**	**1**	**91.7**	**0.267**	**0.3**	**0**	**80**	**0.15**	**0.3**	**0**
		2	**85.85**	**0.4**	**0.3**	**0**	**80**	**0.1**	**0.3**	**0**
		3	**105**	**0.267**	**0**	**0**	**110**	**0.1**	**0.147**	**0**
		4	**105**	**0.4**	**0**	**0**	**120**	**0.6**	**0**	**0**

Finally, V-optimal designs were also determined, starting from the same initial guesses as those used for the D- and A-optimal design computations. For V-optimal designs, a set of operating conditions (where good predictions are desired) must be specified to calculate the Z_{int} matrix in Equation 5.5. Ten operating points that cover the operating region of interest were selected (see Table 5.3). Note that the operating region of interest is irregularly shaped and has

both curved and straight boundaries. Using these 10 operating points, Z_{int} has dimensions 210 by 25.

Table 5.3 Points of interest used to determine the elements of Z_{int}.

Temp (°C)	H_2 / C_2	C_4 / C_2	C_6 / C_2
100	0.4	0	0.15
105	0.4	0	0.1
110	0.4	0	0.05
90	0.6	0.25	0
90	0.6	0.15	0
100	0.6	0	0.05
100	0.6	0	0.1
115	0.2	0	0.01
90	0.6	0	0.25
110	0.2	0.1	0

The V-optimal optimization had similar difficulties with local minima as the D- and A-optimization problems. The results for the V-optimal designs are summarized in Table 5.4. As expected, initial guesses 1 and 2 resulted in the same local optimum, as was the case for the D- and A-optimal designs. The best local optimum obtained (from 3 out of 118 initial guesses) is set 10. This design has one butene run and three hexene runs.

Table 5.4 V-optimal design of experiments. The most V-optimal design is in **bold**.

Set	J		Initial Conditions				V-optimal Runs			
		Run	Temp (°C)	H_2 / C_2	C_4 / C_2	C_6 / C_2	Temp (°C)	H_2 / C_2	C_4 / C_2	C_6 / C_2
1	9.82	1	100	0.4	0	0.15	99	0.6	0	0.282
		2	105	0.4	0.1	0	110.6	0.6	0.139	0
		3	115	0.2	0	0.01	112.4	0.6	0	0.116
		4	90	0.6	0.25	0	80	0.6	0.3	0
2	9.82	1	101	0.41	0	0.16	99	0.6	0	0.282
		2	106	0.39	0.09	0	110.6	0.6	0.139	0
		3	114	0.21	0	0.009	112.4	0.6	0	0.116
		4	91	0.59	0.24	0	80	0.6	0.3	0
3	16.14	1	80	0.1	0	0.01	80	0.1	0	0
		2	80	0.6	0	0.3	80	0.3	0	0.3
		3	120	0.1	0.01	0	112.6	0.1	114	0
		4	120	0.6	0.02	0	114.3	0.6	0.093	0
4	10.75	1	105	0.4	0	0.1	112.3	0.6	0	0.118
		2	105	0.4	0	0.15	98.8	0.6	0	0.285
		3	105	0.4	0.1	0	112.2	0.6	0.12	0
		4	105	0.4	0.15	0	110.1	0.6	0.145	0
5	16.33	1	100	0.4	0.15	0	110.8	0.6	0.136	0
		2	105	0.4	0.1	0	116.2	0.6	0.069	0
		3	115	0.2	0.01	0	116.7	0.1	0	0
		4	90	0.6	0.25	0	80	0.6	0.3	0
6	10.81	1	100	0.4	0	0.15	112.6	0.6	0	0.115
		2	105	0.4	0	0.1	114.6	0.6	0	0.089
		3	115	0.2	0	0.01	107.7	0.1	0	0.174
		4	90	0.6	0	0.25	95.5	0.6	0	0.3
10	**9.45**	**1**	**80**	**0.1**	**0.1**	**0**	**80**	**0.1**	**0.3**	**0**
		2	**105.6**	**0.5**	**0**	**0.2**	**114.4**	**0.6**	**0**	**0.091**
		3	**90**	**0.1**	**0**	**0.1**	**95.5**	**0.6**	**0**	**0.3**
		4	**90**	**0.5**	**0**	**0.1**	**110.5**	**0.6**	**0**	**0.14**

Unlike the D- and A-optimal designs, the V-optimal design does not contain any homopolymerization runs. This is result is not surprising because no homopolymerization runs were specified in the points of interest in Table 5.3. V-optimality focuses on improving model predictions at the points of interest, and it seems that information from homopolymerization runs

is not crucial for obtaining good predictions at the operating conditions specified in Table 5.3. Of the three criteria considered, V-optimality best matches the industrially-relevant objectives of this work, i.e., to produce a model that results in good predictions over the operating region of interest. Table 5.5 compares the three optimal designs obtained using the three different optimality criteria. The objective function values J_D, J_A and J_V were computed for each of three selected designs.

Table 5.5 Optimality over a large range of conditions. Freq. shows the number of times these experiments were selected out of the 118 different initial guesses. J_X is the objective function for the corresponding optimality criterion.

Selection Criterion	Freq.	J_D	J_A	J_V	Run	Temp (°C)	H_2/C_2	C_4/C_2	C_6/C_2
D	1	56.3×10^{60}	3.59	11.05	1	80	0.1	0.3	0
					2	120	0.6	0	0
					3	80	0.1	0	0.3
					4	105.2	0.1	0	0.205
A	1	5.84×10^{60}	2.71	21.3	1	80	0.15	0.3	0
					2	80	0.1	0.3	0
					3	110	0.1	0.147	0
					4	120	0.6	0	0
V	3	8.51×10^{60}	3.8	9.45	1	80	0.1	0.3	0
					2	114.4	0.6	0	0.091
					3	95.5	0.6	0	0.3
					4	110.5	0.6	0	0.14

Comparing the J_D values for the three designs to the locally-optimal objective function values shown in Table 5.1, reveals that the A-optimal and V-optimal designs are quite good in the sense of D-optimality. Similarly, the D-optimal and V-optimal designs in Table 5.5 have good values of J_A (smaller is better), when compared with the local optima in Table 5.2. Comparison of the J_v values from Table 5.5 with the locally optimal values in Table 5.4 shows that the D-

optimal design is reasonably good, but that the A-optimal design has worse V-optimality than any of the local optima in Table 5.4.

5.4 Conclusions and Recommendations

Optimizations were conducted to determine D-, A-, and V-optimal sequential experimental designs. Many local optima were observed because of the nonlinearity of the optimization problem and multi-modal nature of the objective functions. The results of the optimizations were heavily dependent on what initial guesses were used as starting points for the experimental conditions. To address this difficulty, 118 different well-spaced sets of experimental runs were selected as starting points for the optimization. The best local optima obtained are reported.

It is possible that a different numerical optimization algorithm would yield more-reliable results. A more robust optimizer may be desirable, and it is recommended that other optimizers should be investigated to solve the constrained optimization problems formulated in this article. In particular, the suitability of algorithms for global optimization should be investigated.

The best four-run D-optimal design obtained consisted of one butene run, two hexene runs, and a homopolymerization run. The best A-optimal design consisted of three butene runs, and a homopolymerization run. The best V-optimal design consisted of one butene run and three hexene runs. As a result, it is not clear which new experiments should be performed. The V-optimal design is recommended because it is best aligned with the practical goal of improving model predictions at operating points of interest.

5.5 References

[5.1] T. P. Ryan, "*Modern Experimental Design"*, John Wiley & Sons, Inc., Hoboken, New Jersey 2007, pp. 279-282, 504-507.

[5.2] A. C. Atkinson, B. Bogacka, M. B. Bogacki, *Chemometr. Intell. Lab.* **1998**, *43*, 185.

[5.3] W. J. Welch, *Technometrics* **1984**, *26*, 217.

[5.4] P. D. H. Hill, *Technometrics* **1978**, *20*, 15.

[5.5] W. G. Hunter, A. M. Reiner, *Technometrics* **1965**, *7*, 307.

[5.6] D. Ucinski, B. Bogacka, *J. Roy. Stat. Soc. B* **2005**, *67*, 3.

[5.7] B. M. R. Donckels, D. J. W. De Pauw, B. De Baets, J. Maertens, P. A. Vanrolleghem, *Chemometr. Intell. Lab.* **2009**, *95*, 53.

[5.8] O. Krafft, M. Schaefer, *J. Multivariate Anal.* **1992**, *42*, 130.

[5.9] A. C. Atkinson, *Chemometr. Intell. Lab.* **1995**, *28*, 35.

[5.10] R. H. Myers, A. I. Khuri, W. H. Carter, *Technometrics* **1989**, *31*, 137.

[5.11] R. C. St. John, N. R. Draper, *Technometrics* **1975**, *17*, 15.

[5.12] V. Prasad, D. G. Vlachos, *Ind. Eng. Chem. Res.* **2008**, *47*, 6555.

[5.13] J.-L. Dirion, C. Reverte, M. Cabassund, *Chem. Eng. Res. Des.* **2008**, *86*, 618.

[5.14] E. Van Derlinden, K. Bernaerts, J. F. Van Impe, *Int. J. Food Microbiol.* **2008**, *128*, 89.

[5.15] I. Gueorguieva, L. Aarons, K. Ogungbenro, K. M. Jorga, T. Rodgers, M. Rowland, *J. Pharmacokinet. Phar.* **2006**, *33*, 97.

[5.16] E. Balsa-Canto, M. Rodriguez-Fernandez, J. R. Banga, *J. Food Eng.* **2007**, *82*, 178.

[5.17] P. A. K. Covey-Crump, S. D. Silvey, *Biometrika* **1970**, *57*, 551.

[5.18] A. Ruggoo, M. Vandebroek, *Comput. Stat. Data An.* **2004**, *47*, 655.

[5.19] R. H. Myers, *J. Qual. Technol.* **1999**, *31*, 30.

[5.20] L. S. Mayer, A. D. Hendrickson, *Commun. Stat. – Theor. M.* **1973**, *2*, 465.

[5.21] H. P. Wynn, *Ann. Math. Stat.* **1970**, *41*, 1655.

[5.22] O. Dykstra Jr., *Technometrics* **1971**, *13*, 682.

[5.23] G. E. P. Box, *Utilitas Mathematica* **1982**, *21*, 11.

[5.24] W. DuMouchel, B. Jones, *Technometrics* **1994**, *36*, 37.

[5.25] K. Schittkowski, *Ind. Eng. Chem. Res.* **2007**, *46*, 9137.

[5.26] R. H. Myers, D. C. Montgomery, *"Response Surface Methodology: Process and Product Optimization Using Designed Experiments"*, John Wiley & Sons, Inc., New York 1995, pp. 364-373.

[5.27] G. E. P. Box, N. R. Draper, *Biometrika* **1975**, *62*, 347.

[5.28] G. E. P. Box, N. R. Draper, *J. Am. Stat. Assoc.* **1959**, *54*, 622.

[5.29] M. J. Karson, A. R. Manson, R. J. Hader, *Technometrics* **1969**, *11*, 461.

[5.30] J. W. Evans, A. R. Manson, *J. Am. Stat. Assoc.* **1978**, *73*, 171.

[5.31] S. Liu, H. Neudecker, *Stat. Probabil. Lett.* **1995**, *23*, 253.

[5.32] N. François, B. Govaerts, B. Boulanger, *Chemometr. Intell. Lab.* **2004**, *74*, 283.

[5.33] S. Wu, T. J. Harris, K. B. McAuley, *Can. J. Chem. Eng.* **2007**, *85*, 386.

[5.34] P. Rao, *Am. Stat.* **1971**, *25*, 37.

[5.35] N. R. Draper, E. R. Sanders, *Technometrics* **1988**, *30*, 319.

[5.36] D. E. Thompson, K. B. McAuley, P. J. McLellan, *Macromol. React. Eng.* **2007**, *1*, 523.

[5.37] D. E. Thompson, K. B. McAuley, P. J. McLellan, "Parameter Estimation in a Simplified Molecular Weight Distribution Model for HDPE Produced by Ziegler-Natta Catalyst", Accepted for publication in: *Macromol. React. Eng.*, March 2009.

[5.38] WO 01/66610 A1 (2001), BP Chemicals Limited, invs.: J.-R. Llinas, J.-L. Selo.

[5.39] R. Baker, L. E. Swartz, *Ind. Eng. Chem. Res.* **2008**, *47*, 81.

[5.40] A. Wachter, L. T. Biegler, *Math. Program. Ser. A* **2006**, *106*, 25.

5.6 Appendix: Model Assumptions

The model used for design of experiments is a simplified model. There are many phenomena that occur during Ziegler-Natta polymerization that are not included in the model. This appendix presents a summary of the assumptions that were made during the derivation of the model, as well as the basis on which these assumptions were made.

1. The model neglects the effects of catalyst activation and deactivation reactions. During polymerization, reactions occur that activate and deactivate the catalyst. Because this is a steady-state model, it is assumed that the relative amounts of catalyst sites of each type remain fixed, and thus the activation and deactivation reactions do not have an impact on the MWD. Activation and deactivation reactions could still influence the polymer production rate, but this is not included in the model. One justification for this assumption is that residence time (over the range of the industrial data) does not appear to influence MWD. No heat transfer or mass transfer resistances are included in the model, and the effects of catalyst particle break-up on the number of active sites is also neglected. Note that the gas-phase polyethylene production process being modeled includes a prepolymerization reactor, which reduces the influence of these effects in the main gas-phase reactor. The contribution of the prepolymer to the final product is neglected. Temperatures and gas-phase concentrations are assumed to be uniform throughout the reactor.

2. The model ignores the effects of the terminal monomer group. In copolymerization, it is usually assumed that the kinetics of the reactions are influenced by which comonomer was previously added to the growing polymer chain. For instance, ethylene may be added to the polymer chain more quickly if there is an ethylene group at the end of the chain than if there is a hexene group. The model ignores this effect because most of the end-groups are ethylene, especially in HDPE, and because this assumption greatly simplifies the model.
3. It is assumed that the reaction rates are kinetically, rather than diffusionally, controlled and that the amorphous polymer in contact with the catalyst active sites is in phase equilibrium with the gas-phase in the reactor. It is assumed that phase equilibria for hydrogen, ethylene, hexene and butene are governed by Henry's law. The model parameters relate the gas-phase concentrations to the reaction rates, eliminating the need for Henry's law constants to appear explicitly in the model.
4. It is assumed that residence time does not have a significant impact on the MWD or composition of the copolymer produced, and that therefore, residence time is not included in the model. This is based on the observations of correlations between deconvolution parameters and operating conditions presented in Chapter 2.
5. The form of the model used for design of experiments also ignores several chain-transfer reactions that are believed to not have much impact on the MWD (see Chapter 3). In particular, chain transfer to ethylene, hexene, butene, cocatalyst and impurities are ignored.

Chapter 6

Conclusions, Contributions, and Recommendations

6.1 Conclusions

The goal of this work was to develop simplified mathematical models to predict the molecular weight distribution of ethylene copolymers produced using a Ziegler-Natta catalyst. The first step in the model development process was to use deconvolution analysis to examine how the various catalyst active sites respond to changes in the reactor operating conditions. Second, a simplified isothermal model that predicted MWD and comonomer incorporation for ethylene/hexene copolymer produced at 90 °C was developed. The parameter estimates from the isothermal model were used as initial guesses for parameters in a more complex model. In Chapter 4, the isothermal model was extended to account for the effects of butene comonomer and for temperature effects. Finally, optimal sequential experimental designs were selected to provide additional data in order to improve the model predictions. The following specific conclusions can be drawn:

1) Sixteen industrial ethylene/hexene copolymer samples were deconvolved to determine the average molecular weight and relative amount (mass-fraction) of polymer produced by each type of active site on the Z-N catalyst. The deconvolution parameter estimation problem was ill-conditioned and the resulting estimates of the site mass-fraction and molecular-weight parameters were highly correlated, implying that they cannot be believed to be entirely reliable. The deconvolution also revealed that five Flory distributions are required to adequately fit the MWD curves.

2) Analysis of the correlations between the reactor operating conditions and the deconvolution parameter estimates (site mass-fraction and site molecular weight) provided insight into the behaviour of the five different types of active sites on the Z-N catalyst. As expected, high hydrogen-to-ethylene ratios were associated with lower average molecular weights. High hexene-to-ethylene ratios were associated with lower molecular weight, with the possible exception of the lowest-molecular-weight site, which may produce a waxy copolymer. Higher temperatures were found to be correlated with higher average molecular weights. This surprising result was likely the result of the high degree of correlation between temperature and hydrogen. Less hydrogen is present at higher temperatures, and so the higher observed molecular weights at higher temperatures are likely a reflection of reduced chain transfer to hydrogen.

3) The correlations among the deconvolution parameters are consistent with there being only a couple of chemically distinct types of sites on the Z-N catalyst. The three high-molecular-weight sites tend to respond the same way to changes in the reactor operating conditions, and the two low-molecular-weight sites also tend to move together. As a result, it was possible to group some of the kinetic parameters for similar types of sites and to thereby reduce the number of parameters that needed to be estimated.

4) A simplified steady-state model to predict MWDs and comonomer incorporation of ethylene/hexene copolymers produced using Z-N catalysts in industrial gas-phase reactors at 90 °C was developed. The simplified reaction scheme and sharing of rate constants between sites reduced the number of parameters that needed to be estimated to 18 from approximately 100.

5) The deconvolution parameter estimates (site mass-fractions and molecular weights) were used along with comonomer incorporation data to obtain initial estimates for the parameters in the isothermal model. The parameter estimates obtained for the isothermal model provided useful initial parameter guesses for use in parameter estimation for the more complex model.

6) An extended simplified model was developed to predict MWD from ethylene/hexene and ethylene/butene copolymerization at a variety of temperatures. This model accounts for the influences of all of the important reactor operating conditions on MWD and comonomer incorporation. A simplified reaction scheme and sharing rate constants and activation energies between sites reduced the number of model parameters to 25.

7) Estimability analysis and cross-validation were used to determine which model parameters should be estimated from the available industrial data set. Estimability analysis ranked the parameters from most to least estimable and cross-validation was used to determine how many parameters to estimate.

8) Twenty of 25 parameters were estimated, and the model provides good predictions of MWDs and comonomer incorporation. The small mismatch between model predictions and experimental MWD results are similar in magnitude to deviations between MWD curves from replicate experimental runs.

9) D-, A-, and V-optimal designs were found to select four new experiments with the goal of improving model predictions. Multiple initial guesses (118 covering the range of reasonable operating conditions) were used to overcome the presence of local minima in the optimization problem. The best four-run D-optimal design obtained consisted of one

butene run, two hexene runs, and a homopolymerization run. The best A-optimal design consisted of three butene runs, and a homopolymerization run. The best V-optimal design consisted of one butene run and three hexene runs.

10) Constraints were used to keep the experimental runs selected within the range of allowable reactor operation. The Matlab™ optimizer function, fmincon, can readily accommodate the constraints, but appeared to have trouble with the complementarity constraints that ensure that only one comonomer is used.

6.2 Contributions

The specific contributions of this work consist of the following:

1) An understanding of the behaviour of the Z-N catalyst used by our industrial sponsor was obtained by using deconvolution analysis and examining the correlations among the deconvolution parameter estimates and the reactor operating conditions.

2) It was determined that kinetic rate constants and activation energies could be shared between the high-molecular-weight sites that behave in a similar manner and between the low-molecular-weight sites that exhibit similar behaviour.

3) Simplified mechanistic models were developed that can predict MWD and comonomer incorporation for ethylene/hexene and ethylene/butene copolymers produced using Z-N catalysts in industrial gas-phase reactors.

4) Uncertainty-based scaling factors were developed for use in estimability analysis and design of experiments.

5) The use of cross-validation in estimability analysis was demonstrated, and provides a technique for deciding how many parameters should be included in a model estimation

problem. The cross-validation was used to determine how many parameters can be estimated from the ranked list generated by the estimability analysis.

6) Experiments were designed for improving MWD model predictions.

7) Demonstrated how D-, A-, and V-optimality criterion can be used to develop sequential experimental designs for complicated polyolefin models.

6.3 Recommendations

Based on the work presented in this thesis, the following recommendations are made to improve upon this work in the future:

1) This thesis used cross-validation to determine the number of parameters that should be estimated from the ranked estimability list. Unfortunately, this is a computationally intensive system since it requires several rounds of parameter estimation, with more parameters being estimated in each round. The number of parameters that should be estimated can only be seen once the cross-validation parameter estimation has been conducted. It is recommended that a faster and less computationally demanding method be developed for selecting the number of parameters to be estimated from the ranked estimability list.

2) The final model developed in Chapter 4 has good predictive ability, based on the cross-validation. This model should be put online. This would allow for a more rigorous evaluation of the model's predictive abilities and for observation of its performance over a long period of time. This would also make the model more useful for our industrial sponsor.

3) Ultimately, our industrial sponsor would like to be able to predict end-use polymer properties such as Young's Modulus or tensile strength from reactor operating conditions. The MWD models developed in this thesis represent a useful intermediate step between reactor operating conditions and end-use properties, because these end-use properties are highly dependent on the MWD. The MWD model in this thesis should be linked with other models that can predict end-use properties from MWDs. This way, it should be possible to predict end-use properties from reactor operating conditions via the MWD.

4) Other optimization routines should be investigated for use in design of experiments. The optimizer used in this work, fmincon, had difficulty with the complementarity constraints. Other solvers, such as a direct-search solver or IPOPT-C™ (interior point optimization with complementarity constraints) should be investigated. Although it was infeasible to use IPOPT with AMPL™ for the design of experiments because of AMPL™'s lack of matrix algebra abilities, it may be possible to use IPOPT in a different programming environment. In this work, no direct-search optimizer was found that could accommodate the necessary constraints. It may be possible to reformulate the optimization problem using additional variables in order to use a direct-search optimizer. Finally, global optimization techniques should be investigated for solving the optimal experimental design problem.

5) In Chapter 5, optimal experimental designs for improving model predictions were chosen. These experiments could be conducted on a pilot plant reactor to: i) provide the desired improvement in model predictions, and ii) provide some basis for evaluating the effectiveness of the experimental design proposed in Chapter 5.

6) The impact of nonlinearity in the MWD estimation problem should be investigated to determine whether the use of linearization-based methods for inference and for experimental design is sufficiently reliable. All of the techniques used for parameter estimation, estimability analysis, and design of experiments use local linear approximation. Other techniques such as profile likelihood[6.1-6.3] or empirical sampling[6.4, 6.5] should be investigated.

6.4 References

[6.1] D. M. Bates, D. G. Watts, *"Nonlinear Regression Analysis and Its Applications"*, John Wiley & Sons, New York 1988.

[6.2] S. L. Quinn, D. W. Bacon, T. J. Harris, *Commun. Statist.-Theory Meth.* **2000**, *29*, 108.

[6.3] T. A. Severini, *"Likelihood Methods in Statistics"*, Oxford University Press, New York 2000.

[6.4] D. Gamerman, H. F. Lopes, *"Markov Chain Monte Carlo"*, Chapman and Hall, Boca Raton 2006.

[6.5] J. J. Jitjareonchai, P. M. Reilly, T. A. Duever, D. B. Chambers, *Can. J. of Chem. Eng.* **2006**, *84*, 125.